Poole Bay and Harbour Strategy Study

Computational model studies

Report EX4555
June 2003

Poole Bay and Harbour Strategy Study

Computational model studies

Report EX4555
June 2003

HR Wallingford

Address and Registered Office: HR Wallingford Ltd. **Howbery Park, Wallingford, OXON OX10 8BA**
Tel: +44 (0) 1491 835381 Fax: +44 (0) 1491 832233

Contract - Consultancy

This report describes work commissioned by Halcrow Group Ltd, whose representative was Mr L Banyard. The work was carried out under the HR Wallingford project number DDR 3188 by staff in the Ports, Estuaries and Industry Department and the Coastal Department and was managed by Mr T J Chesher in the Estuaries and Dredging Group at HR Wallingford.

Prepared by ..... J. Semmens .....

(name)

..... Project Scientist .....

(Title)

Approved by ..... T J Chesher .....

(name)

..... Project Manager. .....

(Title)

Authorised by ..... T J Chesher .....

(name)

..... Group Manager. .....

(Title)

Date ..... 17/06/03 .....

Summary

Poole Bay and Harbour Strategy Study

Computational model studies

Report EX4555
June 2003

Extensive numerical modelling studies were undertaken to simulate the sediment transport processes within Poole Bay and Harbour, as part of an overall Coastal Defence Strategy Study carried out by Halcrow.

Following set up and calibration of hydrodynamic and a sediment transport model, the HR Wallingford coastal area model, PISCES was used to simulate sediment transport pathways due to tides, with and without the effect of wave stirring, and also due to storm conditions during spring tides.

Detailed resolution of the entrance to Poole Harbour, and the frontage between Poole and Hengistbury Head was used to establish a comprehensive assessment of the coastal sediment regime. Further offshore, the sediment transport pathways in Poole Bay were established, with a particular emphasis on the long term drift patterns throughout the area. As part of this process, a full spring-neap cycle of the sediment transport was simulated.

Results of the numerical model studies were presented to the Poole Bay and Harbour Coastal Group at a series of meetings over the course of the study period. This information has been used by the Poole Bay and Harbour Coastal Group to devise a future coastal defence strategy for the area.

In regard to the sourcing of material for beach nourishment, the effects of placement of material along the coast of the area studied was examined, with particular emphasis on the area of Swanage Bay. Detailed analysis of the littoral drift patterns along the entire coast of the study area were processed to aid this investigation.

The coastal area model was also used to simulate the impact of two dredging scenarios of Swash Channel: one a minor maintenance dredging campaign of localised hot spots, and the other a larger capital dredging campaign of the entire Swash Channel.

Contents

Tables

Contents continued

Figures

Contents *continued*

Contents continued

Appendices

1. INTRODUCTION

In November 2001 HR Wallingford was commissioned by Halcrow to undertake numerical modelling studies as part of the Poole Bay Coastal Defence Strategy Study.

The specific scope of work comprised studies to improve the knowledge of sediment transport patterns under waves and tidal current at Hook Sands and Poole Harbour entrance under spring and neap tides and storm events. In addition there were tasks aimed at modelling the effects of future dredging activity at Poole Harbour entrance and to provide information to feed into a conceptual sediment budget model for Poole Bay.

This report describes the studies undertaken to set up and calibrate a new inner model covering Poole Bay and Harbour, and to analyse the present sediment transport processes over this study area. Results of the numerical model studies were presented to the Poole Bay and Harbour Coastal Group at a series of meetings over the course of the study period. This information has been used by the Poole Bay and Harbour Coastal Group to devise a future coastal defence strategy for the area.

In regard to the sourcing of material for beach nourishment, the effects of placement of material along the coast of the area studied was examined, with particular emphasis on the area of Swanage Bay. Detailed analysis of the littoral drift patterns along the entire coast of the study area were processed to aid this investigation.

The coastal area model was also used to simulate the impact of two dredging scenarios of Swash Channel: one a minor maintenance dredging campaign of localised hot spots, and the other a larger capital dredging campaign of the entire Swash Channel.

2. METHODOLOGY

The aim of the numerical modelling exercise was to provide information to the Coastal Strategy Study in the form of improved knowledge on the sediment transport processes of Poole Bay and Harbour.

As part of studies into the hydrodynamics, sediment transport and morphology of Poole Bay a 2D depth-integrated flow model was used. The model was required to simulate the tidal flow in the area as well as include wave-induced currents in the near-shore region. HR Wallingford had undertaken a number of modelling studies in the area and the present work sought to build on that experience.

The twin requirements of covering a large area and having very fine detail in the areas where waves might break causing wave-induced currents made the state-of-the-art finite element based model TELEMAC2D an ideal choice for the modelling study.

TELEMAC, developed by EDF-LNHE, uses an unstructured triangular grid that gives the user complete control of the model resolution so fine detail can be used in areas where the physical processes require it while larger elements can be used to keep any imposed boundary conditions distant. TELEMAC has also been integrated into the HR sediment transport and morphodynamic modelling framework, PISCES.

PISCES is a state-of-the-art, fully-interactive coastal area modelling framework, capable of simulating the various processes of wave propagation, current distribution, and the resulting sediment transport in complex coastal areas. For this study PISCES comprised the wave propagation model, COWADIS in combination with the finite element flow model TELEMAC and the SANDFLOW sand transport model. Typical application of PISCES comprises setting up a bathymetric database, selection of specific input wave conditions for simulation, calculating the corresponding currents and sand transport pathways and analysing the results. A consequence of detailed model resolution and sophistication of the models means that it is not usually possible to model all wave conditions in a particular climate, and in any event this would not be a practical option since the sequence of wave conditions is not known. Accordingly, PISCES is used to model representative patterns of drift for a selection of waves and the results are integrated to yield the gross and net longshore drift. Details of TELEMAC, COWADIS and SANDFLOW are presented in Appendix 1.

Two models were used for the study, a regional model as used for the Sandbanks Coastal Protection Scheme (Reference 1). This regional model was to be used to generate boundary conditions for a new inner model covering the area from Christchurch Harbour to Swanage Bay with fine resolution in the areas where wave-induced currents might be significant. This inner model would have the same mesh as the COWADIS area wave model enabling direct input of the breaking wave stresses into the flow model allowing wave-induced currents to be added to the tidal simulation. Figure 1 shows the area of study and the areas covered by the inner model.

3. CALIBRATION

3.1 Regional model

The regional model was as that used in Reference 2. It had a 400m model mesh in the area around Poole Bay and covered an area from St Catherine's Point and Calshot in the east to Chesil Beach in the west. The coverage and mesh of the regional model are shown on Figure 2.

3.1.1 Boundary conditions

Boundary conditions for the regional model were generated at 10 points around the boundary from tidal harmonics. This enabled the boundary tide for any required period to be run. Tidal harmonics at Calshot and Chesil Beach were used for the boundary points at those positions. Harmonics for the offshore sites were taken from Reference 3. Linear interpolation was used to provide boundary data at boundary points in between the locations of the tidal predictions.

3.1.2 Regional model calibration

The regional model was run to simulate the period covered by the observations taken for Reference 2, 23-25 April 1990. The predicted tidal range at Poole Harbour Entrance in the Admiralty tide tables showed the range to vary between 1.4m and 2m compared to a mean spring range of 1.7m.

For the regional model water level comparison observations were available at Poole Harbour entrance and Bournemouth. Tidal levels at Calshot, Freshwater Bay, Chesil Beach and also at Poole Harbour Entrance were hindcast using tidal harmonics. The comparison of the model with the hindcast levels and the observations at Bournemouth and Poole Harbour entrance is shown in Figure 3. The location of the water level comparison points is shown on Figure 4.

As can be seen the tidal variation is very complex in the area with the tide shape, range and phasing being very different throughout the model. This phenomenon is linked to the presence of an amphidromic point (point of minimal tidal range) in Poole Bay. The model reproduces many of the features well. One slight discrepancy is the flood tide shape at Bournemouth where the model tends to rise more slowly. The proximity of the amphidromic point makes the tidal level extremely sensitive to the relative phasing and amplitude of the higher harmonics, which are very hard to quantify in offshore areas.

Figure 5 shows the comparison of the model spring tide currents with Admiralty diamonds in the area. The locations of the diamonds are shown on Figure 6. Admiralty diamonds are quoted on charts as typical tidal currents for mean spring and neap tides for the use of mariners. The comparison is generally good with the variation in the peak current and relative phasing of the flood and ebb tides correctly reproduced.

3.2 Local model

3.2.1 Model mesh

To correctly simulate the wave induced currents a finely detailed model mesh was required over the whole area in which waves might break. This included the whole near-shore region of the coastline out to the 5m CD contour and particularly over Hook Sands. The model elements were aligned with the coastline enabling a 20m grid cross-shore resolution to be combined with a mesh size of 80m parallel to the shoreline. A grid size of 50m was used over Hook Sands and in Swanage Bay. The offshore boundary was aligned to the predominate directions of flow as extracted from the regional model and a similar resolution to the regional model used there. Extra resolution over Dolphin Sand was added to ensure accurate representation of its effect on waves. Figure 7 shows the distribution of model mesh sizes in the inner model.

From this definition the TELEMAC system mesh generator produced the unstructured finite element mesh with 42300 nodes and 82100 elements. Figure 8 shows some detail of the final mesh used for the study.

3.2.2 Model Bathymetry

Two bathymetry data sets were assembled, one from the period covered by the calibration data (early 1990's) and one more recent which was used for the 'present' conditions.

The bathymetry for the calibration model was taken directly from the raw data used to set up the models for Reference 2. Within Poole Harbour, bathymetry collected as part of the Middle channel studies (Reference 4) was used. Away from the surveyed areas, Admiralty charts 2611, 2175 and 2172 were digitised to provide bathymetry data.

The bathymetry data for the 'present' condition was taken from the most recent surveys of the area by Poole Harbour Commissioners with Admiralty charts used to provide data in areas not recently surveyed. An additional data source which could be considered for future tidal modelling within the Harbour is the Environment Agency's LiDAR data which provides more intense and accurate coverage of bed levels above mean sea level (e.g. salt marsh) than the Admiralty data. The LiDAR data were not, unfortunately, available at the time of assembling the model.

The bathymetry data sets were combined and set to a common, flat datum of Ordnance Datum (Newlyn) which is 1.4m above Chart Datum at Poole Harbour entrance. The 1990 bathymetry was interpolated onto the model mesh for the calibration run and the more recent data used to produce the model for the baseline condition runs and spring-neap cycle. The baseline model bathymetry is shown on Figure 9.

3.2.3 Boundary conditions

As part of running the regional model, tidal elevation and tidal current components were extracted at 16 locations around the local model boundary. Data for tidal level was used along the western boundary and a tidal current was imposed along the eastern and offshore boundary. The offshore boundary was aligned as closely as possible to the general tidal current direction. Linear interpolation was used to provide boundary data at intermediate points.

3.2.4 Calibration

The local model was run to simulate the spring tide of 24-25 April 1990. Figure 10 shows the comparison with observations at Bournemouth and both measurements and tidal synthesis at Poole Harbour entrance. The reproduction is similar to the regional model with the double high water shape shown.

The modelled tidal currents are compared to data on Figures 11-13. Figure 11 shows the comparison with the data from Reference 2 for 24-25 April 1990. The model represents the observed current well for the peak current magnitudes and the variation in the direction (most noticeably at location BP1). The comparison with the data collected for Reference 5 at the locations SF1, SF2 and SF3 as shown on Figure 12 over Hook Sands also shows good representation of the observations by the model. In particular the direction of the currents is very varied between the 3 sites, a feature that the model represents well. This gives confidence in the simulation of the relation between the water flowing in and out of Poole Harbour and the coastal current. The peak currents are slightly under predicted as these observations were taken over a tide of larger range.

Figure 13 shows the comparison between the model and Admiralty tidal diamonds within Poole Harbour. Currents within Poole Harbour are almost entirely due to the rise and fall of the tide, in turn causing the emptying and filling of the tidal volume of the harbour. The ebb tide currents are well produced but the different shape of the simulated flood tide compared to the observations feed through to alter the shape of the flood tide currents. This effect produces a slightly lower and longer flood tide compared to the tidal diamonds. As mentioned above the tide is highly variable in the area and so the tidal currents within the harbour could also be expected to be highly sensitive to small changes in tide shape.

4. BASELINE SIMULATIONS

4.1 Introduction

Baseline simulations of the existing hydrodynamic and sediment transport within Poole Bay and Harbour were required both to provide an improved understanding of the existing regime and a basis for assessing the potential impact of proposed schemes.

Sediment transport within Poole Bay and Harbour is dependent on the effects of both tides and waves. Tidal action generates the large-scale transport due to bedload as a result of the stress generated by the tidal currents on the seabed, and suspended load as sand is carried by the water column. The effect of waves on sediment transport is two-fold: firstly, they generate a stirring effect that enhances the suspension of sand from the seabed, and secondly they generate local currents in relatively shallow areas as a result of wave breaking.

4.2 Hydrodynamic modelling

Tidal currents are strongest in the offshore areas, and also through the entrance to Poole Harbour, whereas along the coast the effects of wave breaking can generate significant wave-driven currents. The stirring effect of waves is greatest in shallow water.

The penetration of waves generated offshore into Poole Harbour is not great, and wave conditions within the Harbour are dominated by local waves generated by the wind. Wave generation within Poole Harbour has the potential for mobilising sediment, especially as a consequence of wave breaking when the wind blows over the longest fetches and in particular during windy storm periods. During the course of these studies Halcrow considered the effects of local waves on the littoral drift (which also takes into consideration the effect of wave stirring). The effect of wave stirring from locally generated waves on the sediment transport outside the surf zone was assessed by considering relatively large, infrequent wave conditions, and calculating the combined effect of spring tidal currents with these waves. It was anticipated that these locally generated waves do not normally contribute significantly to the overall sediment transport regime (outside the surf zone), and this aspect is considered in more detail in Section 4.4.3.

The baseline conditions to be assessed therefore comprise tidal conditions covering the range from spring tides to neaps, and the effects of relatively small, frequent waves that provide the stirring effect, as well as storm waves that generate currents. The modelling studies undertaken to investigate these aspect are described in the following sections.

4.2.1 Tidal modelling

The calibrated local TELEMAC flow model was used to simulate a full series of tide conditions from springs to neaps. Figure 14 shows peak spring tide flood and ebb currents respectively, and Figure 15 shows the same conditions for neap tides (note the difference in the vector scales). These two Figures, and the time-histories discussed in Chapter 3 highlight the fact that tidal currents are generally weak apart from in the south and offshore areas. Figure 16 shows time histories of water levels at various locations through the study area, for a period of eight days showing the modulation of the tide from spring to neaps. Output from TELEMAC was used as input to the sediment transport model, described in Section 4.3.

4.2.2 Wave modelling

Wave model studies were carried out to provide input to the sediment transport modelling. Wave conditions within the study area were simulated with the wave propagation model, COWADIS, a 2nd generation finite-element spectral wave model. This model is able to simulate the transformation of random directional waves due to the following processes:

- Wave shoaling

- Wave refraction due to the sea-bed
- Depth-induced breaking, bottom friction and whitecapping
- Wave growth due to wind.

Further details of COWADIS are presented in Appendix 1.

For these studies two specific sets of wave conditions were required, one representing the effects of wave stirring on the sediment transport and one representing the effects of larger storm waves which, as well as stirring the seabed, also give rise to wave-driven currents.

The COWADIS model covered the same area as the regional flow model. The stresses due to wave-breaking (which give rise to wave-driven currents) required fine resolution, and these simulations were carried out using the same model mesh and bathymetry as the TELEMAC local flow model. The wave orbital velocity fields, which represent the wave stirring, are more gently varying, and did not require such fine resolution; these fields were calculated on a coarser mesh and interpolated onto the fine grid used for the sediment transport modelling.

Offshore conditions

The offshore wave conditions were derived using the HR Wallingford HINDWAVE model. HINDWAVE uses the JONSWAP wave generation formulation which hindcasts wave conditions at a given location from wind conditions and fetch lengths measured at constant angular increments from the wave prediction point. HINDWAVE produces a set of site-specific offshore wave forecasting tables, giving wave height, period and direction for a wide range of wind speeds, directions and durations. HINDWAVE then uses these tables with the wind data to produce a synthetic wave climate at the offshore wave prediction point.

The offshore point from which the fetches were measured was located at 1°52’0”W 50°36’0”N which lies approximately 6km east of Durleston Head (see Figure 6), which is close to the local model offshore boundary.

In a previous study (Reference 6) HINDWAVE was calibrated to provide a wave climate at the location shown in Figure 6 using wind data from the anemometer at Portland Coastguard Station. This wind record covered 18 years from January 1974 to February 1992. In this study, this data was supplemented with a wave climate derived using HINDWAVE with UK Met. Office European Model wind data. This data-set covers the period October 1986 to March 2001. The offshore wave climate derived from the UKMO winds is given in Table 1a in terms of significant wave height against direction and Table 1b in terms of wave height against mean period.

Simulations of waves for stirring

Having established the offshore wave climate, specific wave conditions were required to be selected on the basis of being representative of the effects of wave stirring on the sediment transport within Poole Bay. The approach used was based on experience from previous studies (Reference 7) and research carried out by HR Wallingford (Reference 8), from which a procedure has been devised that filters the full wave climate into a reduced set of representative conditions. For information, Reference 8 is presented in Appendix 2. This paper describes how the representative wave conditions can be combined to yield a single representative stirring field, and this approach was adopted for this study.

Using the approach described in Reference 7 representative wave conditions for each coastal-propagating wave direction were calculated, and are shown in Table 2 below.

Table 2 Wave conditions used for wave stirring simulations

Direction	110°N	150°N	190°N	230°N
Significant wave height, H_s	1.14m	1.19m	1.62m	1.80m
Mean period, T_m	3.5s	3.6s	4.4s	4.5s
Frequency	12.7%	6.3%	9.8%	33.7%

COWADIS was run for each of these conditions, for the five water levels given in Table 3 below.

Table 3 Water levels at various tidal states

Tide state	Tidal level (m CD)	Tidal level (m OD)
MHWS	2.2	0.8
MHWN	1.7	0.3
MWL	1.57	0.17
MLWN	1.2	-0.2
MLWS	0.6	-0.8

Figure 17 shows example wave heights over the study area for 1.62m 4.4s waves from 190°N at mean high water spring, and Figure 18 shows corresponding wave orbital velocities for the same condition.

For each of the five water levels, the four wave orbital velocity fields (from each direction) were combined into a single orbital velocity field using the relative frequency of occurrence shown in Table 2 as weighting factors. The corresponding orbital velocity field is shown in Figure 19 for waves at mean water level.

This information is passed to the sediment transport model where, at runtime, the appropriate wave stirring field is calculated by interpolating between appropriate fields depending on the actual water level.

Simulations of storm waves

Storm wave conditions were selected from the offshore wave climate (Table 1), and are presented in Table 4 below. These waves were selected in order to identify the relative effect of infrequent (but not the most extreme) storms on the sediment transport regime, which may be important is some areas where sediment transport is only significant during storm periods. The waves shown in Table 4 have a return period of the order of 10 times per year.

Table 4 Wave conditions used for storm simulations

Direction (°N)	140	180	220
Significant wave height (m)	1.55	2.22	2.97
Mean period, T_m (s)	4.4	5.3	5.5

In order to calculate the currents due to wave breaking, COWADIS and TELEMAC were run using the PISCES framework, developed by HR Wallingford, which is a dynamic system that combines the hydrodynamic and sediment transport models into a single operational shell. The structure of PISCES is shown schematically in Figure 20. COWADIS and TELEMAC were run sequentially throughout a spring tidal cycle with updates between the models every 0.5 hours. By this means the true water level (including wave setup) is passed to the COWADIS model, ensuring that wave breaking occurs at the correct location, and the stresses due to wave breaking are passed to the TELEMAC model in order that the currents due to breaking are simulated. The wave orbital velocity (stirring) field is also calculated and stored.

PISCES was run for the three storm wave conditions shown in Table 4 under spring tide conditions. Figure 21 shows example wave-driven currents superimposed on tidal currents at times of spring tide flood and ebb in the vicinity of Hook Sands due to waves from 140N as a means of demonstrating the effects of wave breaking on the current field. Note the change in currents due to wave breaking over Hook Sands and along the coast.

4.3 Sediment transport modelling

Sediment transport simulations were performed with the HR Wallingford model, SANDFLOW. SANDFLOW is a non-cohesive sediment (sand) transport model that simulates the advection and dispersion of suspended sediment due to the effects of both currents and waves. The sediment transport algorithm is based on a formula developed by Soulsby (Reference 9). Further details of SANDFLOW are presented in Appendix 1.

SANDFLOW was used to simulate the sediment transport patterns throughout Poole Bay and Harbour due to tidal conditions alone, and including the effects of wave stirring and storm waves. The resulting sediment transport patterns include only the *potential* for sediment transport, since the information on the actual availability of sediment is not incorporated.

The sediment grain size varies over the study area, especially at the entrance to Poole Harbour where the strong currents are able to sort the material, removing the finer fractions. Although SANDFLOW is capable of simulating transport of mixed sediment grain sizes, the processes associated with the transport of mixed sediments is not well understood. Therefore, for the purposes of this study the more traditional approach of specification of a representative median grain diameter was used, and a value of 0.25mm was defined which is consistent with previous information derived from grab samples (Reference 6). By adopting this approach there is a requirement to interpret the model predictions carefully to account for areas where sediment of this grain diameter does not prevail (for example in the entrance to Poole Harbour). In these cases sensitivity tests were performed to investigate the potential transport of both finer and coarser sediment.

Output from SANDFLOW comprises the net residual potential sediment transport rate over the period simulated, and the corresponding patterns of erosion and deposition. Due to the non-linear nature of sediment transport (which means that increases in currents give rise to disproportionately higher sediment transport rates) the sediment flux patterns are presented on a logarithmic scale so that the full range of transport rates (especially those at the lower end) can be visualised. By way of example, Figure A1 in Appendix 3 shows the same information as that presented in Figure 34 using the more traditional vector plotting where the length of the vector is proportional to the magnitude of the sediment flux, where it is more difficult to discern the transport rates at the lower end of the transport range.

Simulations were performed for a full period of spring-neap tides, with and without the effect of wave stirring (using waves shown in Table 2), and for storm waves (shown in Table 4) during spring tide conditions.

Figure 22 shows the distribution of the sediment flux throughout the study area for the period of spring-neap tides, and the corresponding pattern of erosion and deposition is presented in Figure 23. The effects of wave stirring on the potential sediment transport over the same period is presented in Figures 24 and 25.

The potential sediment transport rate due to tidal currents only, over a spring tide is shown in Figure 26, and the corresponding patterns of erosion and deposition are shown in Figure 27.

Potential sediment transport vectors and patterns of erosion and deposition due to the three storm waves during spring tides are presented in Figures 28 to 33.

4.4 Analysis

Figures 22 and 24 indicate that for much of the coastal zone of the study area, the potential sediment transport rates due to tides and wave stirring are low. Areas of high transport rate are limited to the main headlands at Handfast Point, Peveril Point to Durleston Head, and Hengistbury Head, as well as the entrance to Poole Harbour. The deposition predicted in the navigation channel within Poole Harbour (particularly on the main bend immediately to the east of Brownsea Island) and in the southern part of the Swash Channel (see Figure 25) is consistent with information provided by Poole Harbour Commissioners (pers comm), and gives confidence in the model predictions.

In the deeper areas the general potential sediment transport trend is a net south-westerly drift over much of the area (Figures 22 and 24), although on spring tides there is a net NE transport in the offshore areas (Figure 26). The exception to this pattern occurs at Hengistbury Head, where the net transport is to the east. A consequence of this pattern is that there is a drift divide approximately 5km west of Hengistbury Head, although this is a weak feature and does not correlate with any significant bed features: the location of this divide is considered to be a transient feature.

Wave stirring has the effect of enhancing the potential sediment transport rate, and this effect is sufficient to mobilise the sediment on the Bournemouth coast (Figure 24). Figures 28 to 33 show the potential sediment transport rates and corresponding patterns of erosion and deposition for the storm waves during spring tide conditions. The effects of the storm waves are to generate significant wave-driven currents and sediment transport on the coast, both along the main Bournemouth frontage and in the larger bays (Studland Bay and Swanage Bay). The storm waves also enhance the transport outside the surf zone due to wave stirring.

In order to examine the potential sediment transport patterns in detail, smaller areas of the model were re-plotted and further analysed. The findings are discussed in the following sections.

4.4.1 Durleston Head to Poole Harbour

A key consideration in this region is the sediment regime on the coast and in particular how sand in the two main Bays (Studland Bay and Swanage Bay) is exchanged with that further offshore.

As described earlier, the potential sediment transport rate off the main headlands is very high, and in a net southerly direction. Within the Bays the transport rates are much lower. Figure 34 shows the transport rate over a spring-neap period, and indicates that tidal currents alone are insufficient to mobilise significant amounts of sediment. Wave stirring has the effect of mobilising sediment in the north of Swanage Bay and Studland Bay (Figure 35).

However, the effect of storm waves, shown in Figures 36 to 38, is to transport sediment more effectively. In Swanage Bay the transport on the coast is significantly increased in the northern part of the Bay and Figures 29, 31 and 33 highlights the corresponding erosion in the central section of the Bay and accretion further north. This accretion is likely to be temporary, as the model results indicate that this is an energetic region: wave stirring and strong currents are likely to remove it efficiently. The resulting picture is one of a leakage of sediment out of Swanage Bay through the north.

In Studland Bay there is an indication of a circulation cell in the southern part (Figures 36 and 37) with another in the northern part, with a corresponding apparent source of sediment from the end of the Swash Channel.

4.4.2 Poole Harbour entrance

At Poole Harbour entrance the potential sediment transport patterns are clearly dominated by the tidal flows (Figure 39). As stated in Section 4.3, the sediment grain size defined for the sediment transport studies is not representative of the grain size in the entrance to Poole Harbour, and accordingly, the magnitude of the sediment flux predictions and associated morphological activity requires careful

interpretation. Figure 39 indicates strong transport vectors extending both NW and SE from the entrance to the Harbour around the area of Chapman's Peak, and this zone of rapid divergence (and therefore erosion of this size sediment) is consistent with the regime in this region in that coarser material prevails on the seabed. Further away from the immediate entrance the simulated sediment size of 0.25mm diameter is representative of the seabed type (Reference 6) and the sediment transport patterns can be more reliably interpreted.

Throughout the Swash Channel the net sediment transport direction is toward the south, joining the prevailing southerly transport beyond Swash Channel as part of the overall sediment drift pattern as described in Section 4.4.

Between Swash Channel and the coast to the west, tidal currents are insufficient to transport sediment of the grain size simulated. Similarly, to the NE of Hook Sands the tidal currents are also weak and unable to transport significant quantities of sediment. Outside the Harbour therefore, the effect of the tidal filling and emptying of Poole Harbour gives rise to very high potential transport rates in the main Swash Channel and also (to a lesser degree) over Hook Sands. Over the northern part of Hook Sands in the East Looe Channel tidal currents are able to transport sediment, although at a lower rate than in the Swash Channel.

Wave stirring has the effect of enhancing the transport rates over Hook Sands and along the Poole coast (Figure 40), and also in the region to the west of Swash Channel. Hook Sands acts as a significant wave break so that the small wave heights within the Swash Channel have little stirring effect and therefore do not contribute significantly to the sediment transport.

Storm waves (Figures 41 to 43) have a more pronounced effect, both on the magnitude of the transport and direction both outside and immediately within Poole Harbour. Under these conditions the storm waves generate an additional current due to wave breaking, and this process, combined with the stirring effect of these larger waves gives rise to sediment transport over a wider area. Under storm conditions, sediment transport takes place over much of the entrance to the Harbour including the region to the west of Swash Channel and also on the eastern side of Hook Sands. Over Hook Sands the transport rates are high, and the direction is generally to the NW as a result of the wave-generated currents due to breaking, and this transport direction is in contrast to that in the Swash Channel. Inevitably, the storm waves give rise to a flux of sediment off Hook Sands and into the Swash Channel which is then transported south. As the power of the tidal currents diminished in the southern part of Swash Channel, the sediment transporting capacity reduced and the sediment accumulates: this process explains the mechanism that gives rise to infill and the requirement to maintain the southern end of Swash Channel.

Wave breaking along the coast of the Poole frontage (and further east) also generates an additional littoral current which (together with the wave stirring) gives rise to littoral drift.

As stated at the start of this Section, the sediment grain size defined over the entire model area was not representative of the sediment in the entrance to Poole Harbour, and that the corresponding model predictions should be treated with caution. In order to investigate this aspect in more detail, the SANDFLOW model was re-run for spring tide conditions using coarser 2mm sediment grain size which is more consistent with the sediment in the area around Chapman's Peak (Reference 6).

Figure 44 shows the predicted change in bed deposits indicating erosion and deposition in Poole Harbour entrance for the 0.25mm grain size and 1mm grain size sediment. Clearly, the 0.25mm sediment is more mobile than the 2mm sediment. Furthermore, although both grains indicate erosion of sediment from Chapman's peak, the extent and magnitude of erosion is greater for the finer sediment, and in fact accretion of the 2mm sediment also occurs. It is likely that sediment coarser than 2mm is also present at Chapman's Peak and from the results of this sensitivity test would explain why this material is able to remain at this site, although the source of this size material is not evident.

4.4.3 Poole Harbour

The pattern of sediment distribution within Poole Harbour was described in Reference 7 and reflects the varying wave/current environment, as follows.

Generally the upstream gradient of declining tidal energy away from the entrance into the sheltered parts of the harbour, is reflected in decreasing sediment size, increasing incidence of net accretion as opposed to erosion, and increasing incidence of unconsolidated as opposed to consolidated beds. Similarly across the channel cross-sections there is a decrease in sediment coarseness and consolidation towards the channel margin, though this is modified at channel bends. Thus within the Harbour entrance, the most current-scoured section of Poole Harbour, the channel is more than 15m deep and sediments range from medium and coarse sand at the channel peripheries, to stones, boulders and consolidated clays at the channel centre. At the other extreme, typical upstream profiles, for example in upper Holes Bay, may hardly bottom out below Chart Datum level and the profile may be entirely of soft mud.

Superimposed on this pattern of tidal-induced sorting are the effects of waves on the northern and north-eastern shores which are exposed to the longest fetches. Sand dominates in these areas, occasionally with a narrow shingle or shell upper beach. Large cobbles and boulders are found at several locations derived from erosion of the seawalls and breakwaters built up to 120 years ago. In sheltered parts of the bays muds prevail.

Given the complex nature of the sedimentological characteristics of Poole Harbour in order to assess the corresponding sediment transport regime simplifications have to be made including interpreting the *potential* for sediment transport on the assumption that sediment of the grain size simulated actually exists. The results presented in the section, however, are considered to be indicative of the sediment transport pathways, although the magnitude of the transport will depend strongly on the characteristics of the particular sediment in question.

Figure 45 shows the net pattern of potential sediment transport within the Harbour over a spring-neap period, and indicates that the areas of strongest transport rates are the deep channels in the east of the Harbour: elsewhere the currents are low, and it is in these areas that finer sediments predominate.

Figure 46 shows the net sediment transport pattern over a spring-neap cycle including the effects of waves that have propagated into the Harbour from offshore. The relatively low penetration of wave energy has little effect on the patterns of sediment transport due to tides. Similarly, penetration of storm waves within the Harbour is also restricted and the simulations with storm waves also showed little effect on the sediment transport.

Wave generation within Poole Harbour has the potential for mobilising sediment, especially as a consequence of wave breaking when the wind blows over the longest fetches and in particular during windy storm periods. During the course of these studies Halcrow considered the effects of local waves on the littoral drift (which also takes into consideration the effect of wave stirring). The effect of wave stirring from locally generated waves on the sediment transport, was assessed by considering relatively large, infrequent wave conditions, and calculating the combined effect of spring tidal currents with these waves. Figure 47 shows the net tidal magnitude of the sediment transport rate through two sections within Poole Harbour for the case with spring tides with and without local wave stirring. In this case the wave height was determined from the results of a previous study (Reference 6) and set to 0.44m and the wave period was set to 3s which is appropriate for typical wind speeds and fetch lengths within the Harbour. Waves of this magnitude (and larger) occur approximately 10% of the time. Note that for the purposes of this assessment the sheltering effect of islands was not considered and it was assumed that the wave conditions would persist for the entire tidal period (this is a conservative estimate since the fetch length would reduce substantially at low water). Figure 47 shows that the effect of locally generated waves is to increase the magnitude of the sediment transport rate by approximately 10% in the intertidal and shallow

subtidal. On this basis it is concluded that, in so far as a coastal strategy study is concerned, the effects of wave stirring on the sediment transport processes is relatively minor.

4.4.4 Bournemouth to Hengistbury Head

Potential sediment transport on the coast between Bournemouth and Hengistbury Head is insignificant under tidal conditions alone (Figure 48). Wave stirring mobilises the sediment in the nearshore (Figure 49), and the overall transport rate along the coast is from west to east, although at the top of the beach there is an indication from the model that the drift is in the opposite direction (east to west). In any event, the littoral drift will be strongly dependent on the effects of wave breaking which are assessed separately by Halcrow taking into consideration all waves in the wave climate. The effects of discrete storm waves were simulated with the PISCES model and are described below.

Storm waves are far more effective at transporting the sediment (Figures 50 to 52). Wave from the SE and S (Figures 50 and 51) produce transport from Hengistbury Head eastwards as far as Bournemouth, with the larger southerly waves giving rise to higher transport rates. Waves from the SW produce transport from west to east along much of the frontage (Figure 52), although at Hengistbury Head refraction of the waves means that they arrive at the coast shore-normal, and the transport direction is more erratic. Note that over Christchurch Ledge the transport rate is persistently from west to east.

5. DREDGED SIMULATIONS

5.1 Dredging of Swash Channel to the originally specified dredged profile

The Swash channel is presently not maintained at the originally specified dredged profile which comprises a base width of 100m at 6.8mCD (7.0mCD in the outer part) and side slopes of 1:30.

Halcrow compared the existing bathymetry with the original channel plan and identified two areas on the channel slope on the east side where significant volumes of material had accumulated (relative to the original profile). This information was used to define two areas where the original profile was re-instated, including an allowance for an over-dredge of 300mm. Figure 53 shows the existing bathymetry in the region, and Figure 54 shows the change in bathymetry following the dredging, indicating that bed levels are lowered by up to 2-3m, especially at the southern tip of Hook Sands.

Sand transport patterns were simulated for spring tides under calm conditions and including the effects of storm waves from 140^{o}N as shown in Table 4. The modelling approach was based on simulation of specific tidal and wave conditions for the pre-and post-dredged scenarios as a means of determining the impact of the scheme on the present conditions.

Spring tide peak flood and ebb currents are presented in Figures 55 and 56 for the existing scenario and following dredging, and Figure 57 shows the difference in peak speed for these two stages of the tide. The dredging only marginally affects the strength and direction of the currents.

Figure 58 shows the net tidal sand transport patterns under spring tides under existing conditions and following the dredging, and Figure 59 shows the corresponding pattern of net erosion/deposition under existing conditions and the change in this field following the dredging. In the absence of waves significant bed level changes are restricted to the entrance to Poole Harbour. The predicted patterns of potential erosion and deposition occur in narrow bands rather than larger discrete areas, and this response is indicative of high transport rates through this region and suggest that the model is attempting to smooth out the small fluctuations in the seabed resolved in the model. Only relatively small scale morphological activity takes place. Predictions of larger areas of erosion and deposition should be treated with caution and it is noted that the area of Chapman's Peak and the route of the Bramble Ferry show significant erosion and deposition respectively. Chapman's Peak is a complex feature with a large distribution of sediment grain sizes, particularly coarser material and it is likely that the specified median grain diameter is not representative of conditions at this specific location. The pattern of erosion and deposition may also change with the tidal conditions, so that simple extrapolation of the model predictions to the longer term may be misleading. However, the modelling approach does allow the *relative* change in the potential sediment transport rates due to the scheme to be determined. It can be seen that the dredging only affects the potential sediment transport rates locally, and that there are no discernible effects outside the vicinity of the deepened areas. The deepening has only a marginal effect on the pattern of erosion and deposition and this is restricted to the lee of Hook Sands.

Figures 60 and 61 show the net tidal sand transport patterns under spring tides including storm waves from 140^{o}N, and the corresponding patterns of erosion and deposition. Under these storm wave conditions the area influenced by the dredging is larger, though still limited to the vicinity of the entrance to Poole Harbour.

The conclusions from this analysis are that the relatively small amount of dredging, on the eastern side of the Swash channel has little significant effect on the potential sediment transport at the entrance to Poole Harbour.

5.2 Deeper dredging of Swash Channel

The model simulations described in Section 5.1 were repeated to study the impact of a deeper dredge of Swash Channel. In this case the main channel was deepened 2m below its existing permitted profile to 8.8mCD (10.2mODN), maintaining the same channel width, and the side slopes were set at 1:15 for 60m within the base channel, flattening to 1:30 thereafter. Figure 62 shows the existing bathymetry in the region, together with the limits of permitted maintenance dredging of the Swash Channel, and Figure 63 shows the change in bathymetry following the dredging, indicating that bed levels are lowered typically by 1.5m to 2m, but in some areas, notably on the east side of the channel adjacent to Hook Sands the depth change is as much as 4.5m. In the numerical model this depth change is equivalent to a capital dredge volume of 1.14Mm^3.

Sand transport patterns were simulated for spring tides under calm conditions and including the effects of storm waves from 140^{o}N as shown in Table 4. The modelling approach was based on simulation of specific tidal and wave conditions for the pre-and post-dredged scenarios as a means of determining the impact of the scheme on the present conditions.

Spring tide peak flood and ebb currents are presented in Figures 64 and 65 for the existing scenario and following dredging, and Figure 66 shows the difference in peak speed for these two stages of the tide. These figures indicate that the dredging has a significant effect on the tidal currents in the region. The overall effect is generally one of an increase in the tidal discharge in the main Swash Channel which leads to a reduction in the current speed on either side of the channel over the banks. On the flooding tide there is a small increase in the current speed in the southern half of Swash Channel, whereas further inland in the channel the effect is mixed, with increases in some areas of the channel and decreases in others. A decrease in speed is possible despite the increase in the flux of water due to the increased water depth. There is also a marked effect on the East Looe Channel adjacent to the Sandbanks frontage, and generally over the northern part of Hook Sands. On the ebbing tide the general effect of the dredging is one of a reduction in current speed, due to an increase in the volume of ebbing water in the main (deepened) channel and corresponding reduction of flow over the banks.

Figure 67 shows the net tidal sand transport patterns under spring tides under existing conditions and following the dredging, and Figure 68 shows the corresponding pattern of net erosion/deposition under existing conditions and the change in this field following the dredging. Even under tidal conditions alone, the dredging has an effect on the sediment fluxes in the area, and corresponding patterns of accretion and erosion. In general the deepened part of the channel are subject to infill, although the increased currents appear to promote deepening of the northern end of the channel. On the sides of the channel the changes to the tidal currents cause a general redistribution of the bed, shown as sequential patterns of erosion and deposition. The model also predicts a small change in the area of Chapman's Peak in the entrance to Poole Harbour, and although the bed in this area comprises coarser material to that modelled, it can still be concluded that the dredging would alter the behaviour of the morphology in this region. No impacts outside the area shown were predicted.

Figures 69 and 70 show the net tidal sand transport patterns under spring tides including storm waves from 140^{o}N, and the corresponding patterns of erosion and deposition. Under these storm wave conditions the area influenced by the dredging is larger than that due to tides alone. The net landward sediment flux over Hook Sands is reduced as a consequence of the reduced currents over this bank, and the net ebb fluxes out through the Swash Channel are generally increased. Figure 70 indicates that under existing conditions, these storm conditions give rise to significant changes in the distribution of sediment on the seabed, most notably with erosion on the top of Hook Sands and deposition in its lee. The impact of the dredging shown in the lower half of Figure 70 is not confined to the channel. Changes in the wave propagation give rise to an impact on the coast at Studland Bay, and also on the bank along the edge of the present training wall. There is a general tendency for infill of the deepened parts of Swash Channel, particularly at the northern end, and the changes in the pattern of deposits over Hook Sands would suggest that the configuration of the banks would be affected. The changes around East Looe Channel would also indicate that this area

would be affected, and given the reduction in current speed, especially on the flooding tide it is anticipated that this area would shoal: in effect the Swash Channel would take a greater proportion of the tidal flow at the expense of the East Looe Channel and as a consequence it is anticipated that the East Looe Channel would suffer infill. This tendency for deposition in East Looe Channel is indicated in the lower part of Figure 70. No impacts outside the area shown were predicted.

The conclusions from this analysis are that the large amount of capital dredging simulated in this study would have a significant effect on the potential sediment transport at the entrance to Poole Harbour. Should this option be considered in the future there would also be a requirement to consider additional impacts including those arising from the dredging and disposal process.

6. CONCLUSIONS

Extensive numerical modelling studies were undertaken to simulate the potential sediment transport processes within Poole Bay and Harbour, as part of an overall Coastal Defence Strategy Study carried out by Halcrow.

Following the setting up and calibration of wave and current hydrodynamic models and a sediment transport model, the HR Wallingford coastal area modelling framework, PISCES was used to simulate potential sediment transport pathways due to tides, with and without the effect of wave stirring, and also due to storm conditions during spring tides.

Detailed resolution of the entrance to Poole Harbour, and the frontage between Poole and Hengistbury Head was used to establish a comprehensive assessment of the coastal sediment regime. Further offshore, the potential sediment transport pathways in Poole Bay were established, with a particular emphasis on the long term drift patterns throughout the area. As part of this process, a full spring-neap cycle of the potential sediment transport was simulated.

Results of the numerical model studies were presented to the Poole Bay and Harbour Coastal Group at a series of meetings over the course of the study period. This information has been used by the Poole Bay and Harbour Coastal Group to devise a future coastal defence strategy for the area.

In regard to the sourcing of material for beach nourishment, the effects of placement of material along the coast of the area studied was examined, with particular emphasis on the area of Swanage Bay. Detailed analysis of the littoral drift patterns along the entire coast of the study area were processed to aid this investigation.

The coastal area model was also used to simulate the impact of two dredging scenarios of Swash Channel: one a minor maintenance dredging campaign of localised hot spots, and the other a larger capital dredging campaign of the entire Swash Channel.

7. REFERENCES

1. Sandbanks coast protection scheme. HR Wallingford Report EX 3083, December 1994

2. Poole Bay. Phase II – Hydraulic study. HR Wallingford Report EX 2228, February 1991

3. Baptista, Westerink, Turner Tides in the English Channel and Southern North Sea. A frequency domain analysis using model TEA-NL. Advances in Water Resources, Vol 12, No 4. December 1989

4. Poole Harbour Commissioners. Middle Channel Study. HR Wallingford Report EX 2160. July 1990

5. Poole Bay. Sediment study. HR Wallingford Report EX 2153, June 1990

6. Poole Borough Coastal Strategy Study. HR Wallingford Report EX2881, February 1995

7. Poole Bay. Phase II Hydraulic Study. HR Wallingford Report EX2228, February 1991

8. Chesher TJ, and Miles, GV (1992). The concept of a single representative wave for use in numerical models of long term sediment transport predictions. In Hydraulic and Environmental Modelling: Coastal Waters. Proceedings of the Second International Conference on Hydraulic and Environmental Modelling of Coastal, Estuarine and River Waters, Volume 1. Falconer, Chandler-Wilde and Liu (Eds). Ashgate

9. Soulsby RL (1997). Dynamics of Marine Sands. Thomas Telford Publications

Tables

HR Wallingford

Table 1a Offshore wave climate for significant wave height against wave direction. Data in parts per hundred thousand

H1 To H2		P(H>H1)	Wave direction in degrees North																	
			-10	10	30	50	70	90	110	130	150	170	190	210	230	250	270	290	310	330
			10	30	50	70	90	110	130	150	170	190	210	230	250	270	290	310	330	350
0.00	0.20	0.99197	362	434	478	504	467	487	419	393	440	383	371	397	395	398	810	636	876	333
0.20	0.40	0.90616	1920	1286	1001	1036	1360	1169	406	149	135	127	175	788	2413	1741	1106	951	794	1131
0.40	0.60	0.72928	572	999	1010	898	1062	186	560	880	854	856	1109	1108	729	1375	474	264	234	308
0.60	0.80	0.59447	351	307	333	544	1064	1758	539	338	304	341	555	946	2621	1076	456	214	203	260
0.80	1.00	0.47237	187	262	212	425	563	940	1127	276	151	157	262	1628	3229	566	81	24	18	31
1.00	1.20	0.37098	27	102	180	282	633	1565	299	529	658	755	1238	1498	993	235	18	5	7	2
1.20	1.40	0.28072	17	25	32	109	259	246	555	114	113	109	234	1447	2249	127	2	0	2	0
1.40	1.60	0.22432	0	1	23	20	89	688	297	323	368	522	1082	1567	2023	44	1	0	1	0
1.60	1.80	0.15383	0	0	3	5	51	214	242	22	0	0	33	439	367	25	2	6	0	0
1.80	2.00	0.13974	0	0	2	0	7	137	130	84	98	147	386	1917	1108	9	0	0	0	0
2.00	2.20	0.09951	0	0	0	0	16	138	27	116	144	233	625	545	462	4	0	0	0	0
2.20	2.40	0.07643	0	0	0	0	7	185	103	27	60	119	290	703	400	6	0	0	0	0
2.40	2.60	0.05743	0	0	0	0	0	59	93	33	51	121	335	827	177	0	0	0	0	0
2.60	2.80	0.04046	0	0	0	0	0	9	70	13	2	2	167	208	17	0	0	0	0	0
2.80	3.00	0.03559	0	0	0	0	0	20	25	0	27	59	6	431	382	0	0	0	0	0
3.00	3.20	0.02608	0	0	0	0	0	3	28	20	31	50	258	577	10	0	0	0	0	0
3.20	3.40	0.01631	0	0	0	0	0	5	13	3	15	29	84	321	179	0	0	0	0	0
3.40	3.60	0.00982	0	0	0	0	0	0	3	10	9	4	1	240	31	0	0	0	0	0
3.60	3.80	0.00683	0	0	0	0	0	0	0	0	0	10	136	90	47	0	0	0	0	0
3.80	4.00	0.00399	0	0	0	0	0	0	0	0	2	11	0	71	27	0	0	0	0	0
4.00	4.20	0.00288	0	0	0	0	0	0	0	0	0	2	10	106	17	0	0	0	0	0
4.20	4.40	0.00153	0	0	0	0	0	0	0	0	0	6	4	49	4	0	0	0	0	0
4.40	4.60	0.00090	0	0	0	0	0	0	0	0	0	0	4	2	0	0	0	0	0	0
4.60	4.80	0.00084	0	0	0	0	0	0	0	0	0	0	0	28	6	0	0	0	0	0
4.80	5.00	0.00050	0	0	0	0	0	0	0	0	0	0	0	9	7	0	0	0	0	0
5.00	5.20	0.00033	0	0	0	0	0	0	0	0	0	0	0	0	2	0	0	0	0	0
5.20	5.40	0.00031	0	0	0	0	0	0	0	0	0	0	0	16	5	0	0	0	0	0
5.40	5.60	0.00010	0	0	0	0	0	0	0	0	0	0	0	0	2	0	0	0	0	0
5.60	5.80	0.00008	0	0	0	0	0	0	0	0	0	0	0	0	0	0	0	0	0	0
5.80	6.00	0.00008	0	0	0	0	0	0	0	0	0	0	0	1	4	0	0	0	0	0
6.00	6.20	0.00003	0	0	0	0	0	0	0	0	0	0	0	0	0	0	0	0	0	0
6.20	6.40	0.00003	0	0	0	0	0	0	0	0	0	0	0	0	1	0	0	0	0	0
6.40	6.60	0.00002	0	0	0	0	0	0	0	0	0	0	0	0	2	0	0	0	0	0
Parts per thousand for each direction			34	34	33	38	56	78	49	33	35	40	74	160	179	56	29	21	21	21

Table 1b Offshore wave climate for significant wave height against mean wave period. Data in parts per hundred thousand

H1 To H2		P(H>H1)	Mean wave period in seconds (Tm)									
			0	1	2	3	4	5	6	7	8	9
			1	2	3	4	5	6	7	8	9	10
0	0.2	0.99197	264	8316	0	0	0	0	0	0	0	0
0.2	0.4	0.90616	0	6315	11374	0	0	0	0	0	0	0
0.4	0.6	0.72928	0	5	13476	0	0	0	0	0	0	0
0.6	0.8	0.59447	0	0	9886	2324	0	0	0	0	0	0
0.8	1	0.47237	0	0	1027	9112	0	0	0	0	0	0
1	1.2	0.37098	0	0	3	9023	0	0	0	0	0	0
1.2	1.4	0.28072	0	0	0	3001	2639	0	0	0	0	0
1.4	1.6	0.22432	0	0	0	647	6403	0	0	0	0	0
1.6	1.8	0.15383	0	0	0	17	1391	0	0	0	0	0
1.8	2	0.13974	0	0	0	2	4021	0	0	0	0	0
2	2.2	0.09951	0	0	0	0	2071	238	0	0	0	0
2.2	2.4	0.07643	0	0	0	0	360	1540	0	0	0	0
2.4	2.6	0.05743	0	0	0	0	7	1689	0	0	0	0
2.6	2.8	0.04046	0	0	0	0	2	486	0	0	0	0
2.8	3	0.03559	0	0	0	0	0	950	0	0	0	0
3	3.2	0.02608	0	0	0	0	0	969	8	0	0	0
3.2	3.4	0.01631	0	0	0	0	0	167	482	0	0	0
3.4	3.6	0.00982	0	0	0	0	0	7	292	0	0	0
3.6	3.8	0.00683	0	0	0	0	0	1	283	0	0	0
3.8	4	0.00399	0	0	0	0	0	0	111	0	0	0
4	4.2	0.00288	0	0	0	0	0	0	135	0	0	0
4.2	4.4	0.00153	0	0	0	0	0	0	63	0	0	0
4.4	4.6	0.0009	0	0	0	0	0	0	6	0	0	0
4.6	4.8	0.00084	0	0	0	0	0	0	13	21	0	0
4.8	5	0.0005	0	0	0	0	0	0	0	17	0	0
5	5.2	0.00033	0	0	0	0	0	0	0	2	0	0
5.2	5.4	0.00031	0	0	0	0	0	0	0	20	0	0
5.4	5.6	0.0001	0	0	0	0	0	0	0	2	0	0
5.6	5.8	0.00008	0	0	0	0	0	0	0	0	0	0
5.8	6	0.00008	0	0	0	0	0	0	0	3	2	0
6	6.2	0.00003	0	0	0	0	0	0	0	0	0	0
6.2	6.4	0.00003	0	0	0	0	0	0	0	0	1	0
6.4	6.6	0.00002	0	0	0	0	0	0	0	0	2	0
Parts per thousand for each period			3	146	358	241	169	60	14	1	0	0

Table 2 Wave conditions used for wave stirring simulations

Direction	110°N	150°N	190°N	230°N
Significant wave height, H_s	1.14m	1.19m	1.62m	1.80m
Mean period, T_m	3.5s	3.6s	4.4s	4.5s
Frequency	12.7%	6.3%	9.8%	33.7%

Table 3 Water levels at various tidal states

Tide state	**Tidal level (m CD)**	**Tidal level (m OD)**
MHWS	2.2	0.8
MHWN	1.7	0.3
MWL	1.57	0.17
MLWN	1.2	-0.2
MLWS	0.6	-0.8

Table 4 Wave conditions used for storm simulations

Direction (°N)	140	180	220
Significant wave height (m)	1.55	2.22	2.97
Mean period, T_m (s)	4.4	5.3	5.5

Figures

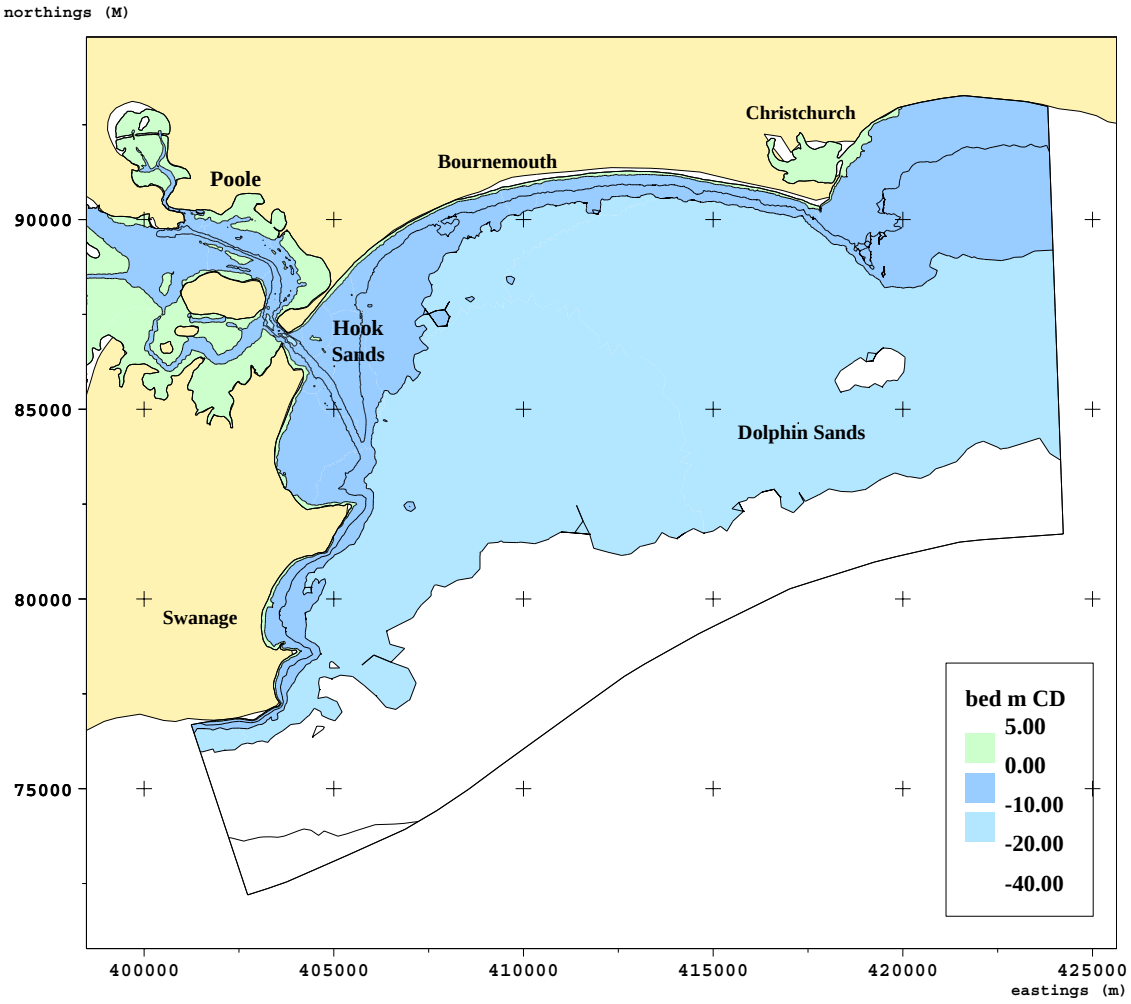

Figure 1 Area of study

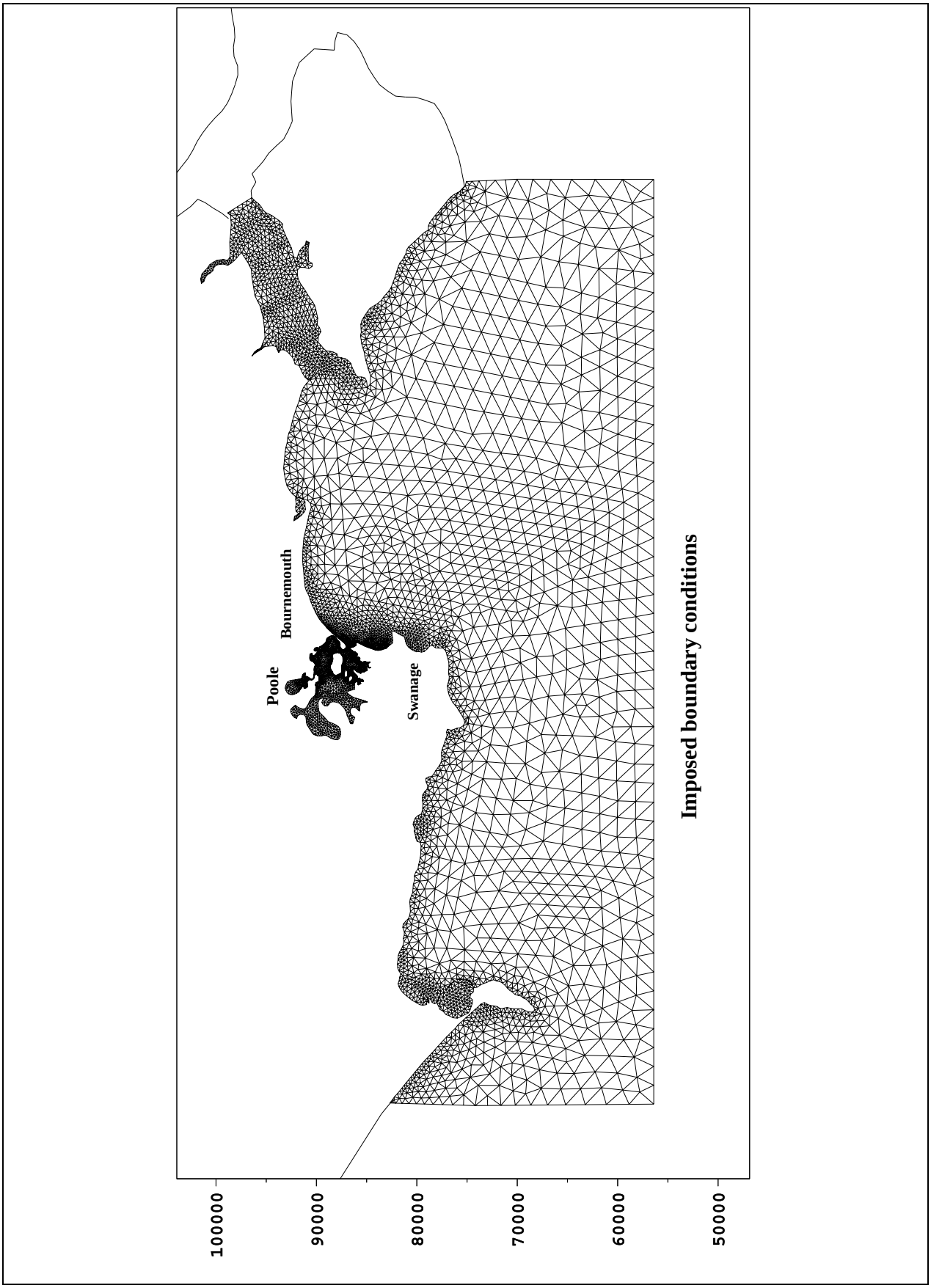

Figure 2 Regional model area and model grid

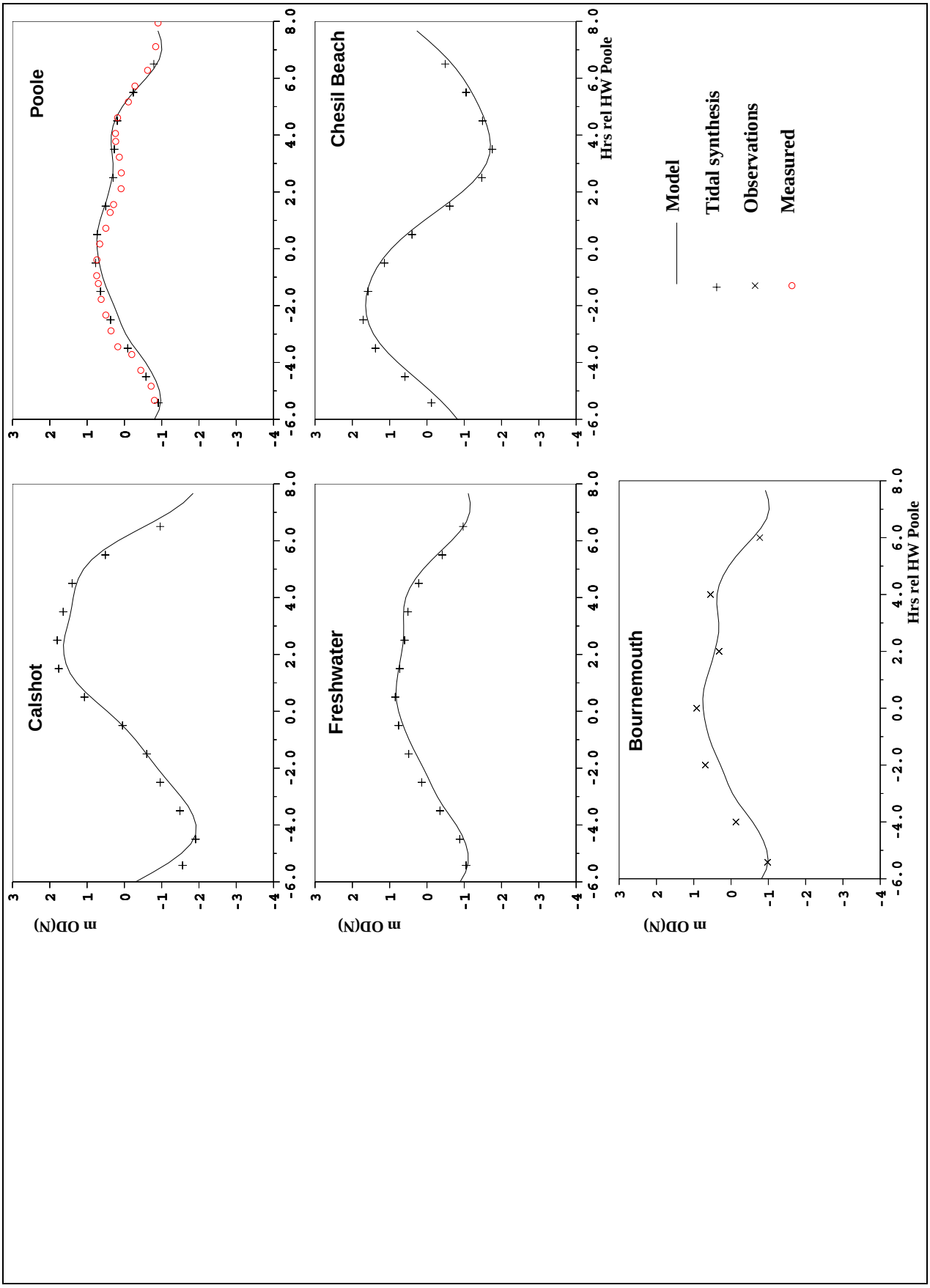

Figure 3 Comparison of regional model simulated tidal elevations with data

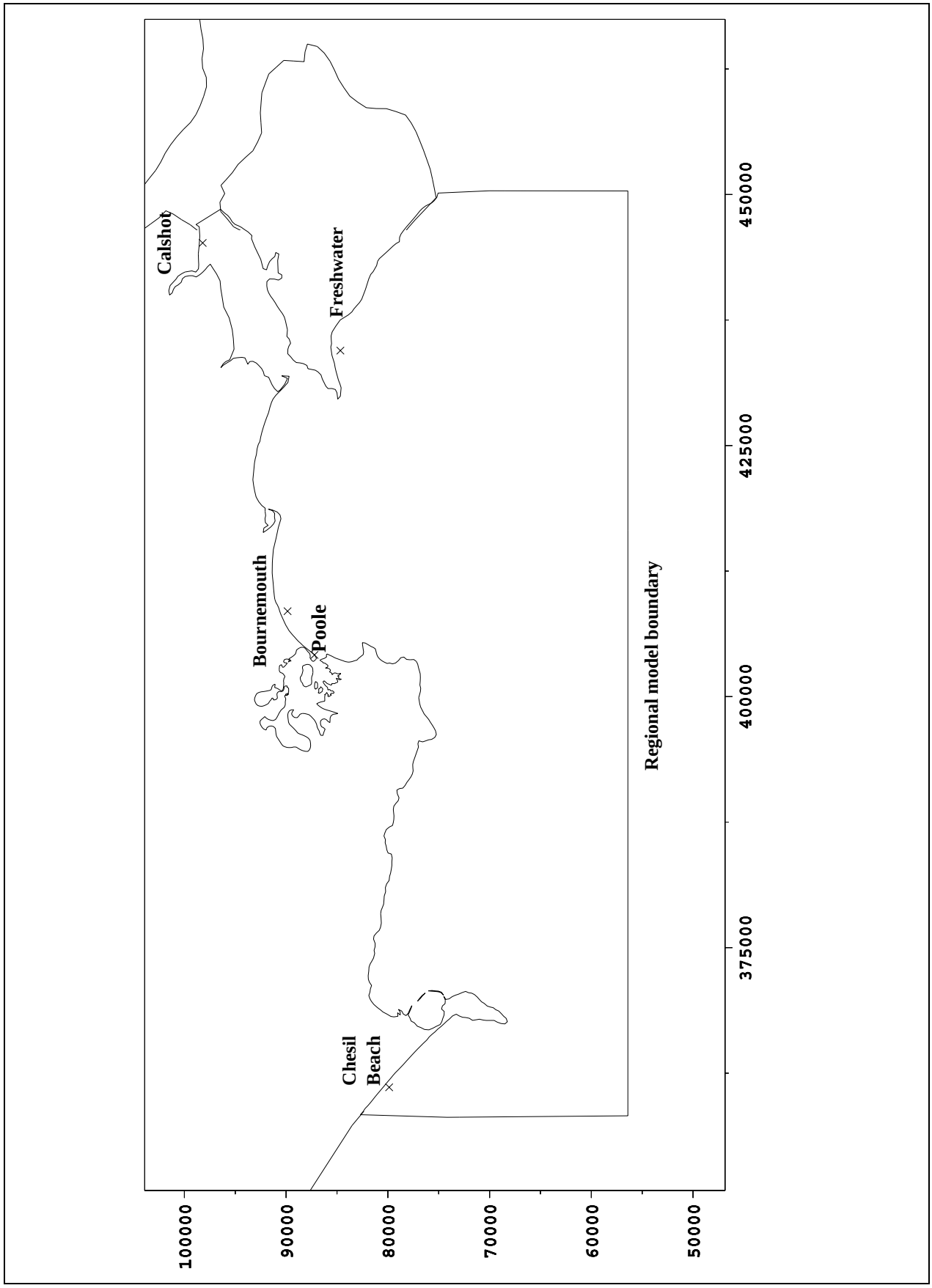

Figure 4 Location of water level comparison points

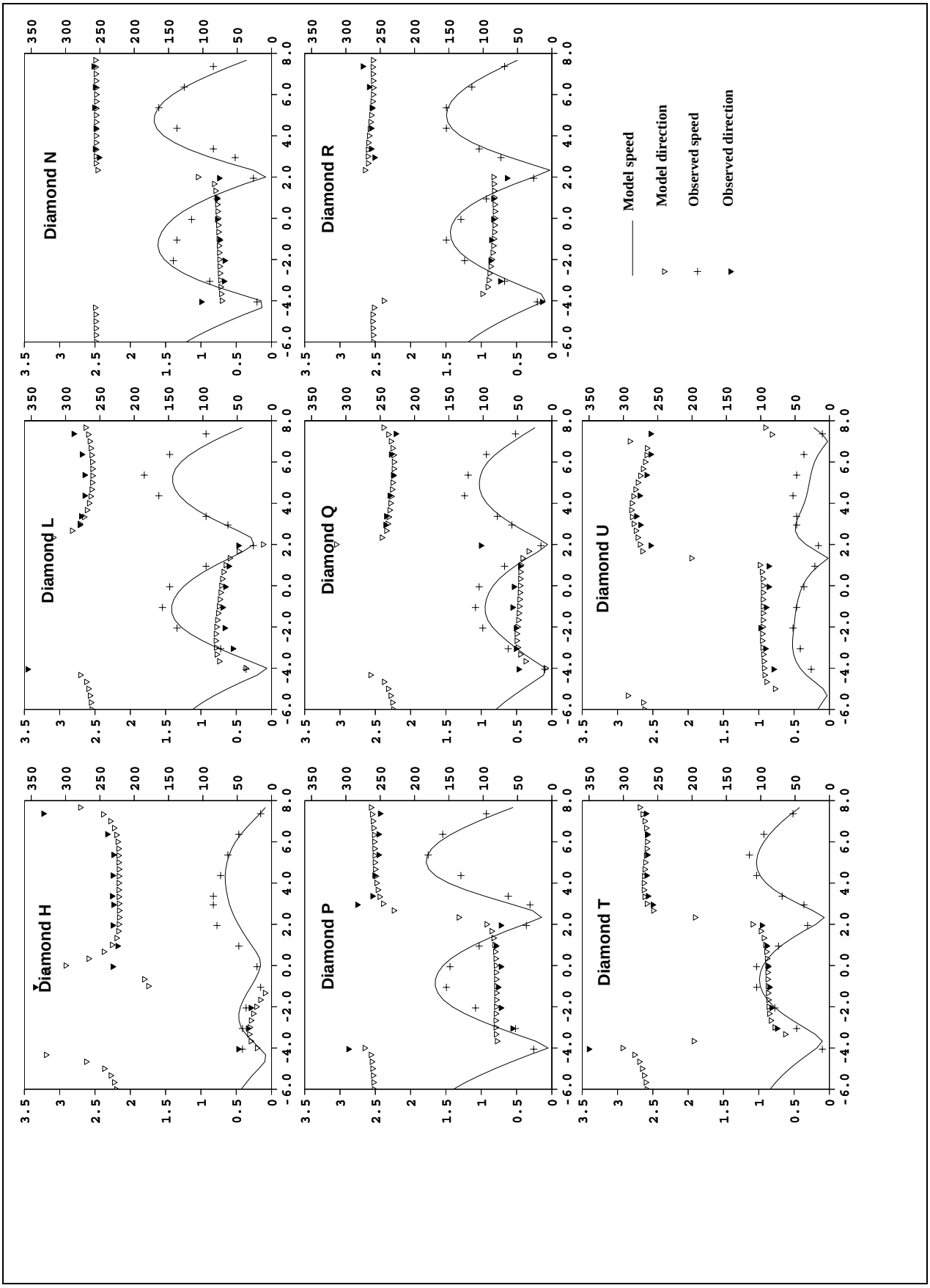

Figure 5 Comparison of regional model simulated tidal elevations with Admiralty diamonds

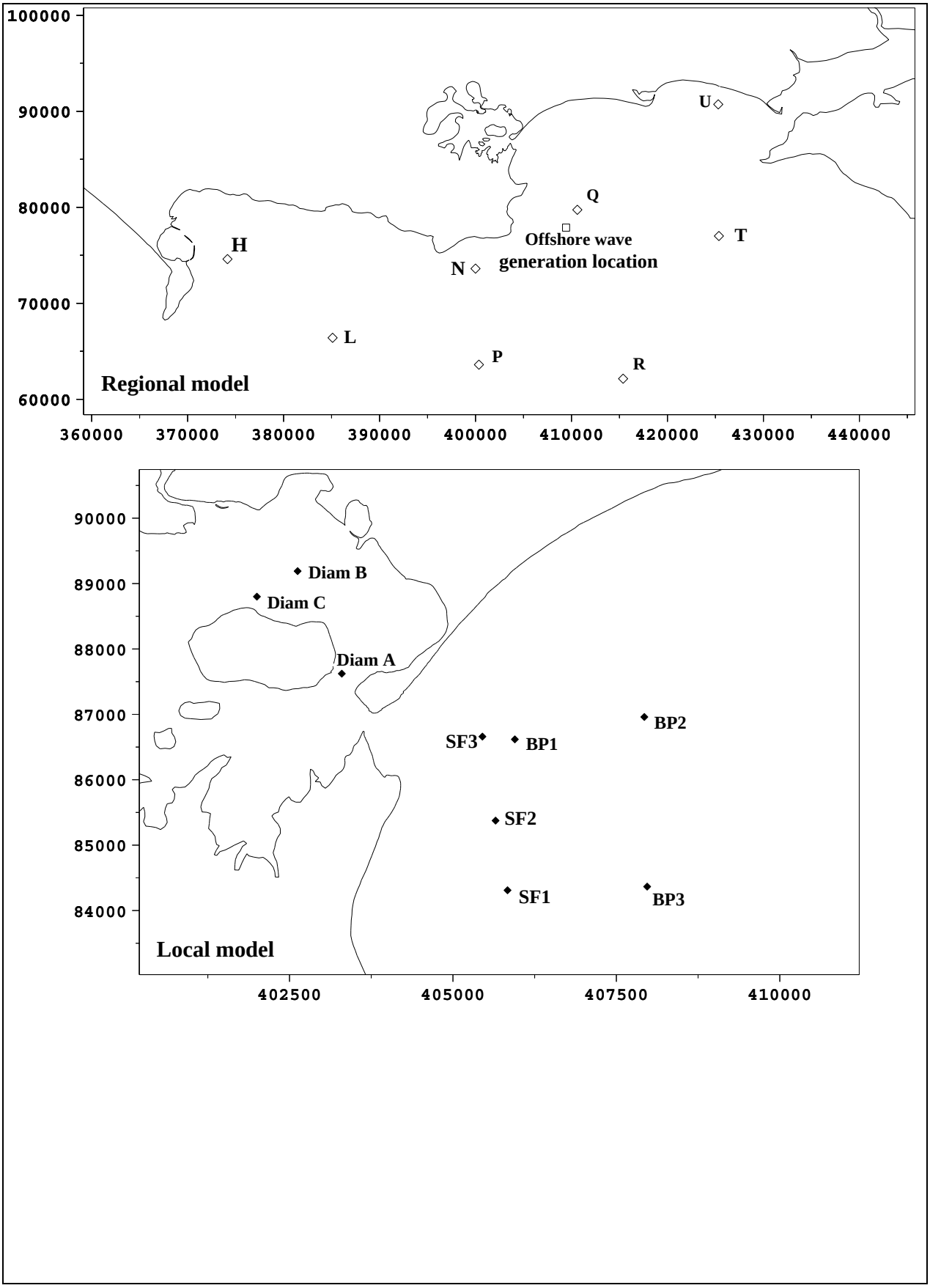

Figure 6 Location of tidal current comparison points

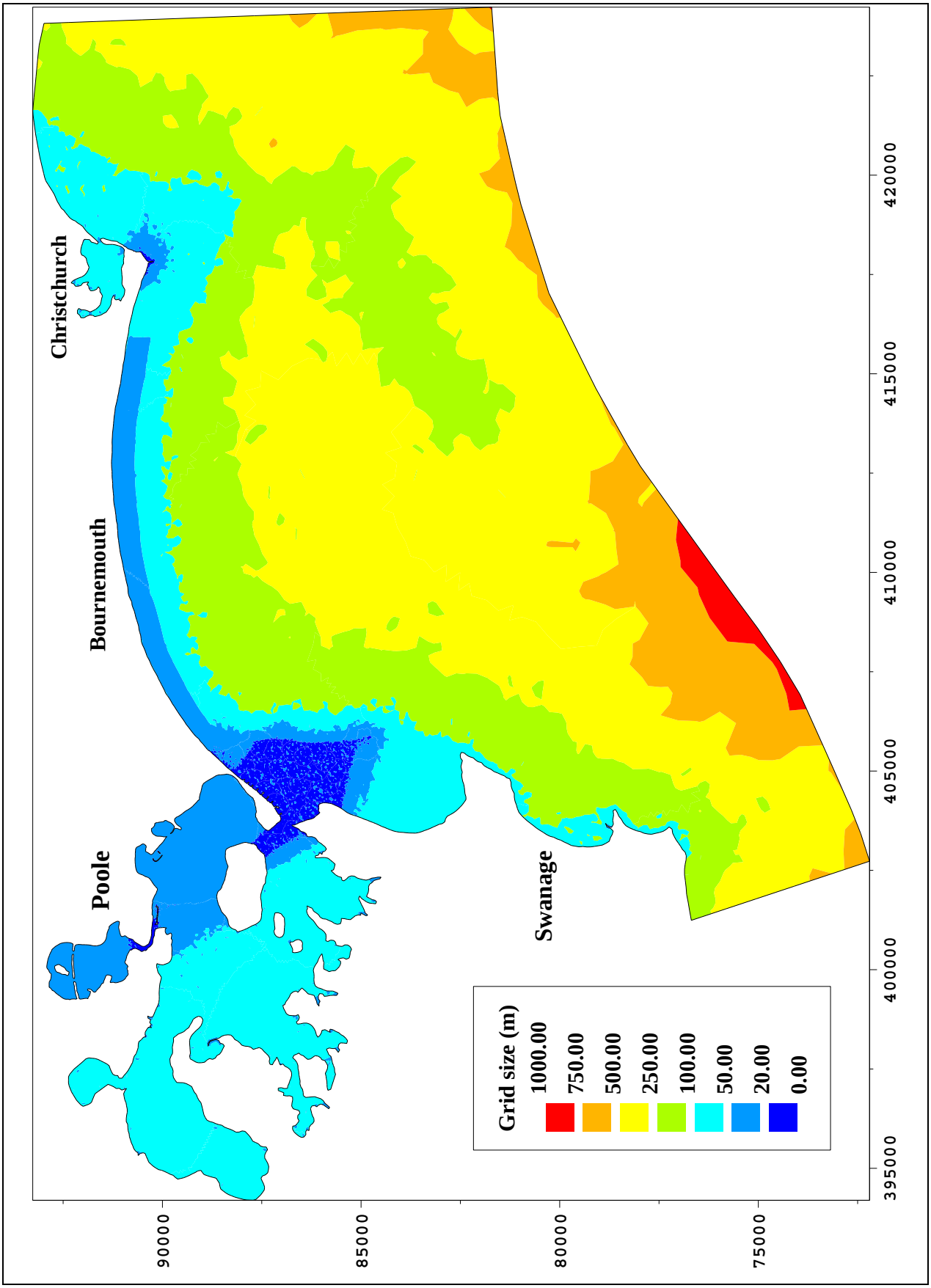

Figure 7 Local model mesh size

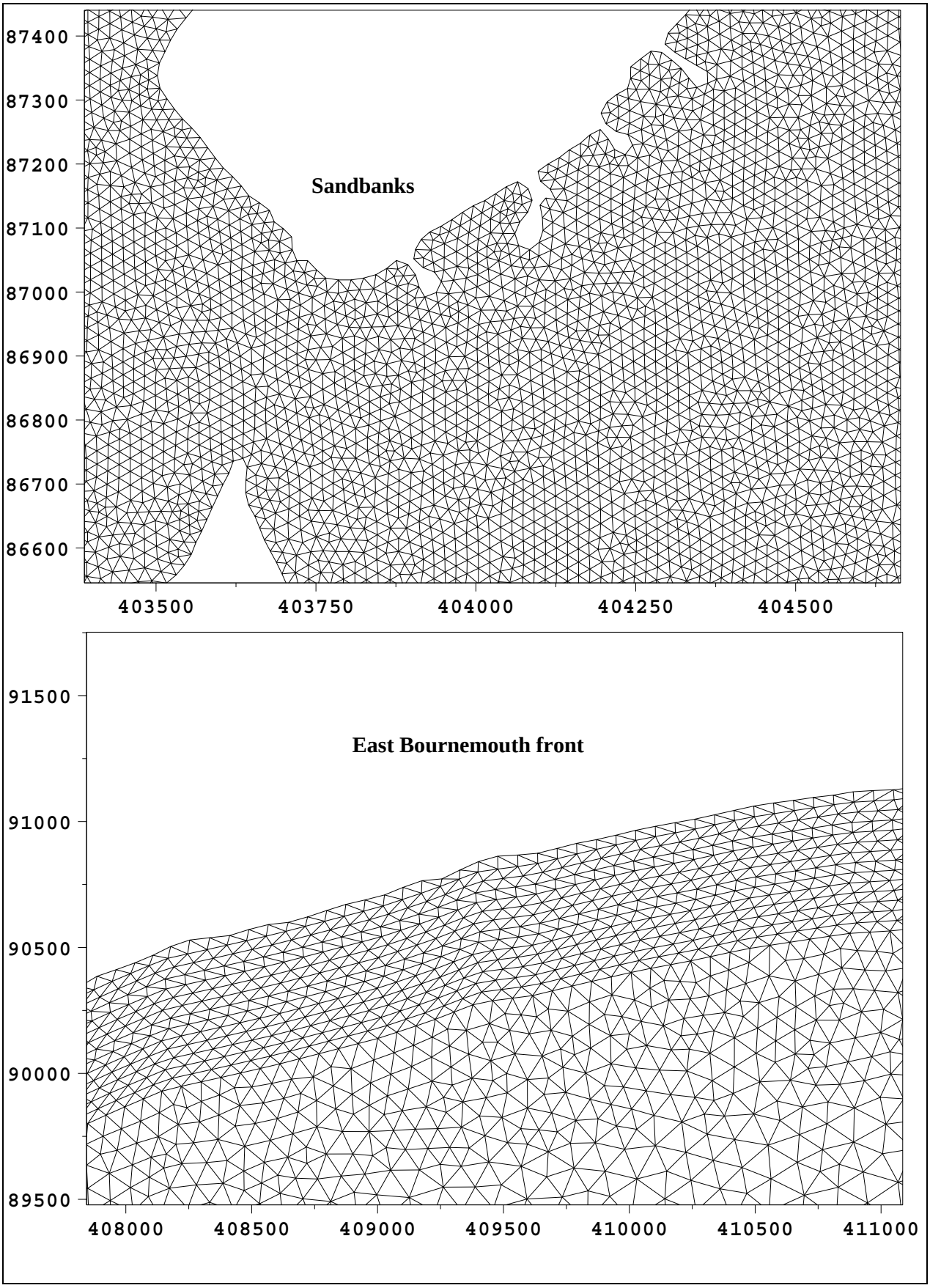

Figure 8 Details of local model mesh

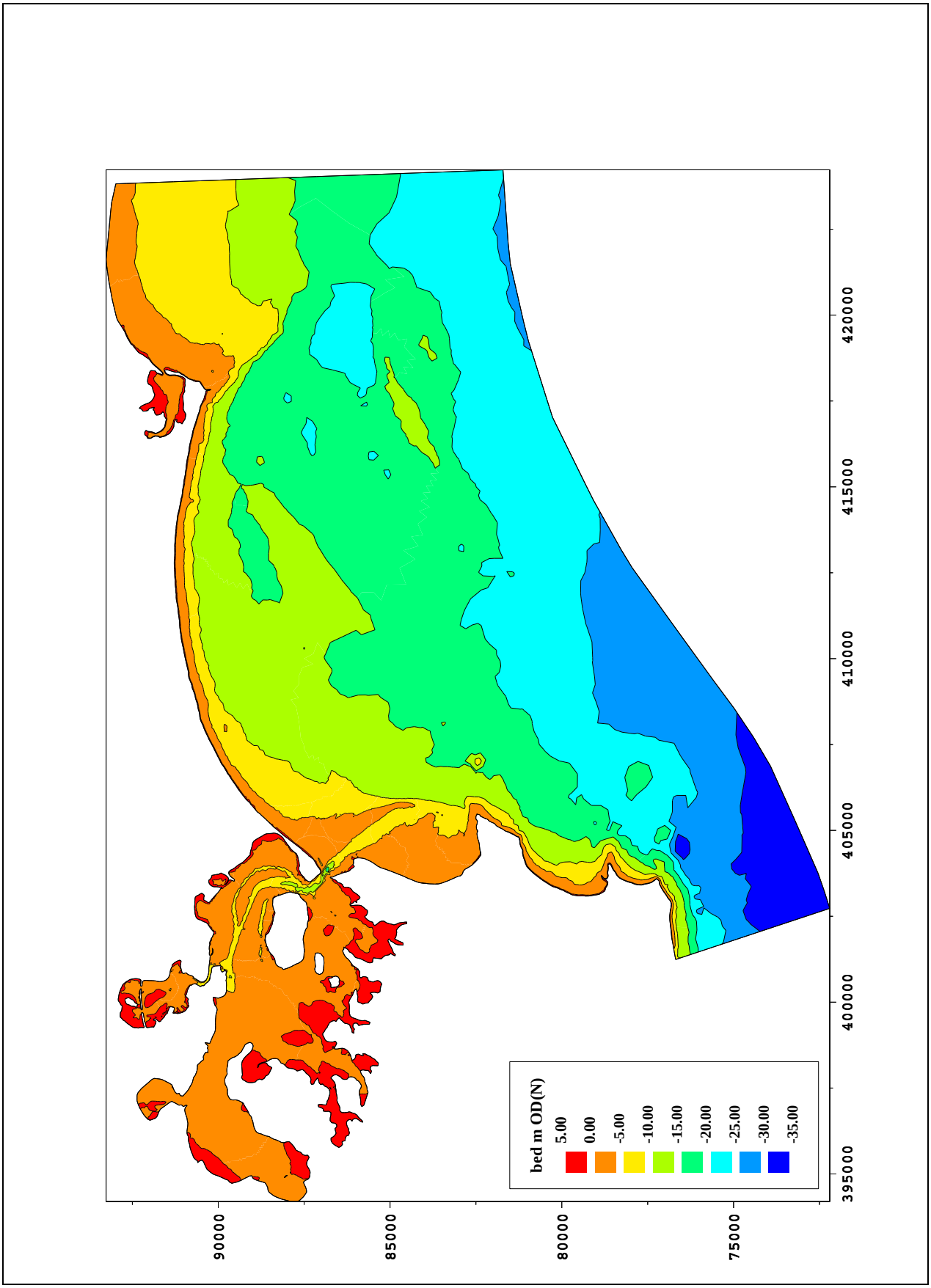

Figure 9 Local model bathymetry

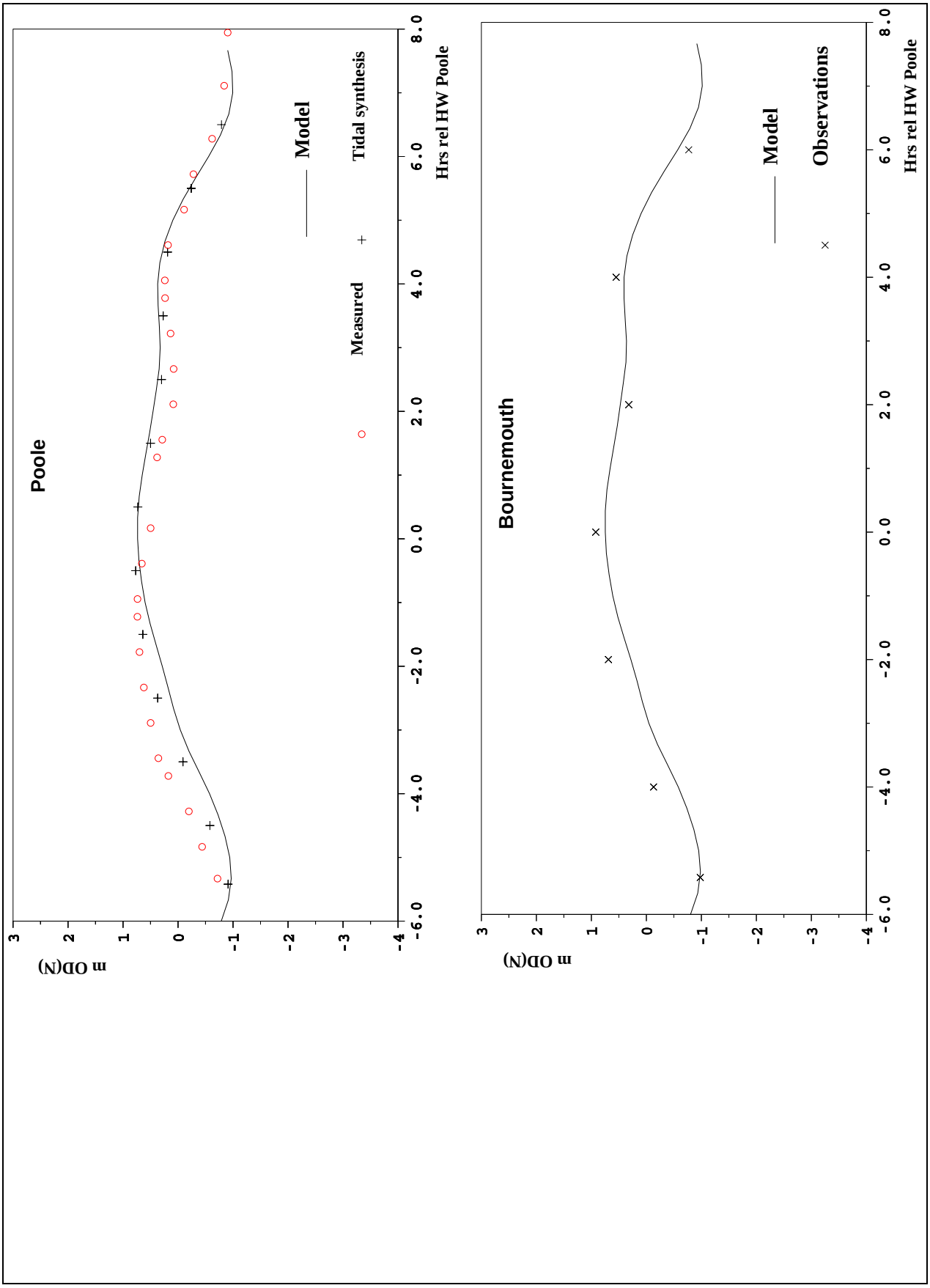

Figure 10 Comparison of local model simulated tidal elevation with data

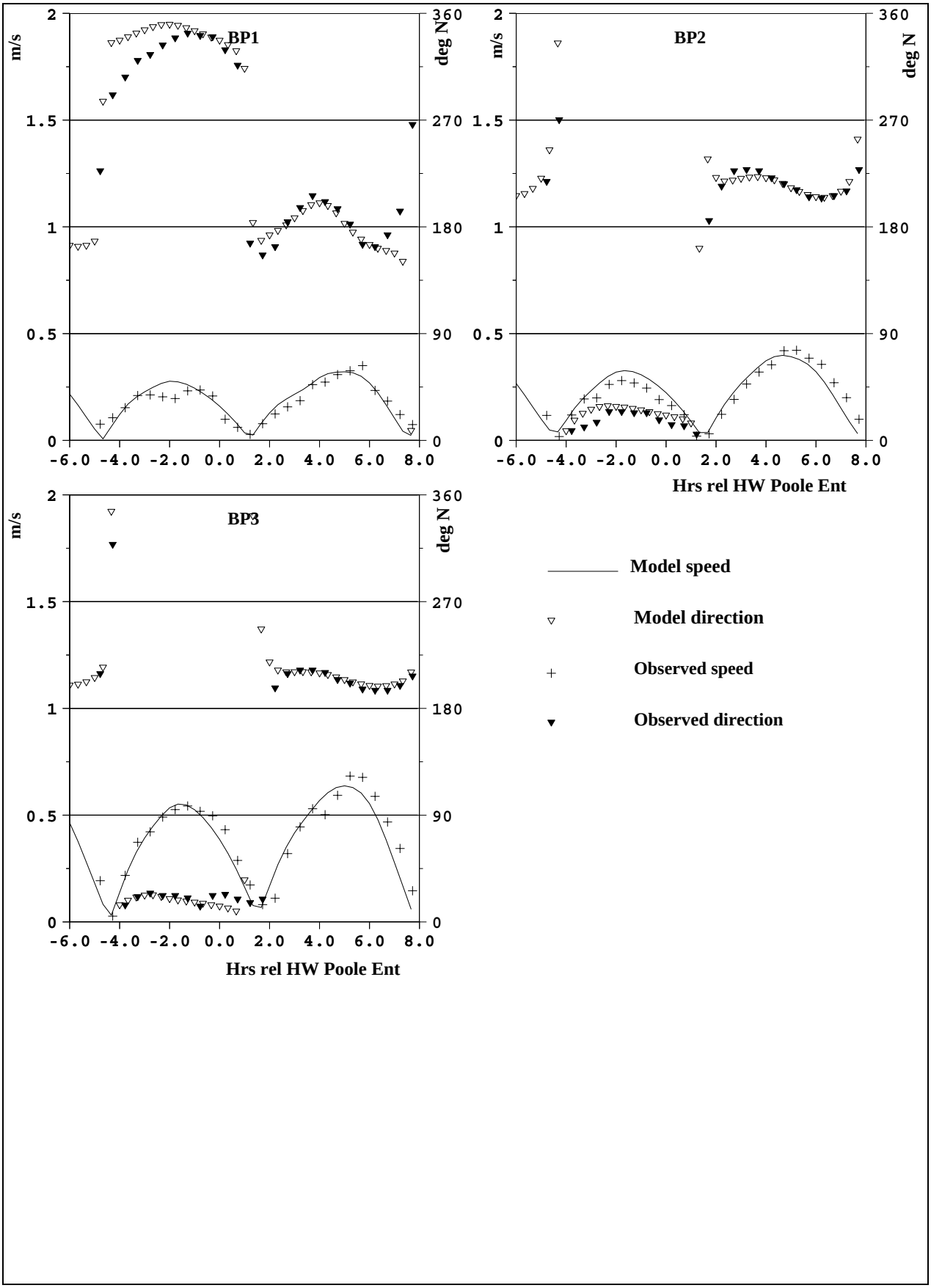

Figure 11 Comparison of local model simulated tidal currents with data 24-25 April 1990

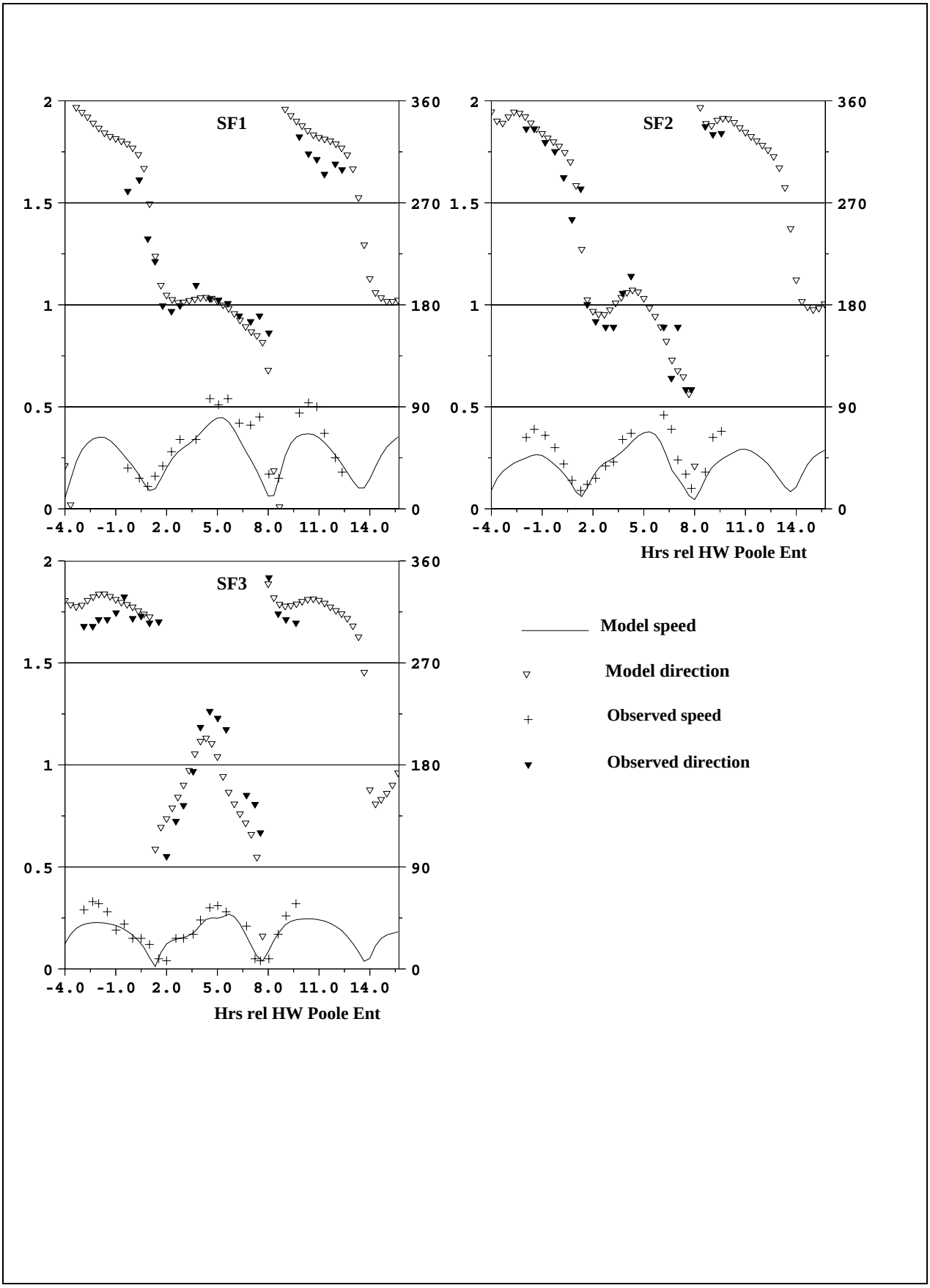

Figure 12 Comparison of local model simulated tidal currents with data 24-27 May 1990

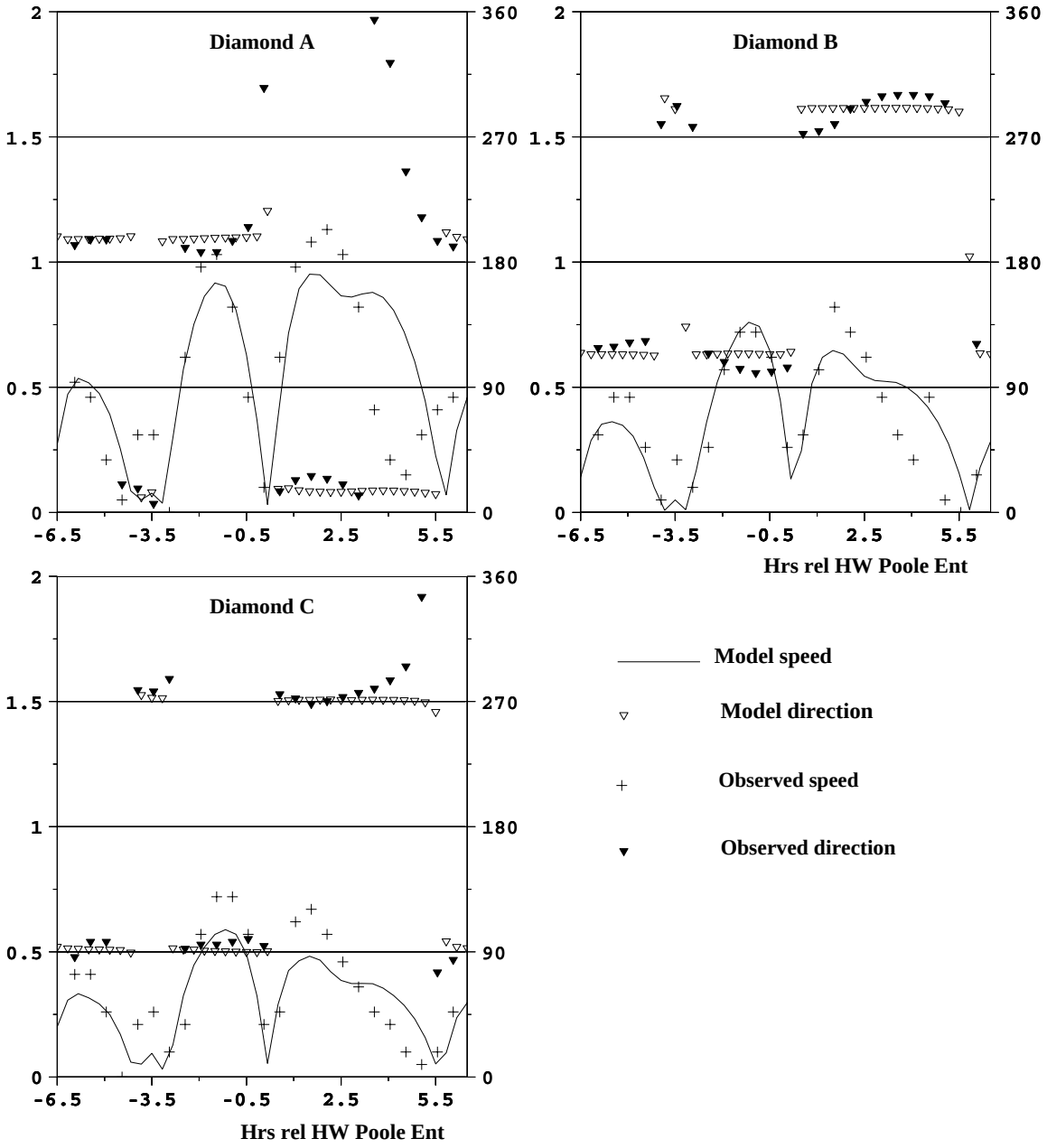

Figure 13 Comparison of local model simulated tidal currents with Admiralty diamonds

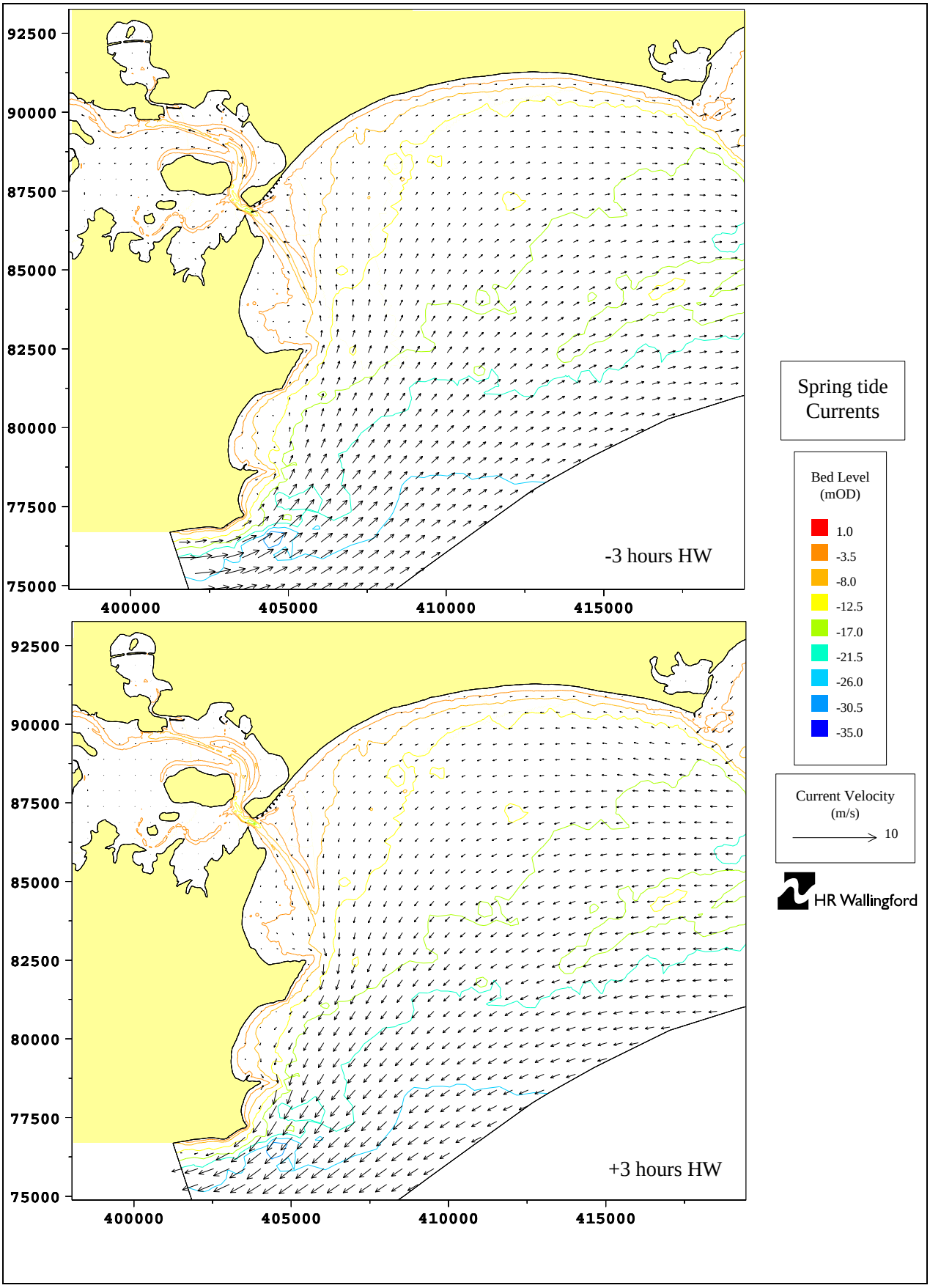

Figure 14 Spring tide flood and ebb currents

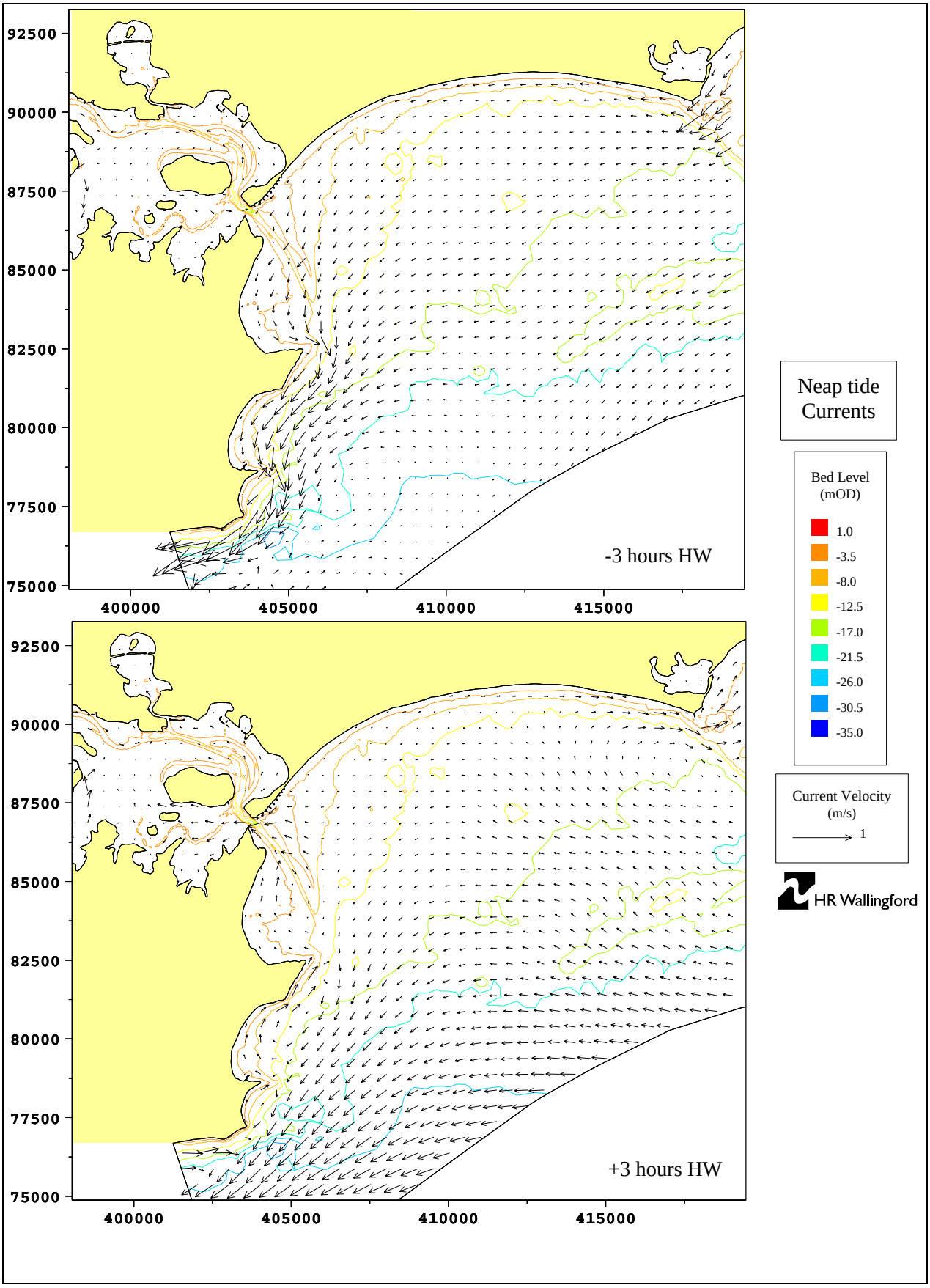

Figure 15 Neap tide flood and ebb currents

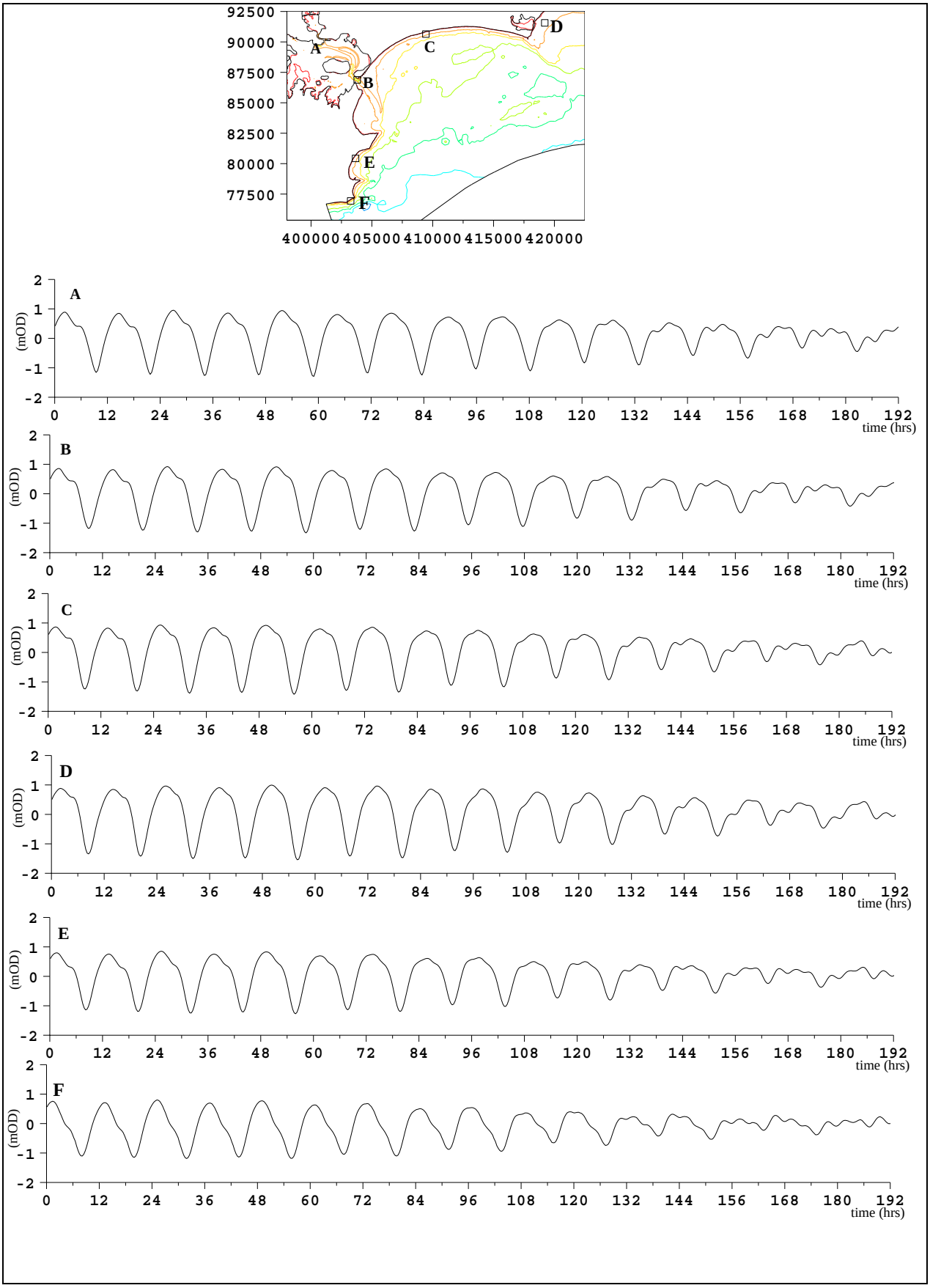

Figure 16 Spring-neap water levels

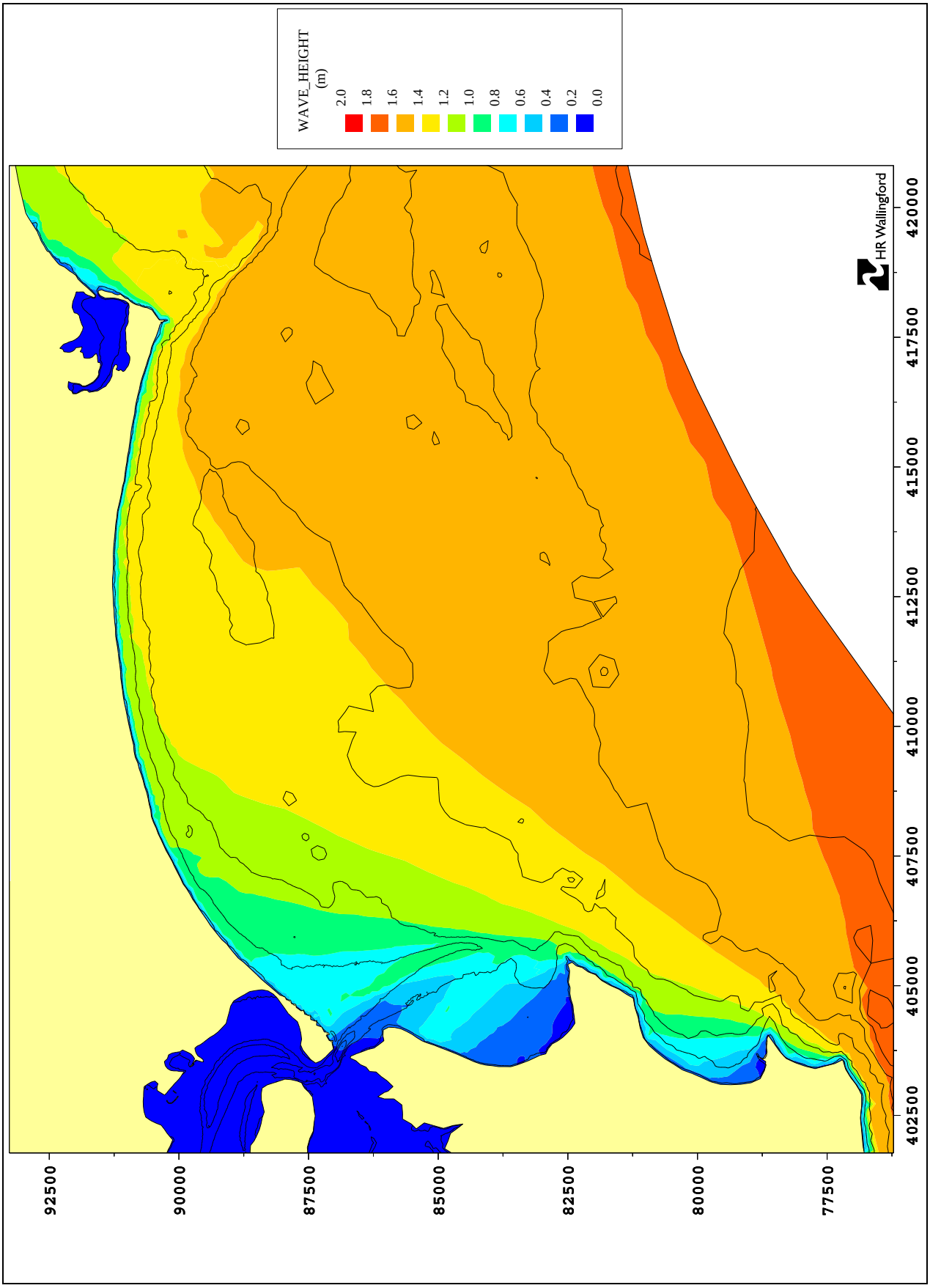

Figure 17 Wave height field from 1.62m, 4.4s offshore waves from 190N at MHWS

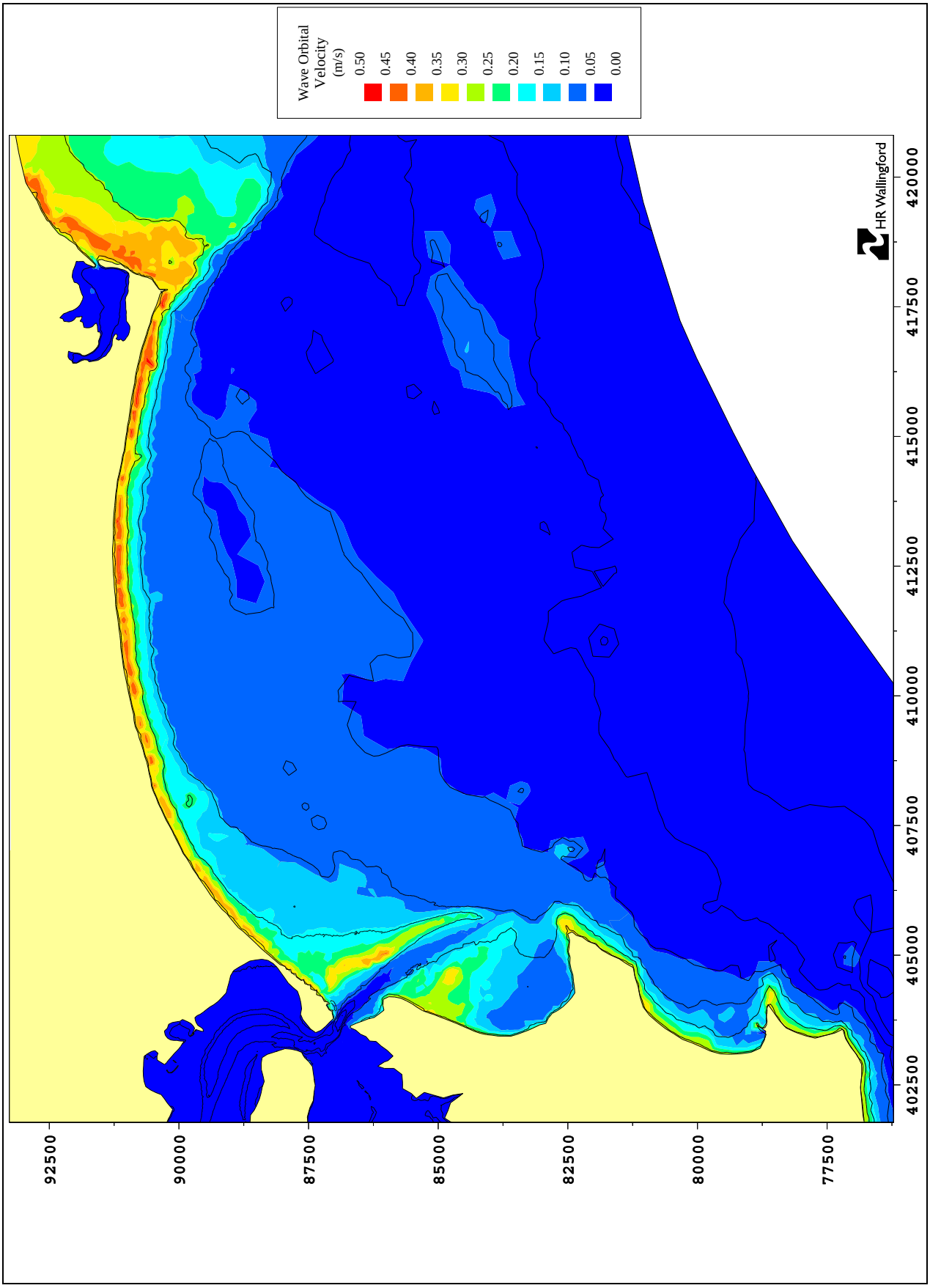

Figure 18 Wave orbital velocity field from 1.62m, 4.4s offshore waves from 190N at MHWS

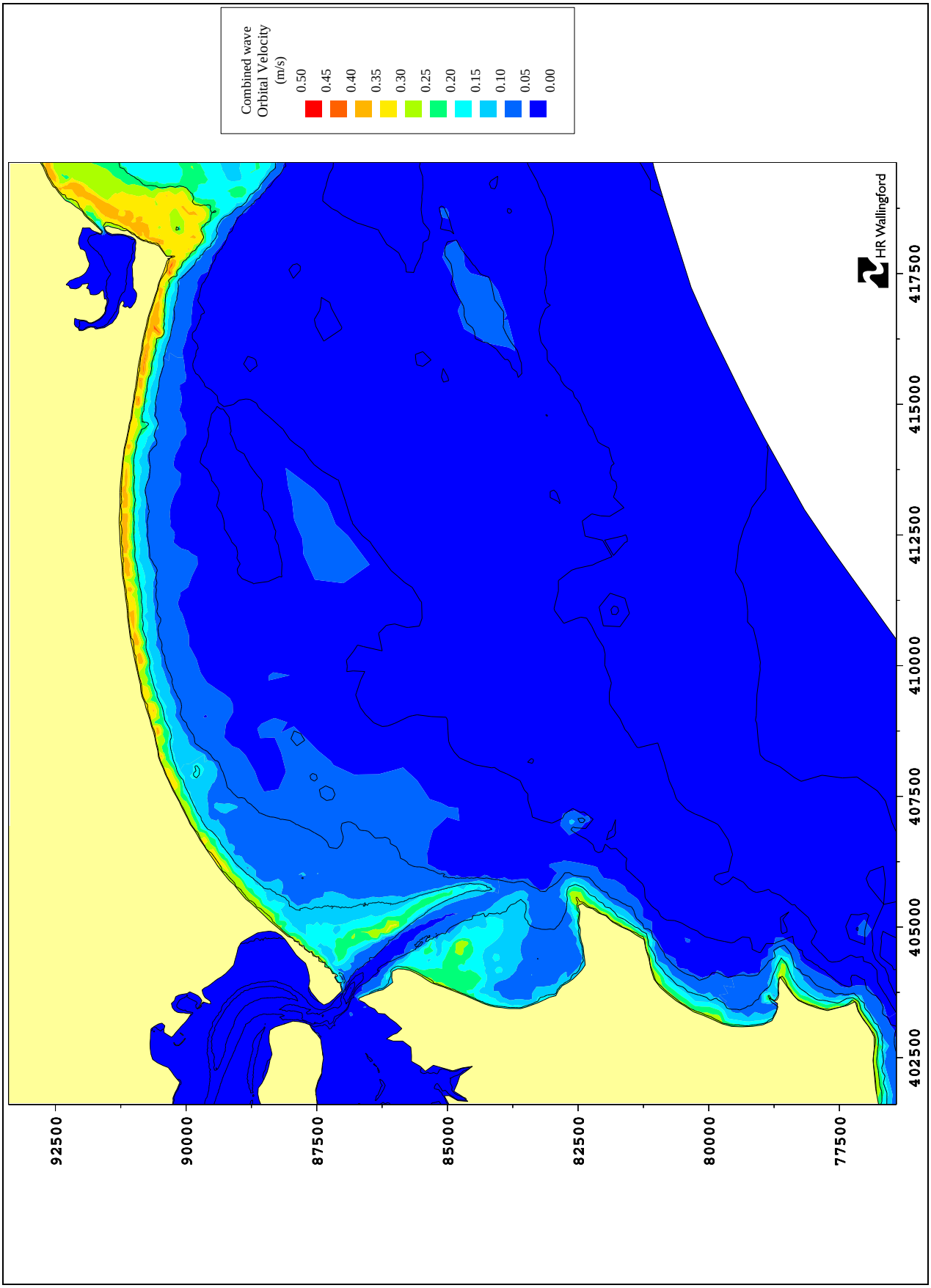

Figure 19 Combined wave orbital velocity field at MWL

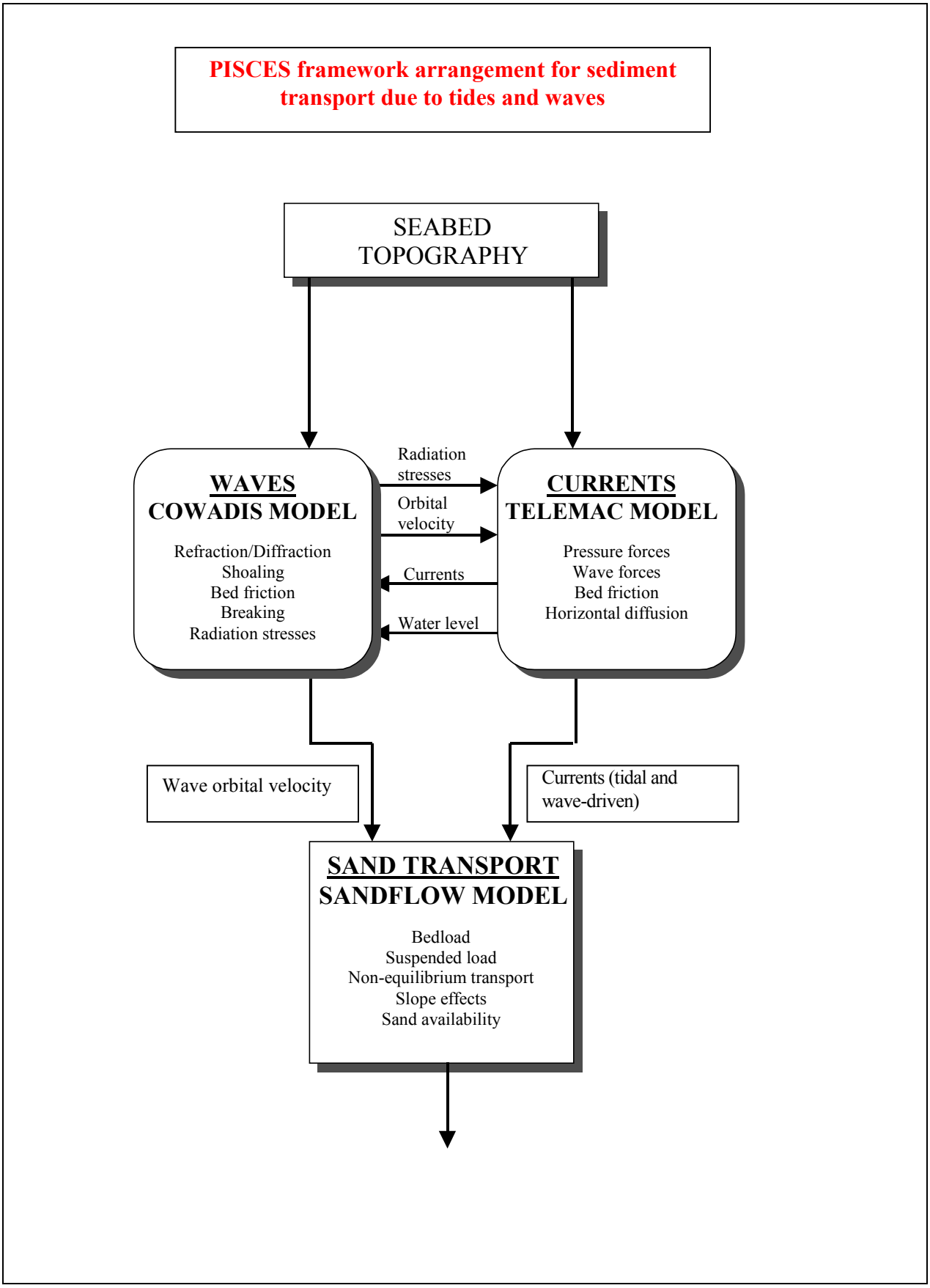

Figure 20 PISCES model flow diagram

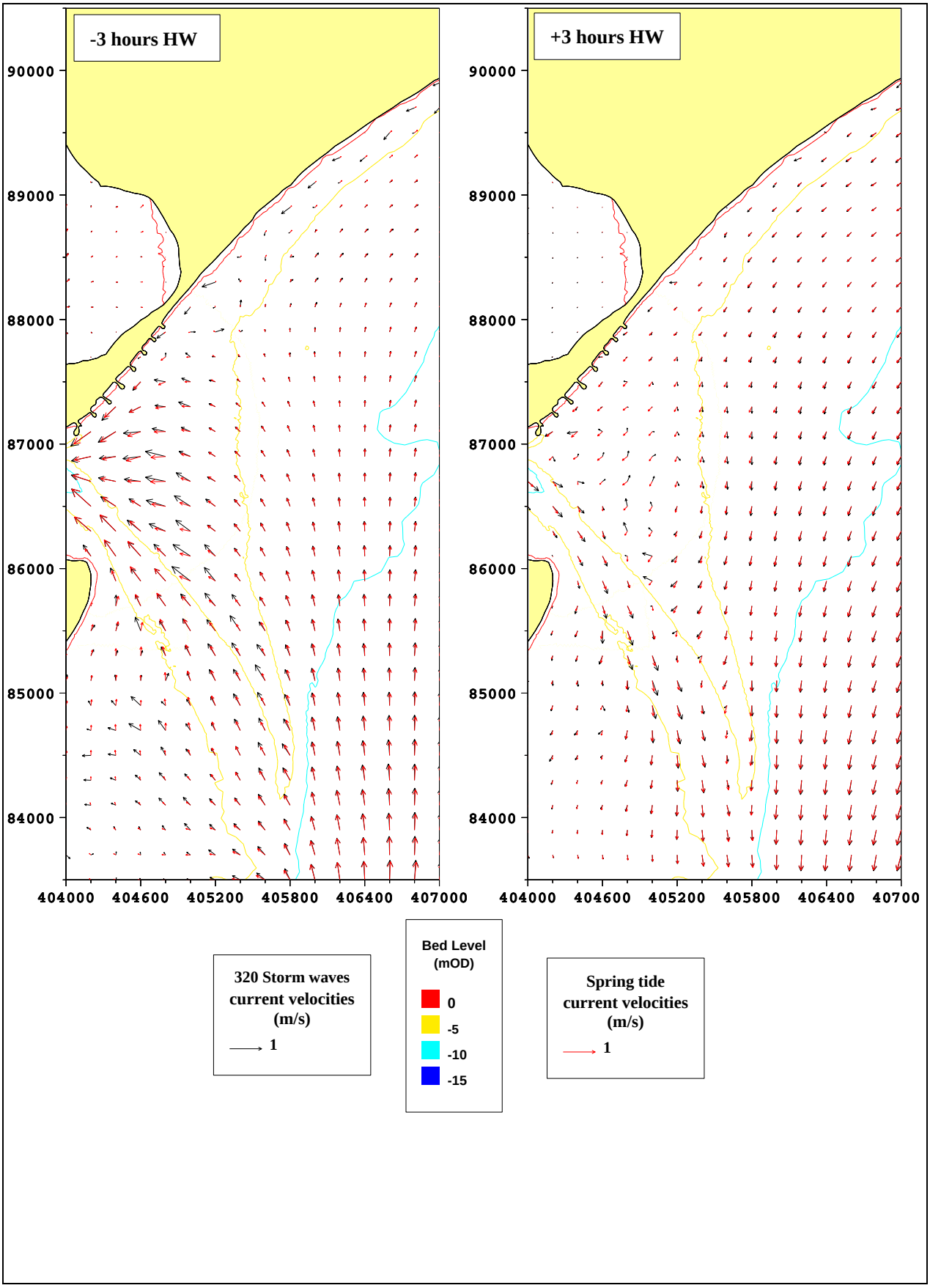

Figure 21 Flood and Ebb currents due to spring tides and storm waves from 140N

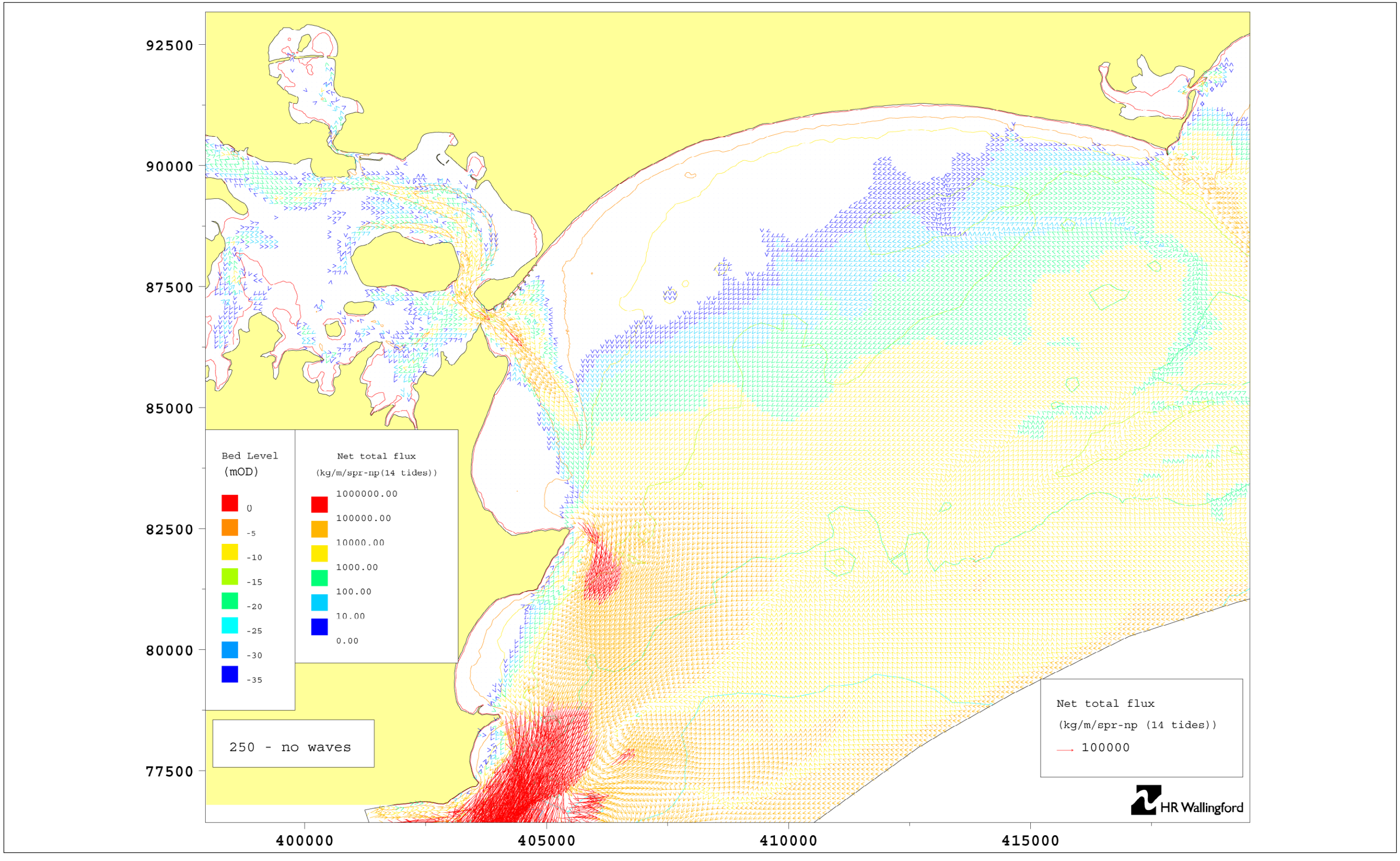

Figure 22 Net sediment flux over spring-neap period

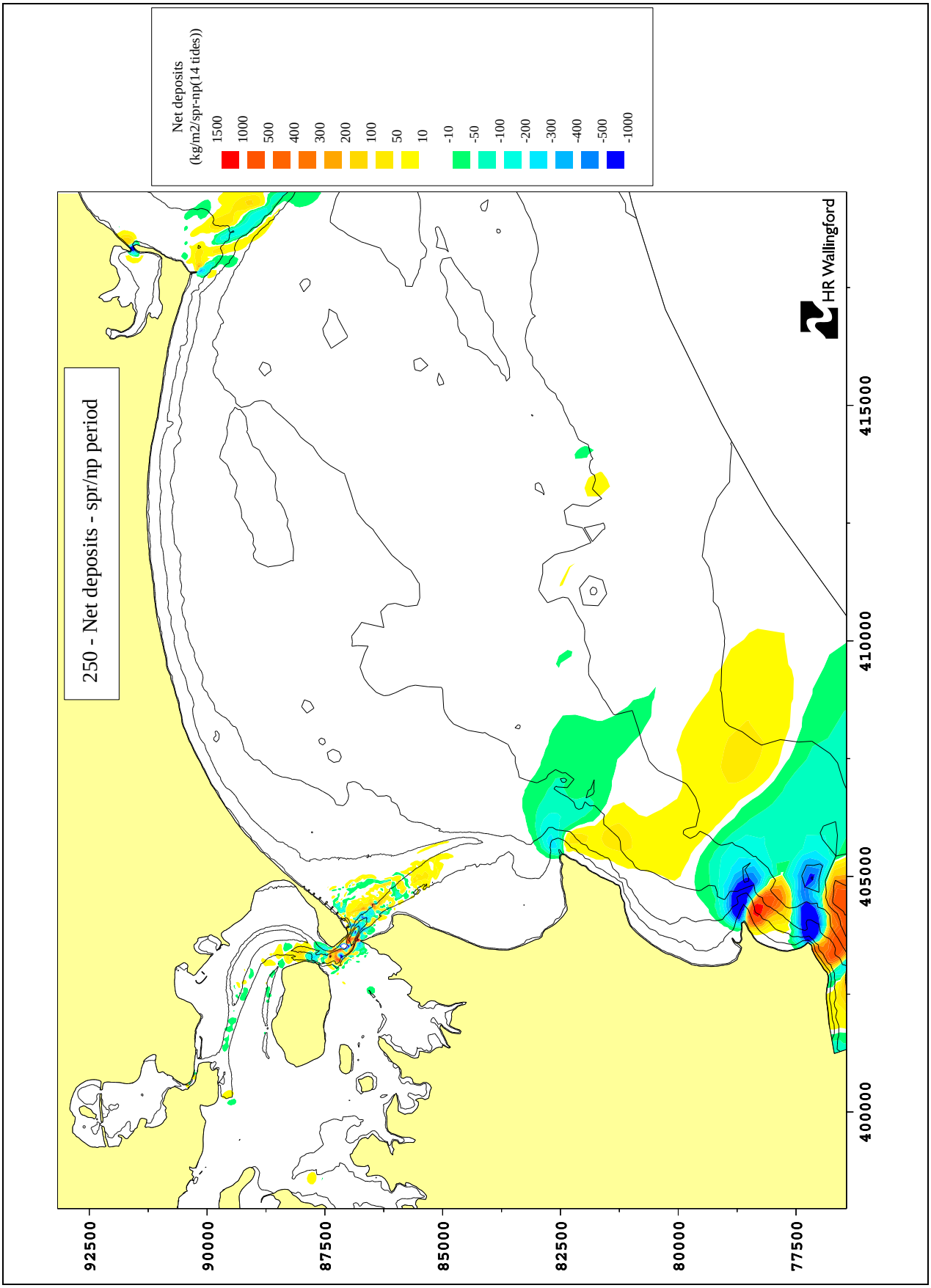

Figure 23 Net patterns of erosion and deposition over spring-neap period

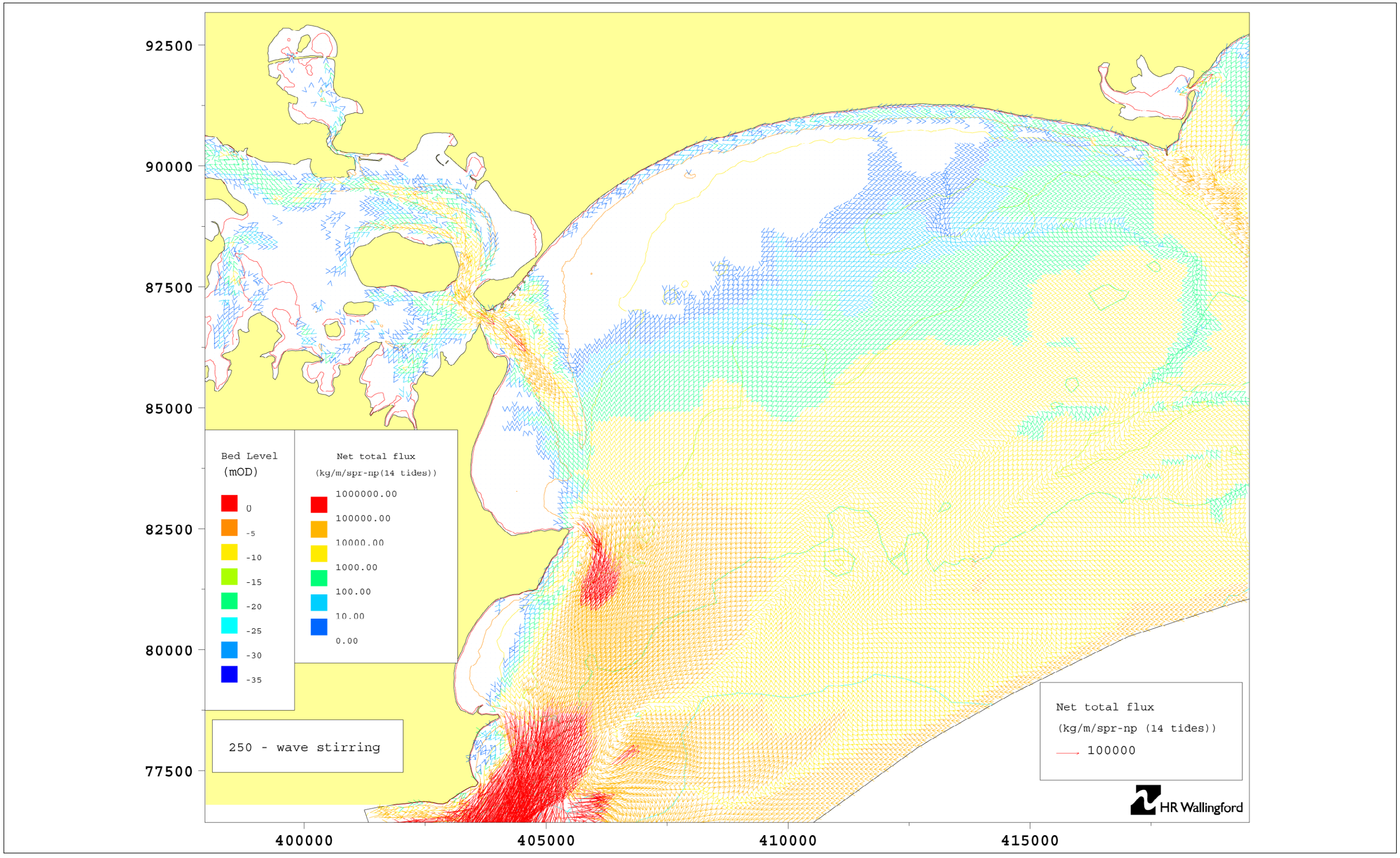

Figure 24 Net sediment flux over spring-neap period, including wave stirring

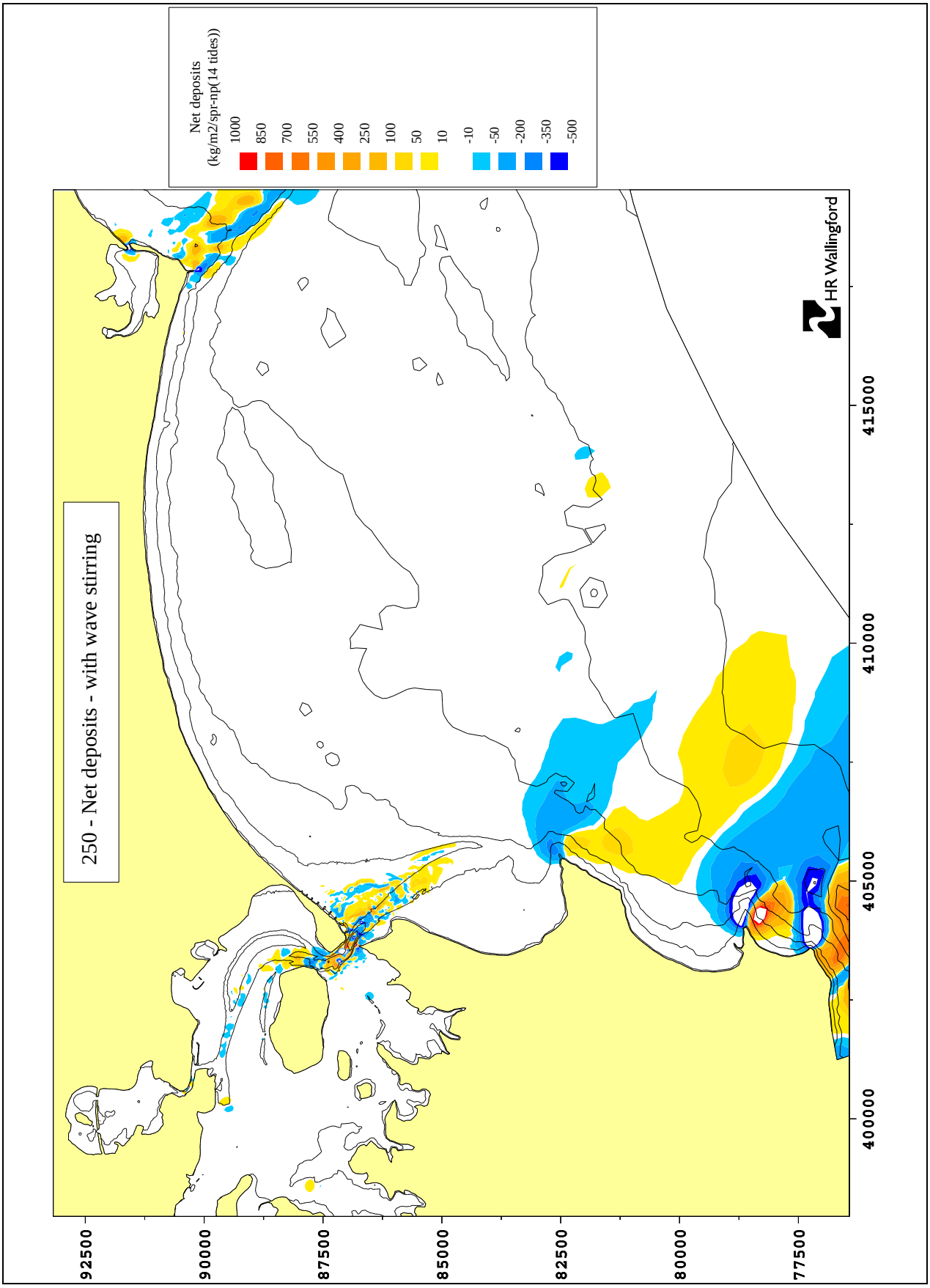

Figure 25 Net patterns of erosion and deposition over spring-neap period, including wave stirring

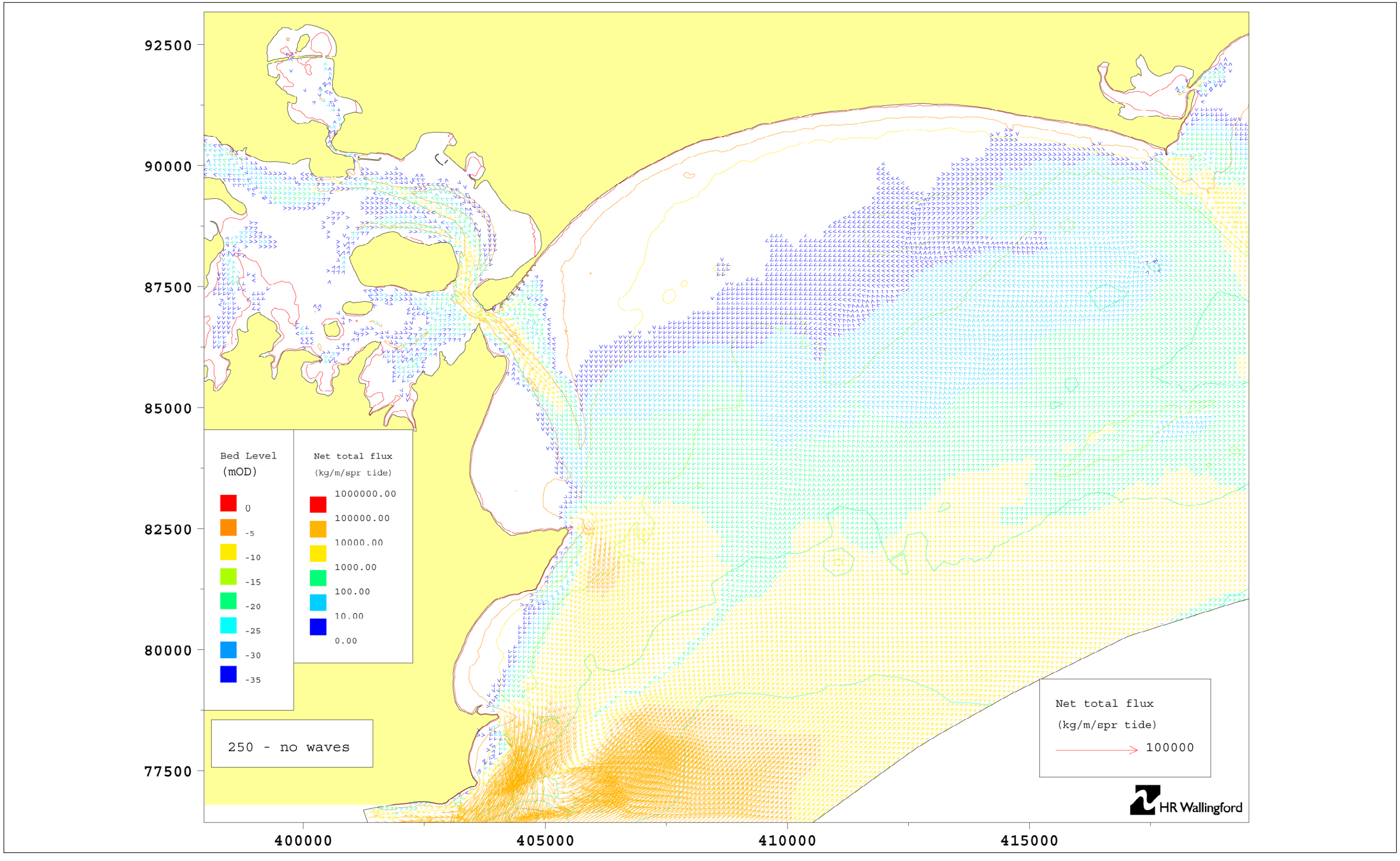

Figure 26 Net sediment flux over spring tide

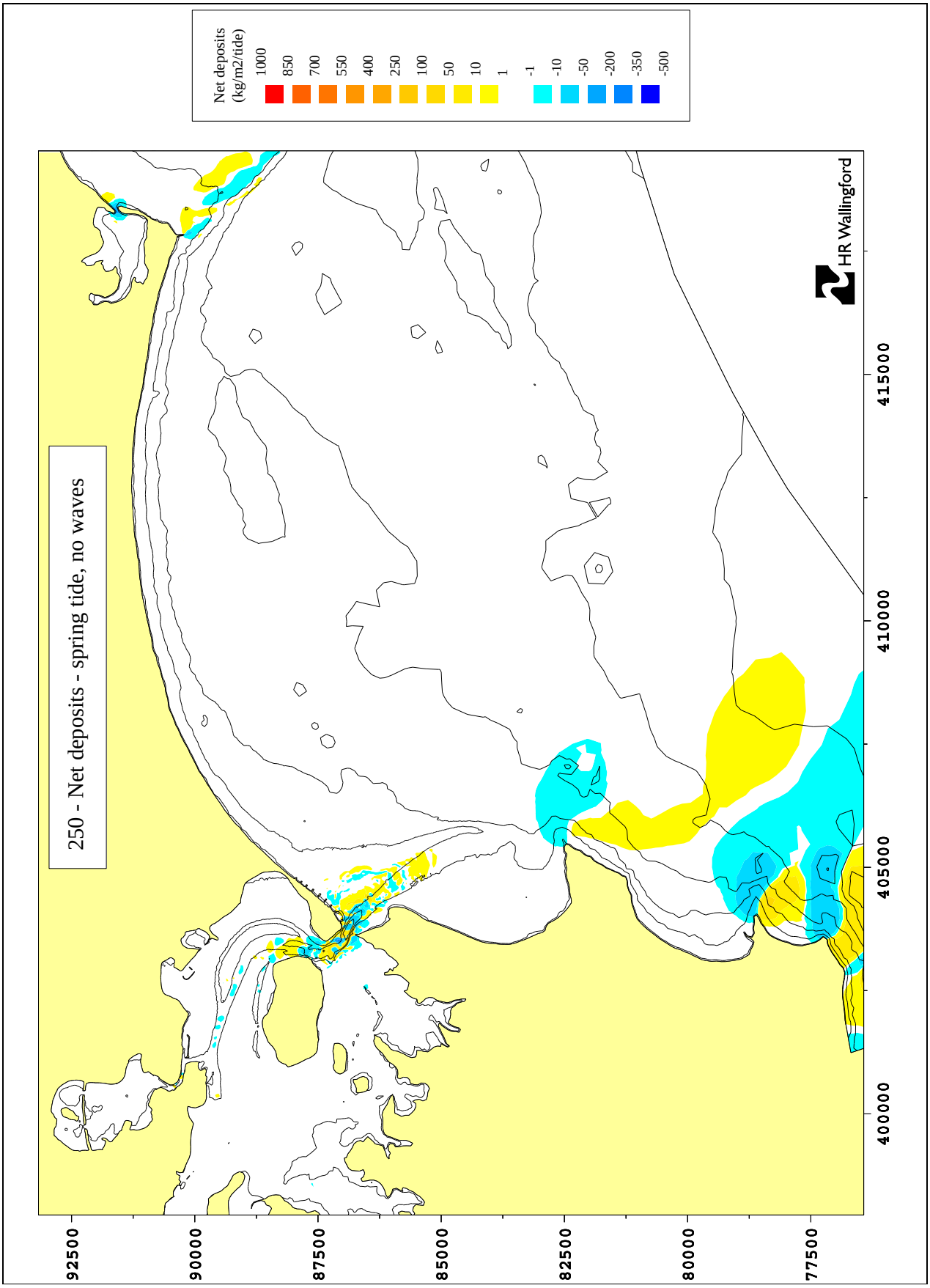

Figure 27 Net patterns of erosion and deposition over a spring tide

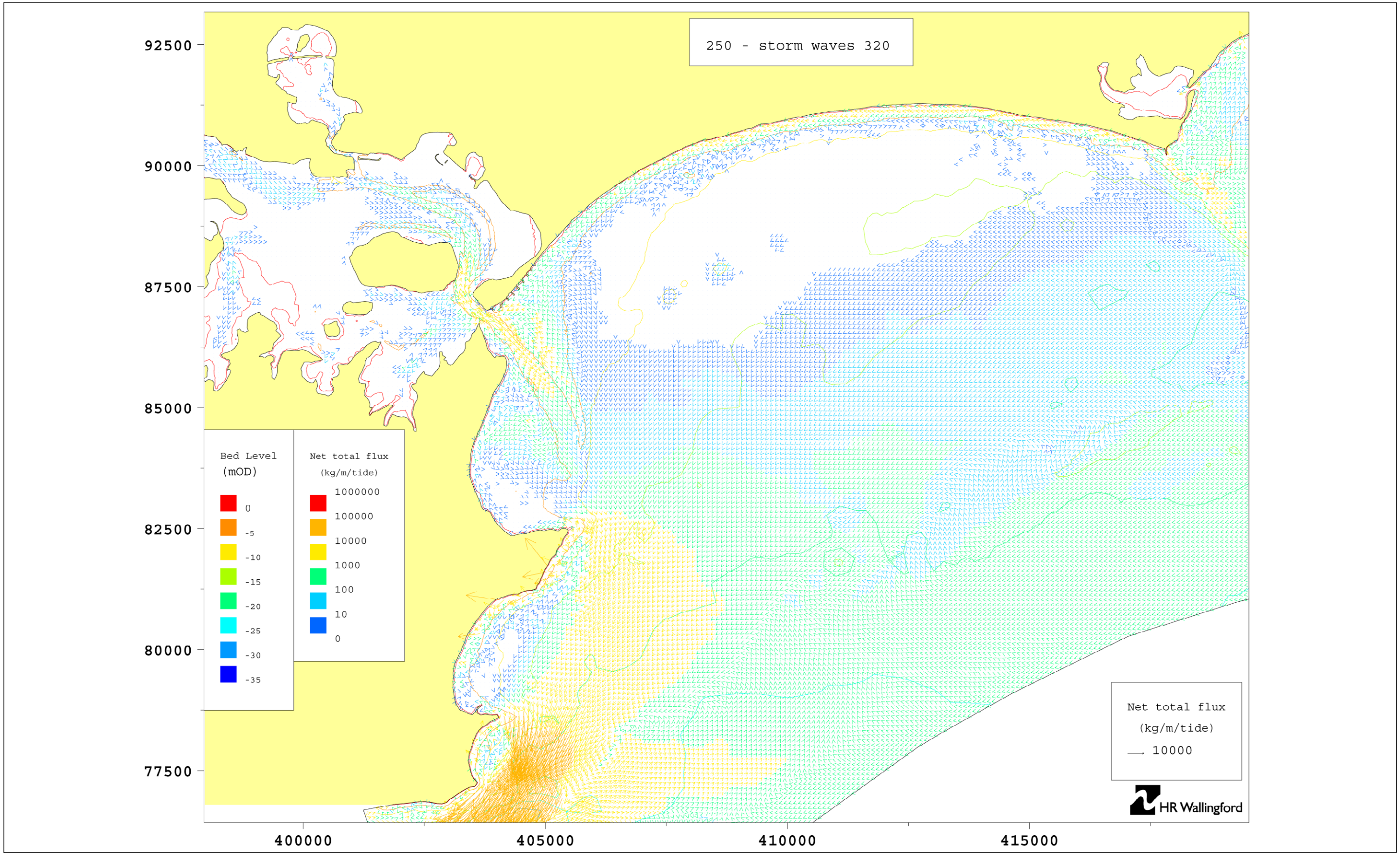

Figure 28 Net sediment flux over spring tide with storm waves from 140N

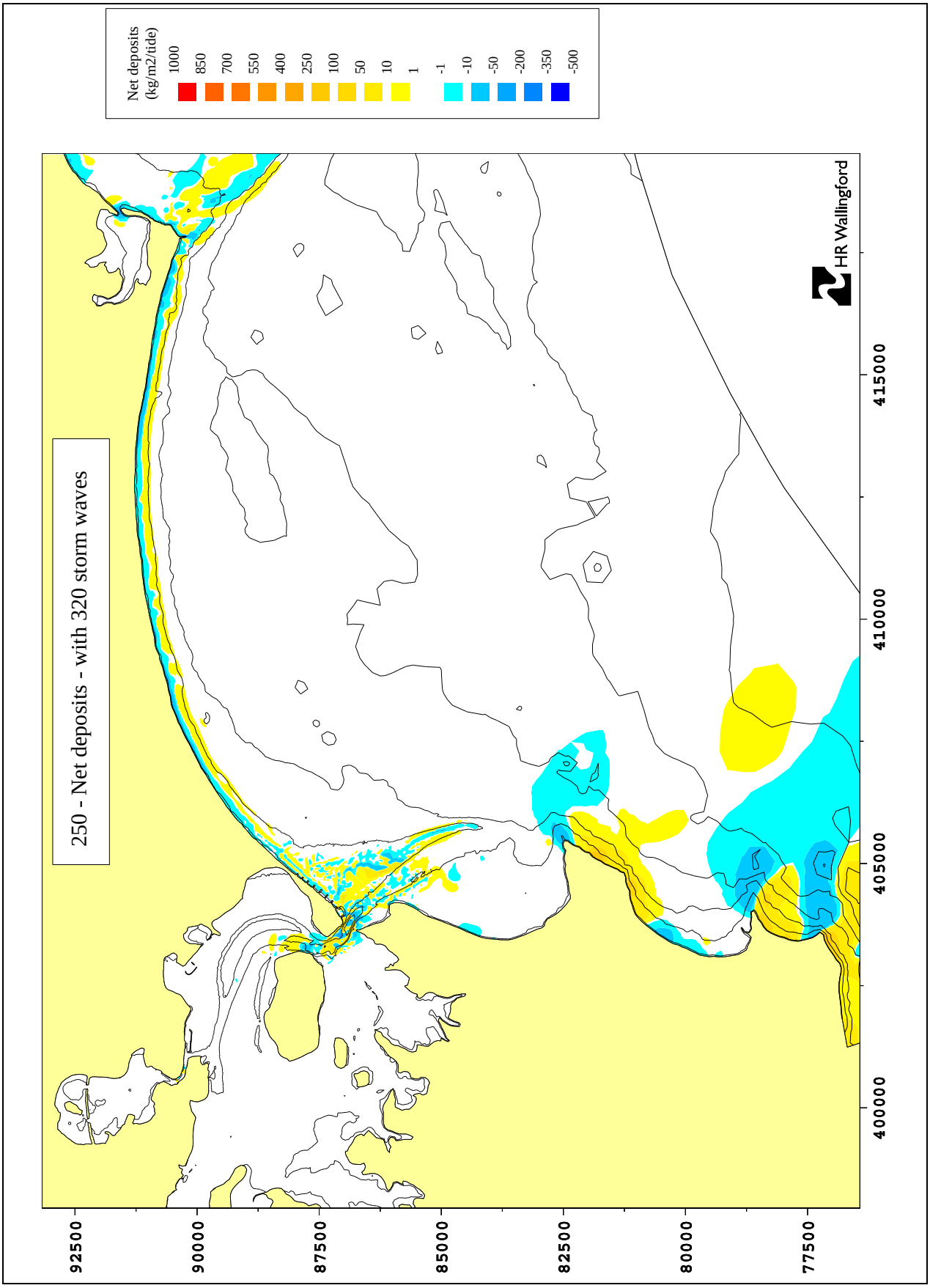

Figure 29 Net patterns of erosion and deposition over a spring tide with storm waves from 140N

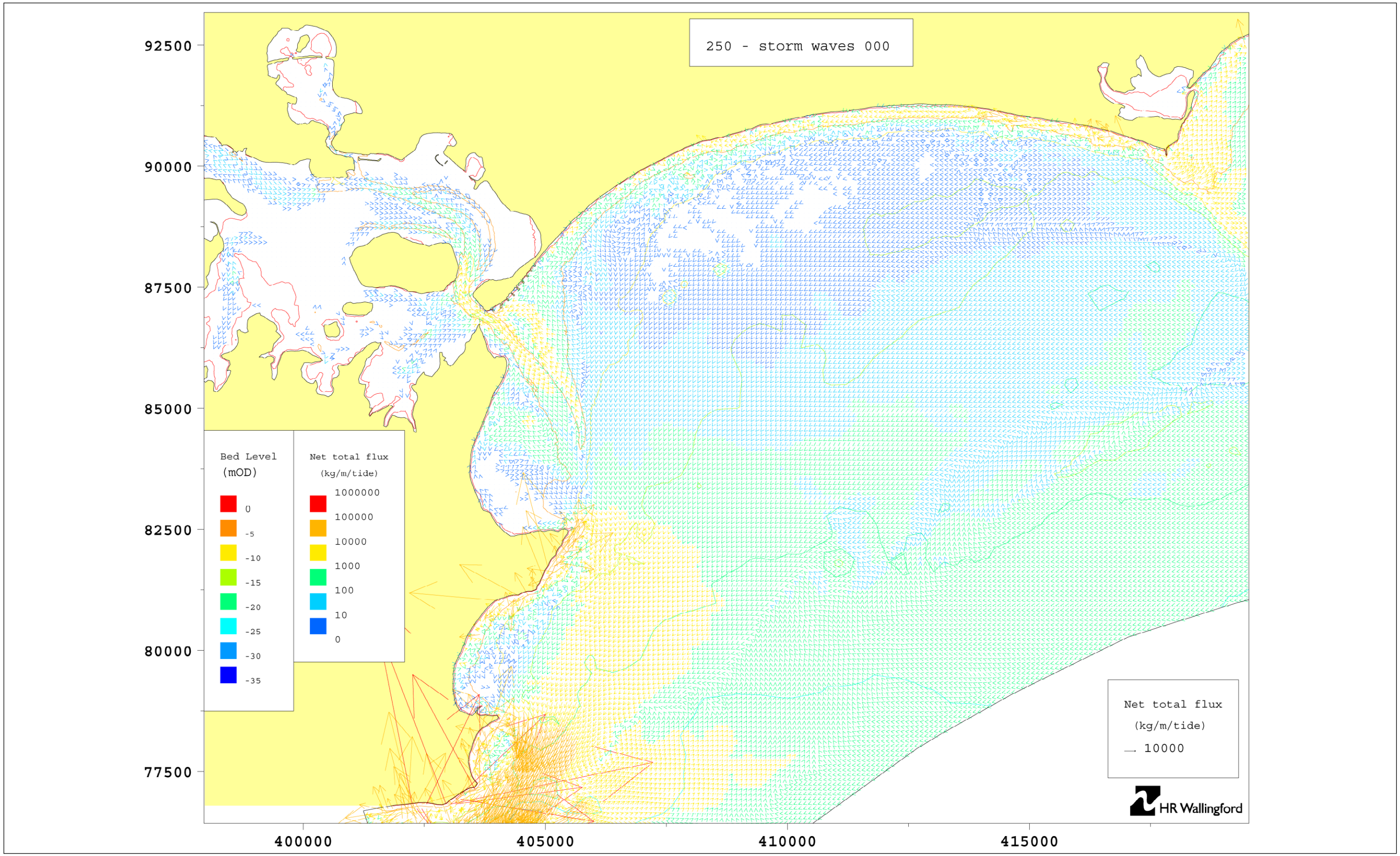

Figure 30 Net sediment flux over spring tide with storm waves from the South

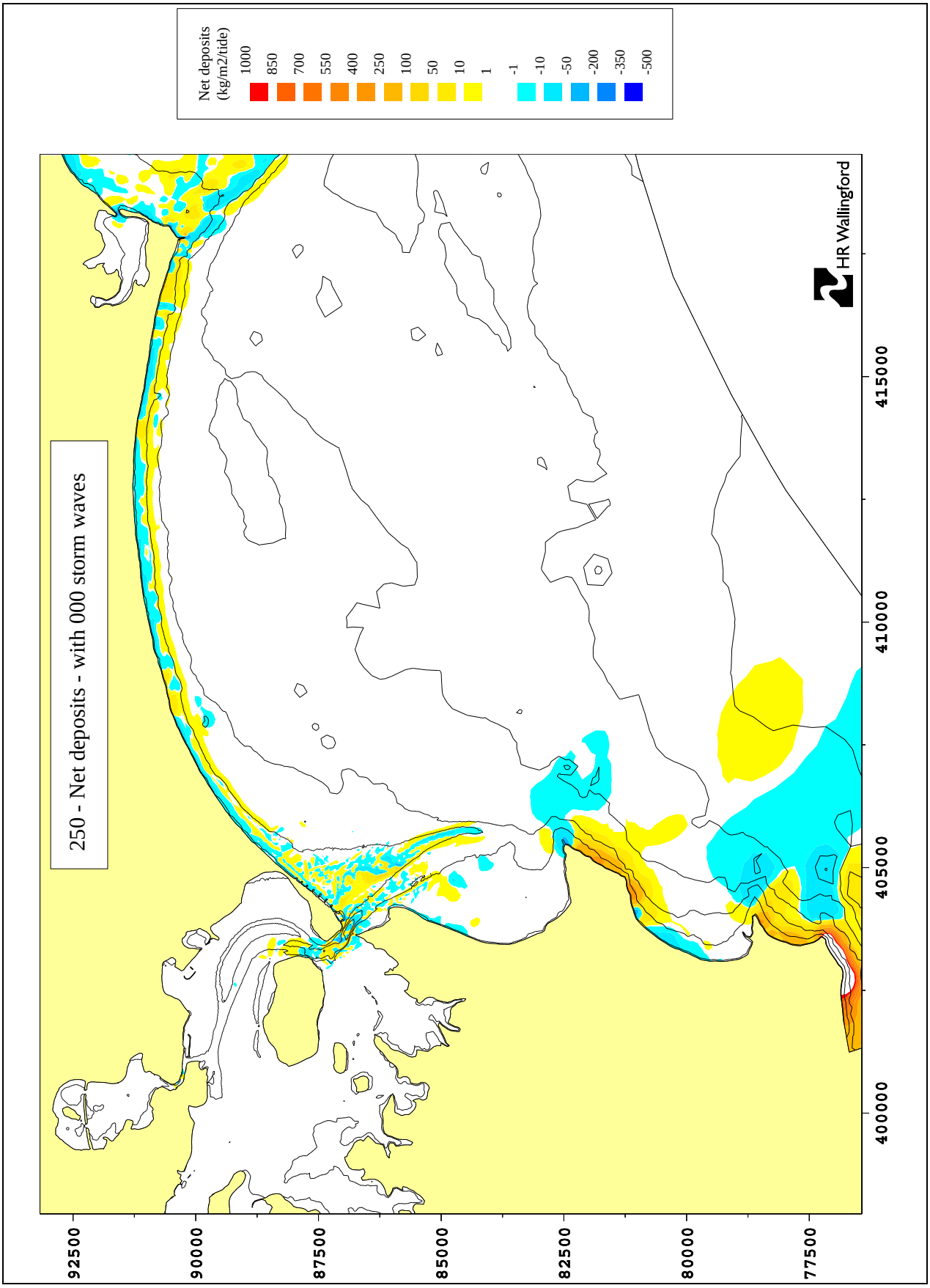

Figure 31 Net patterns of erosion and deposition over a spring tide with storm waves from the South

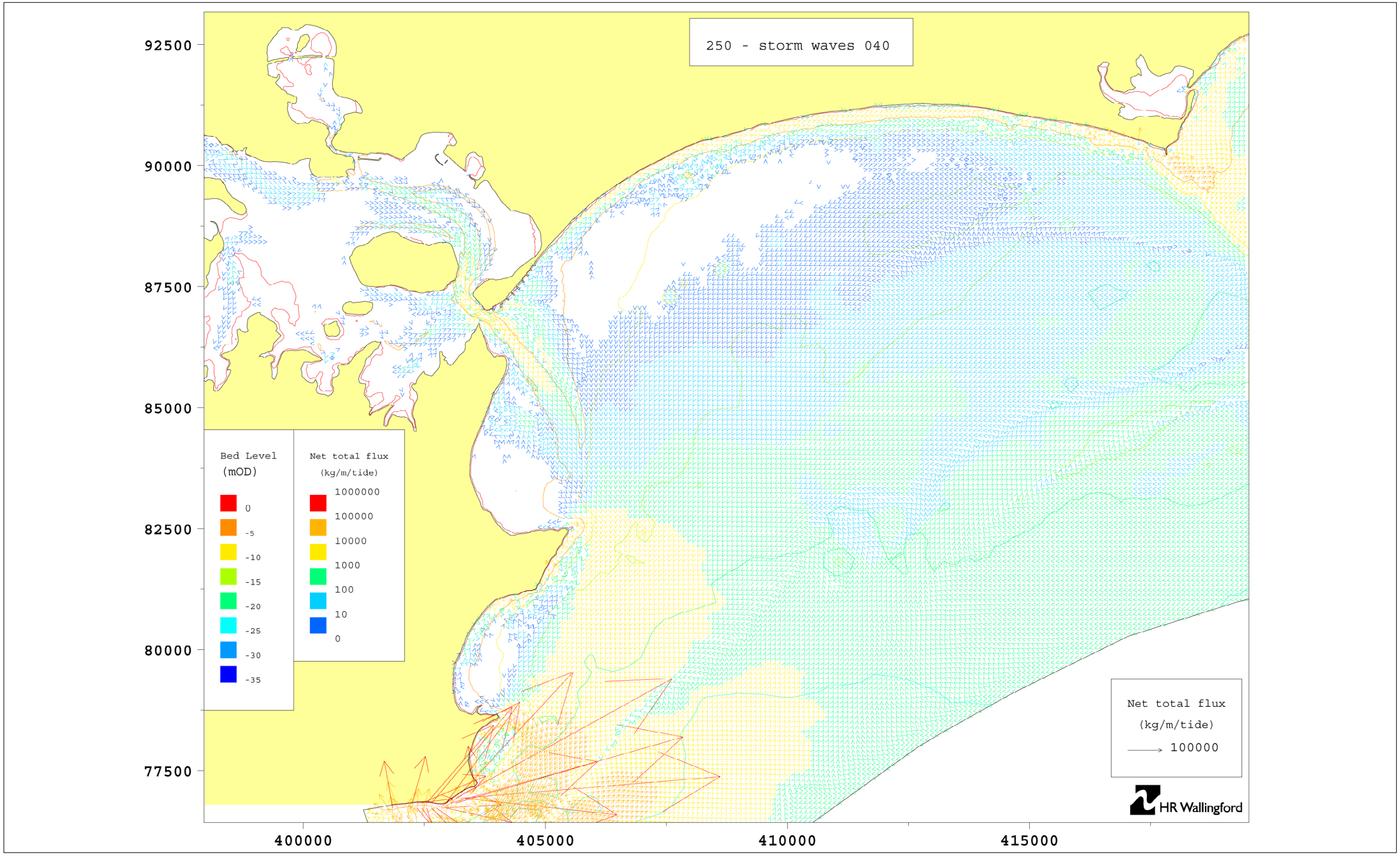

Figure 32 Net sediment flux over spring tide with storm waves from 220N

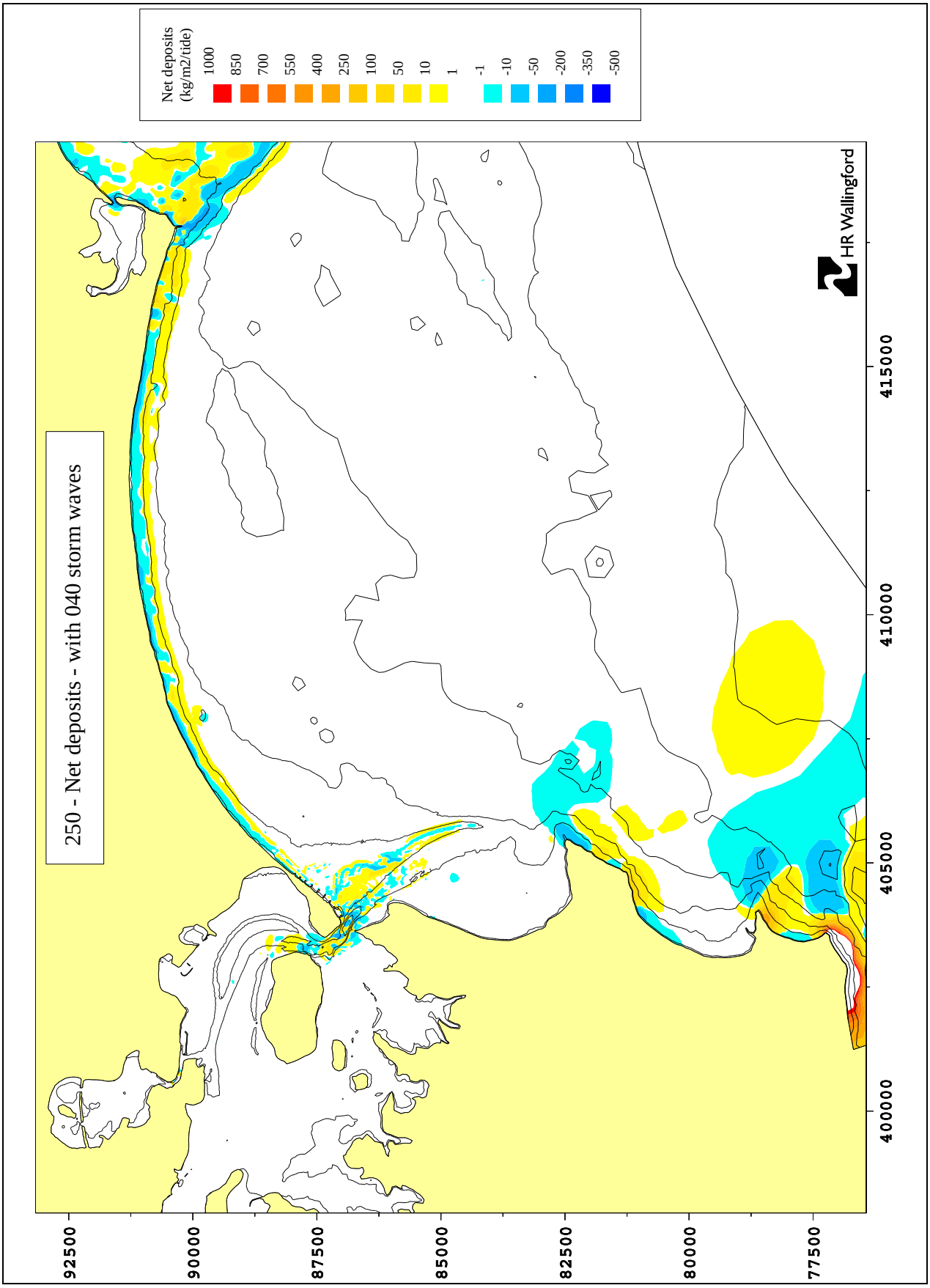

Figure 33 Net patterns of erosion and deposition over a spring tide with storm waves from 220N

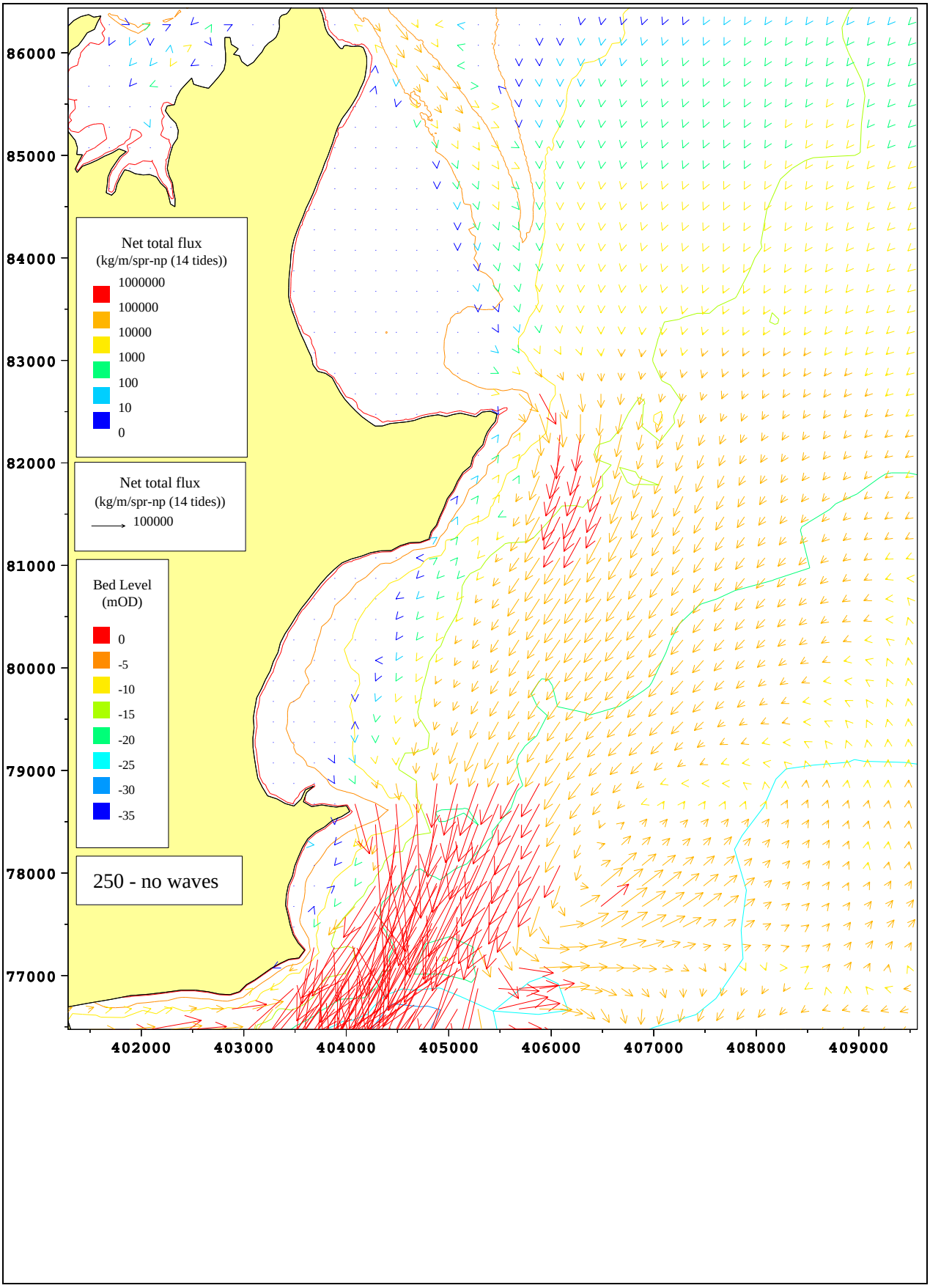

Figure 34 Net sediment flux over spring/neap period, Durleston Head to Poole Harbour

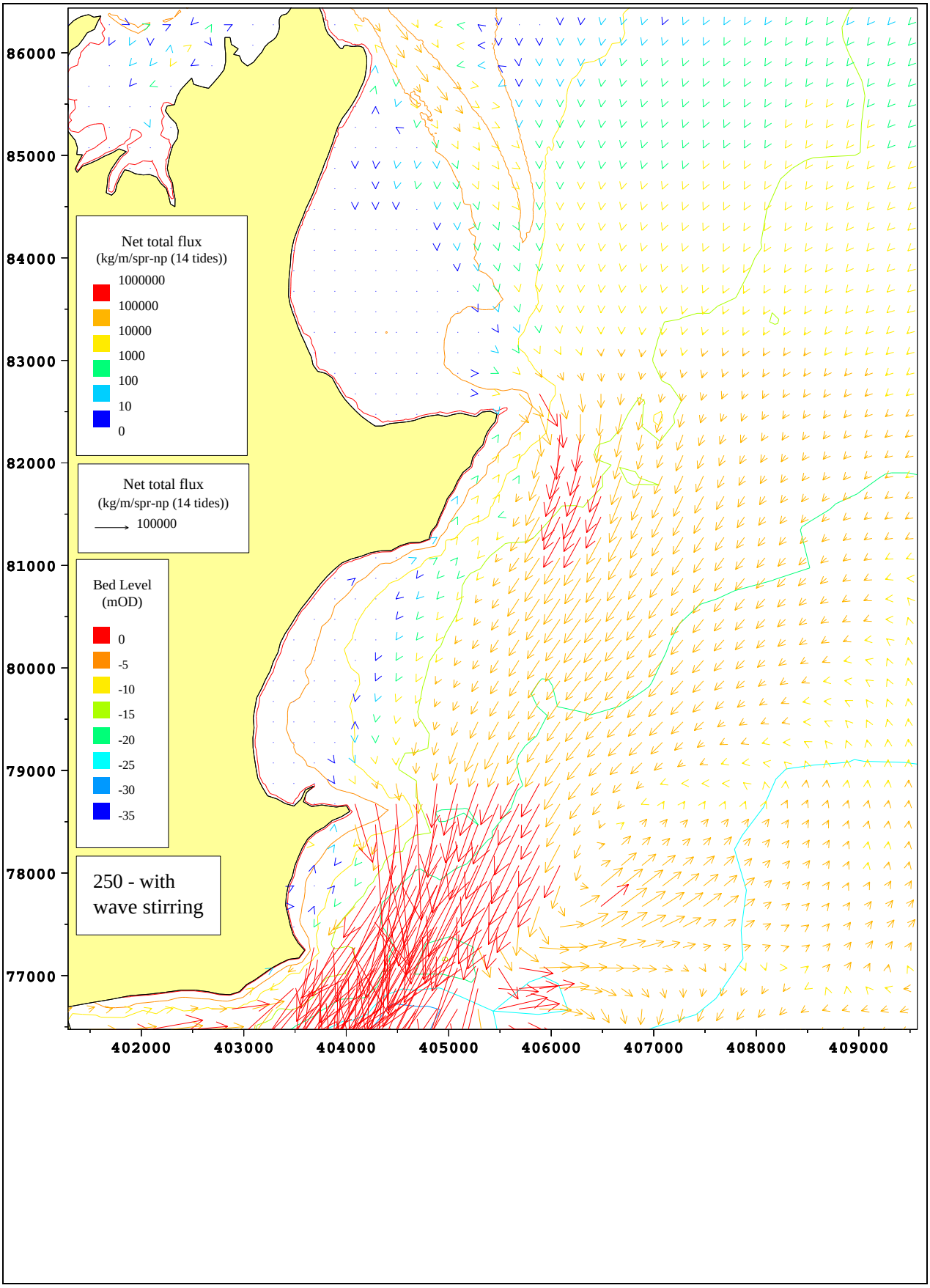

Figure 35 Net sediment flux over spring/neap period with wave stirring, Durleston Head to Poole Harbour

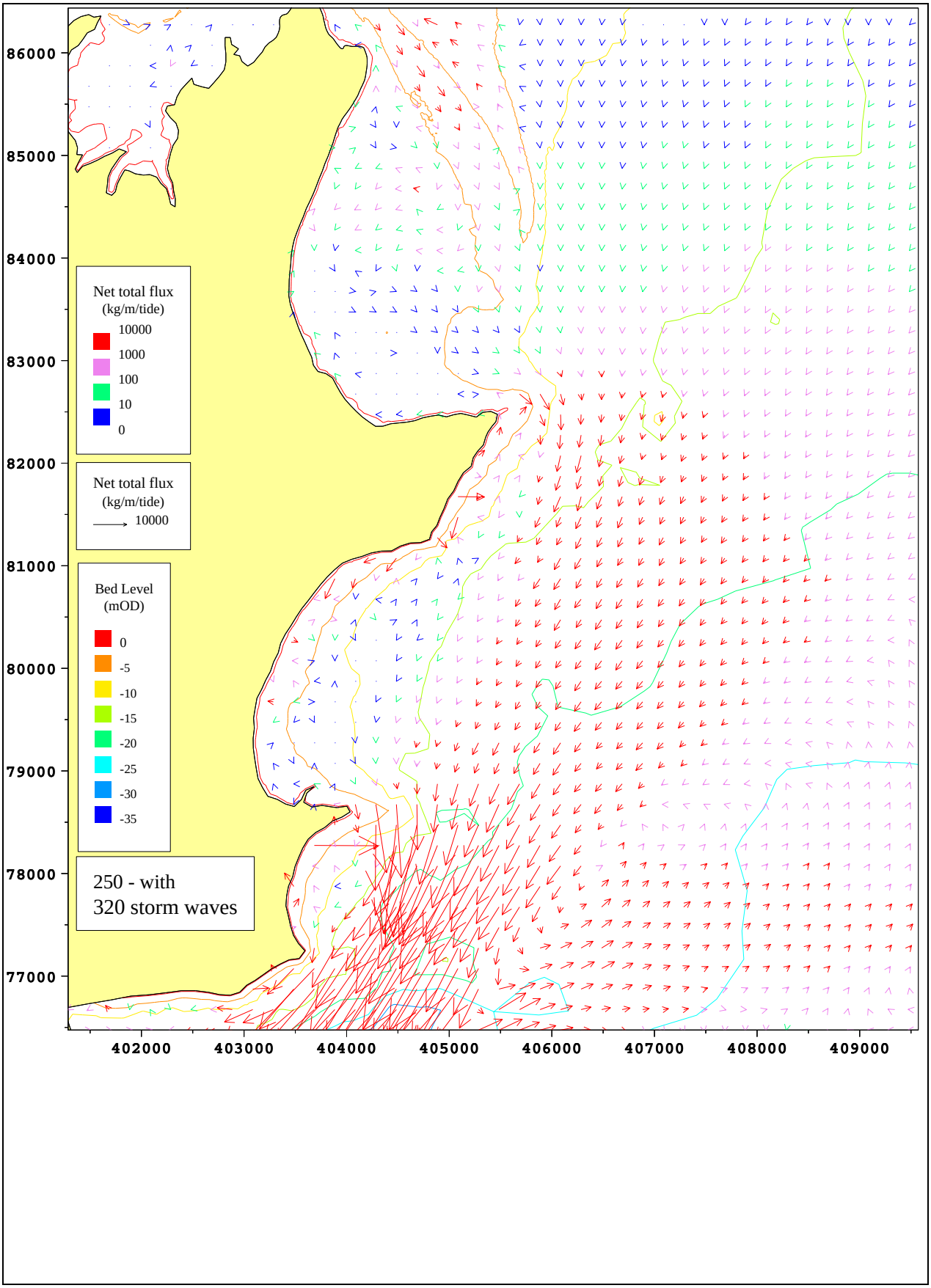

Figure 36 Net sediment flux over spring tide with storm waves from 140N, Durleston Head to Poole Harbour

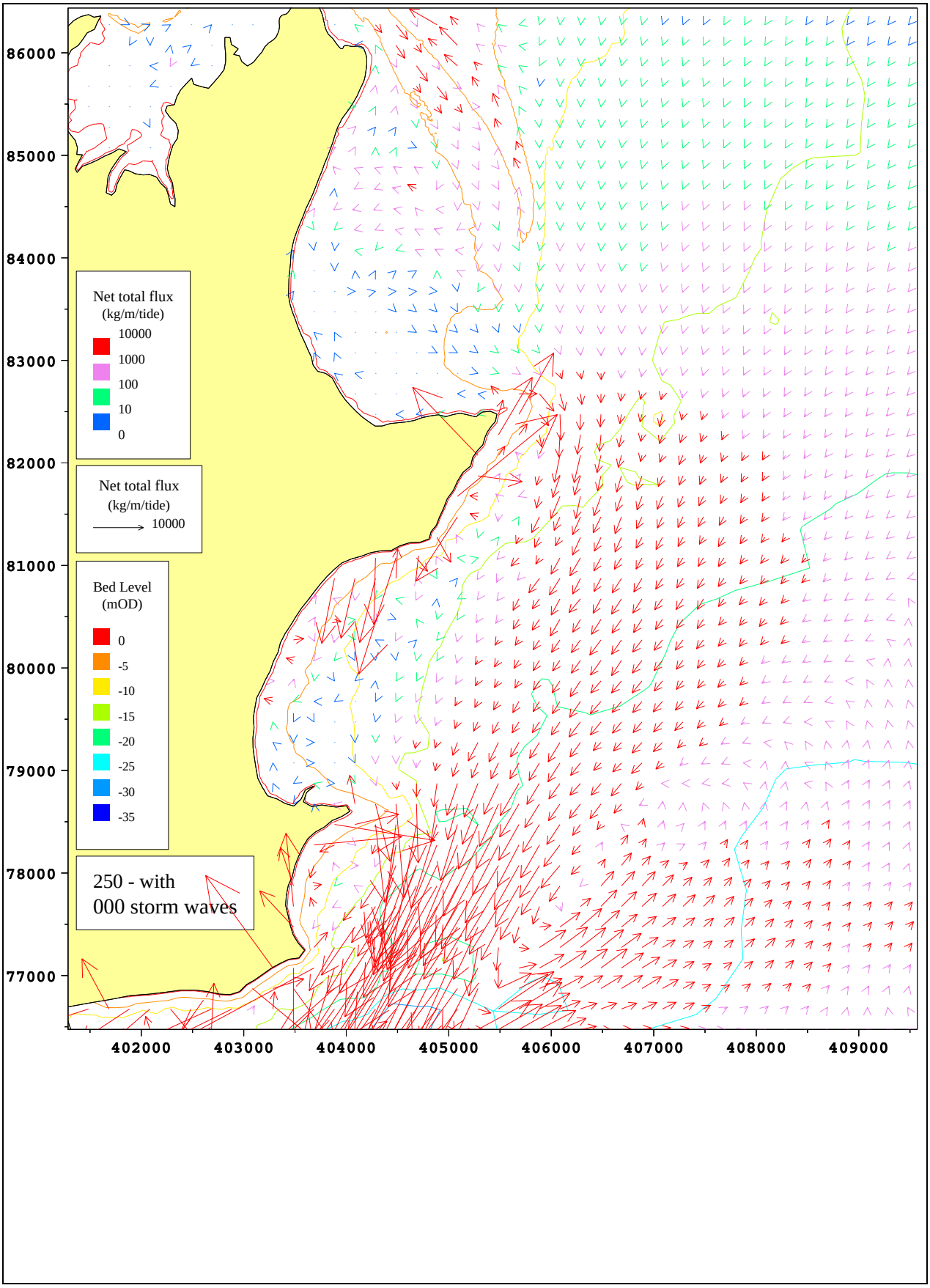

Figure 37 Net sediment flux over spring tide with storm waves from the South, Durleston Head to Poole Harbour

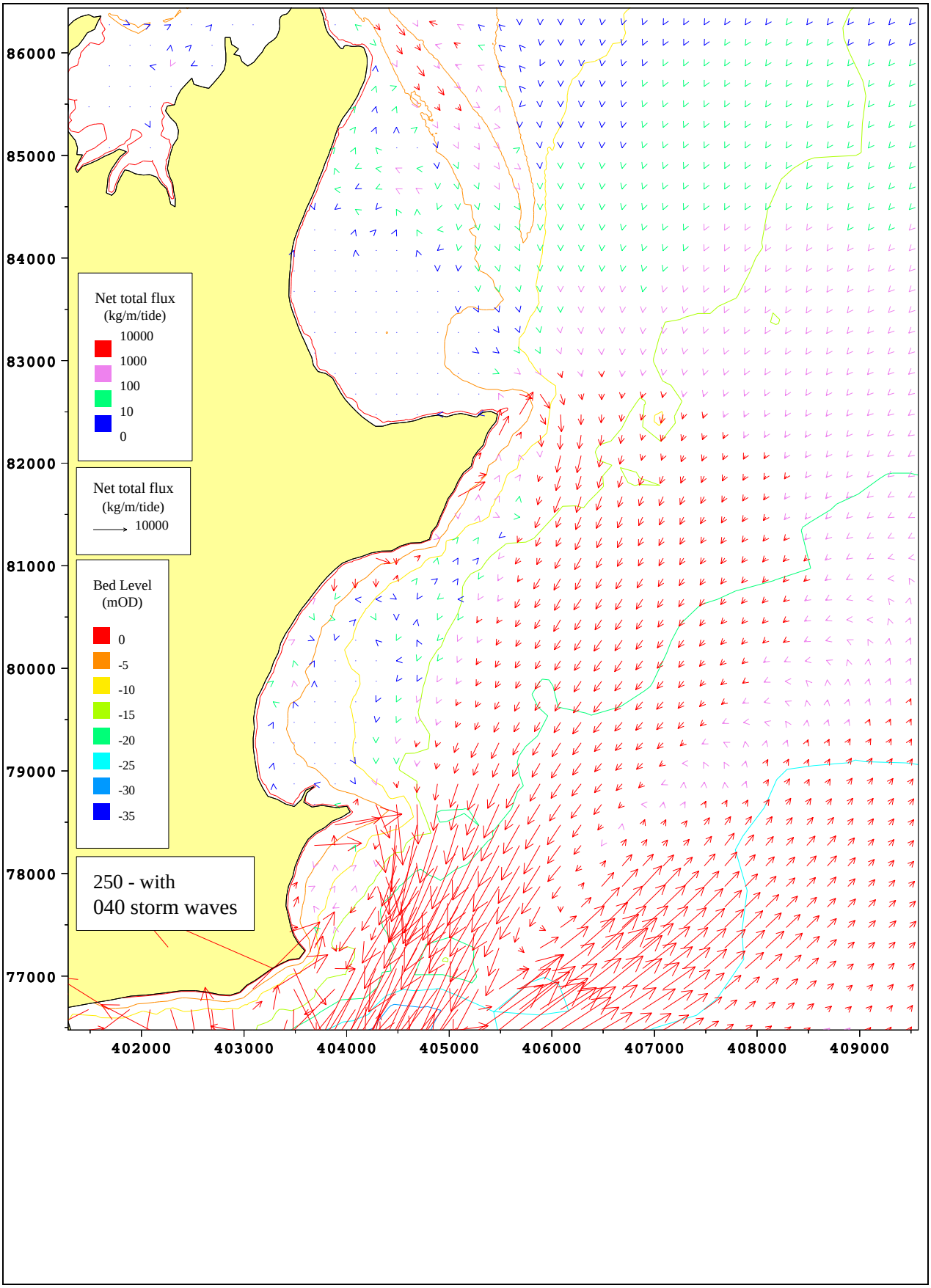

Figure 38 Net sediment flux over spring tide with storm waves from 220N, Durleston Head to Poole Harbour

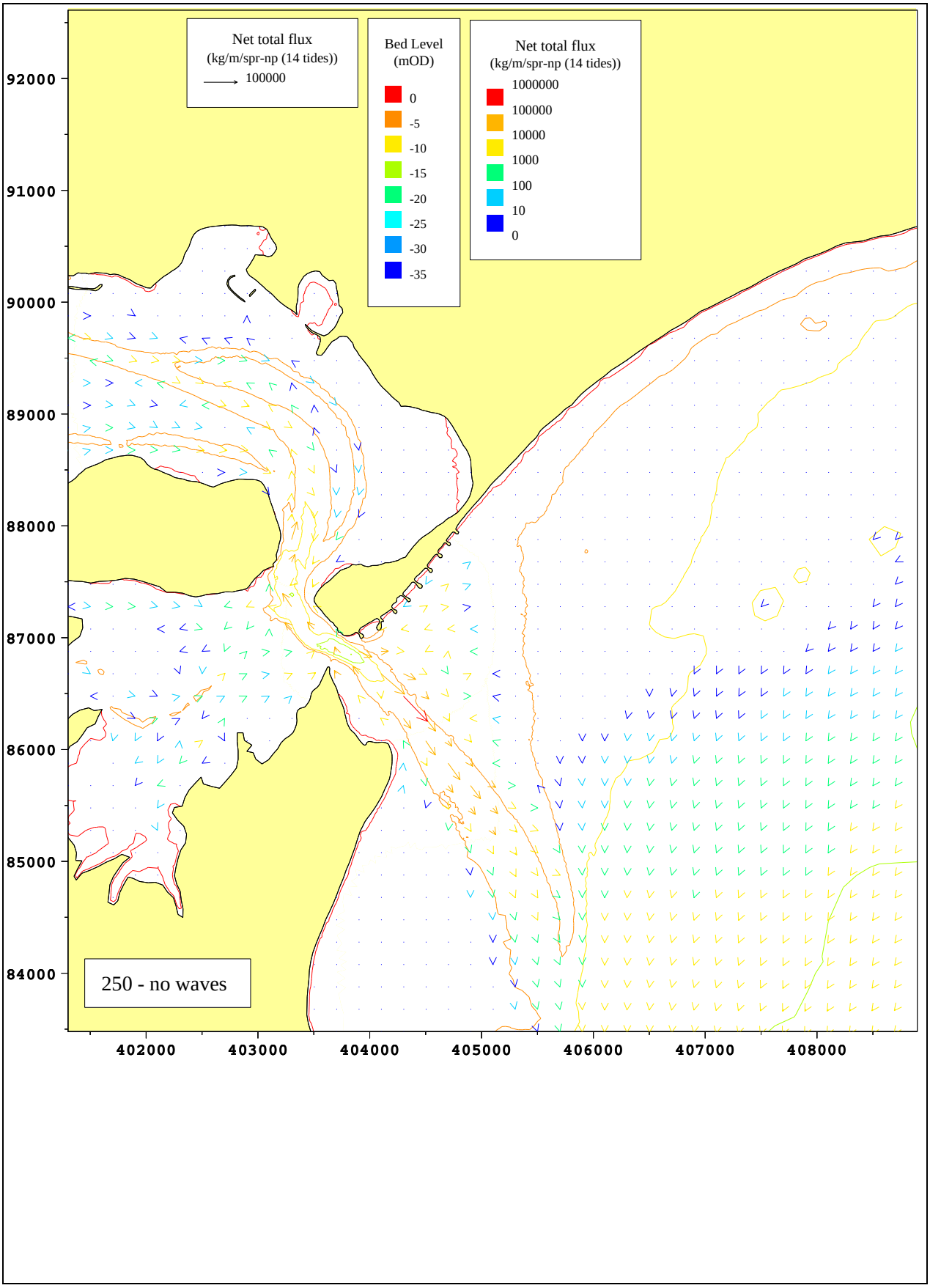

Figure 39 Net sediment flux over spring/neap period, Poole Harbour Entrance

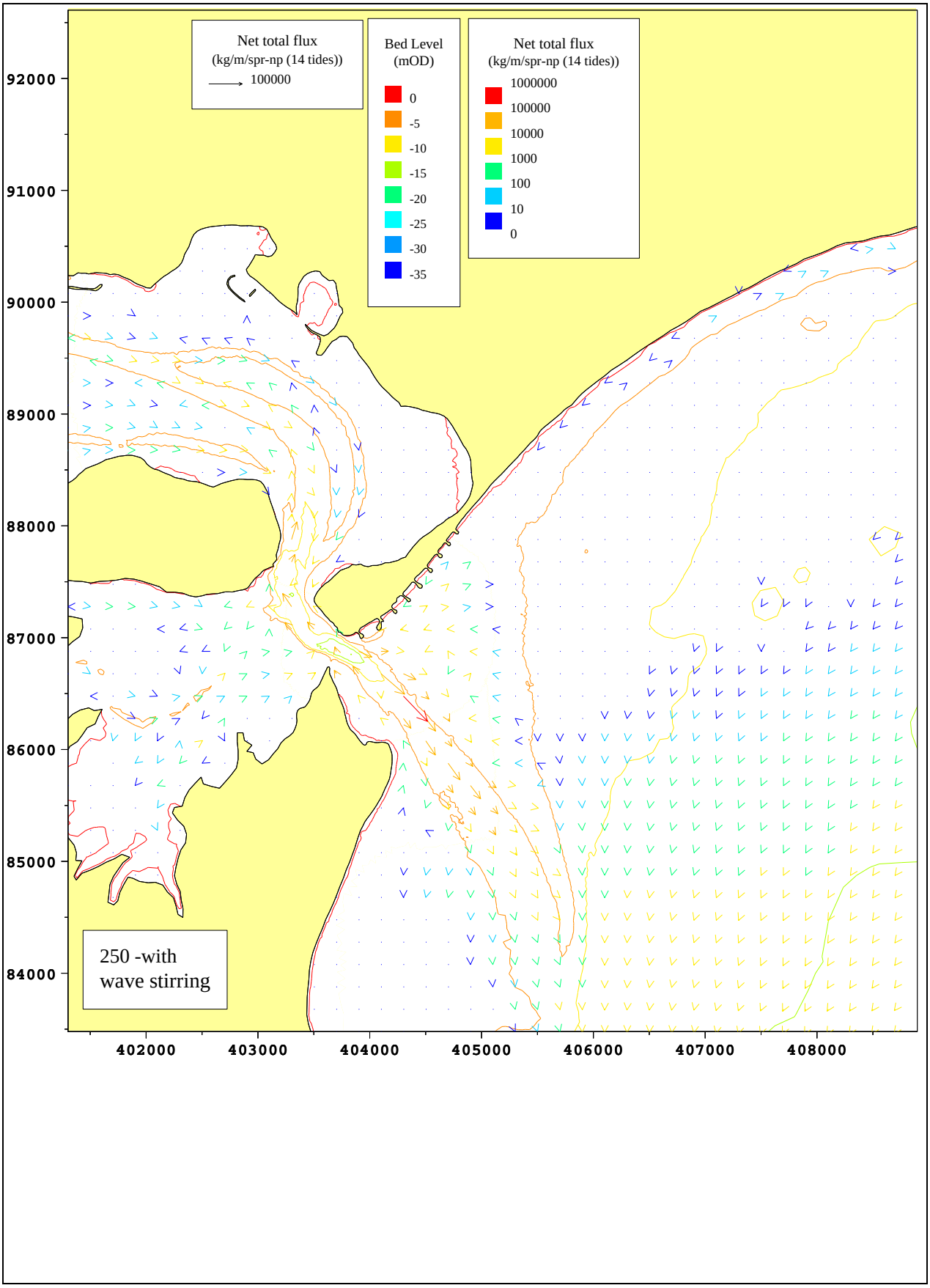

Figure 40 Net sediment flux over spring/neap period with wave stirring, Poole Harbour Entrance

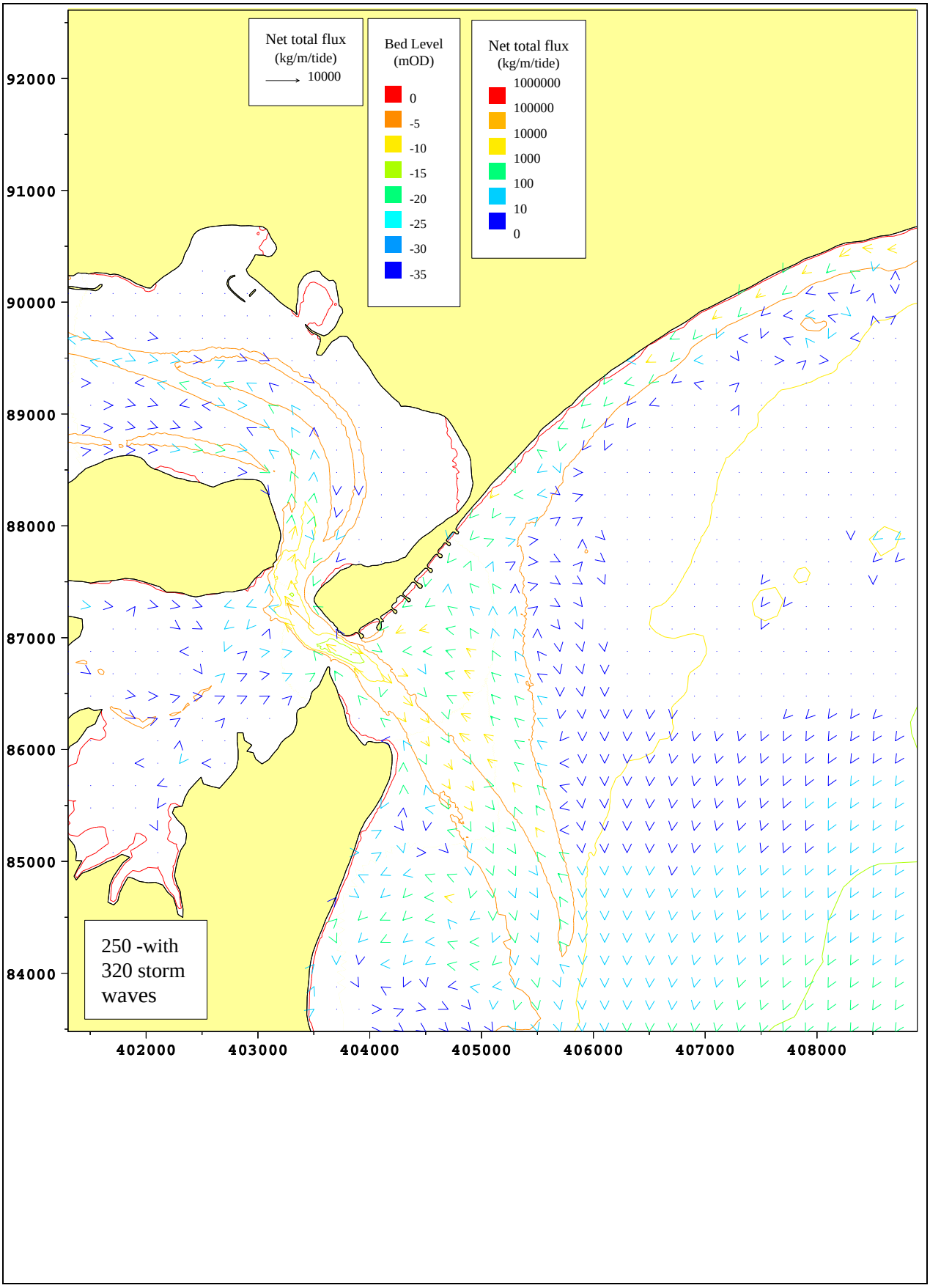

Figure 41 Net sediment flux over spring tide with storm waves from 140N, Poole Harbour Entrance

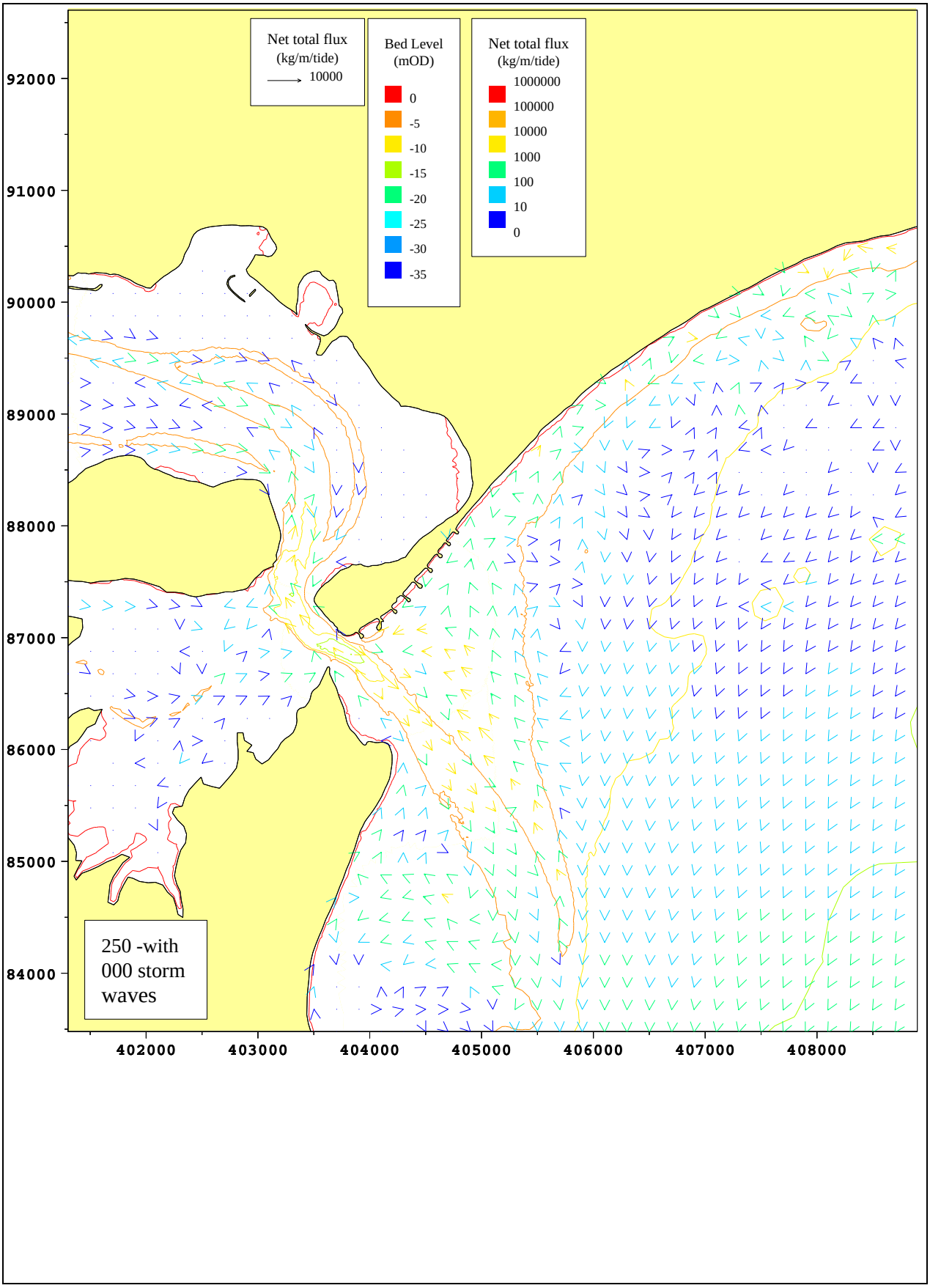

Figure 42 Net sediment flux over spring tide with storm waves from the South, Poole Harbour Entrance

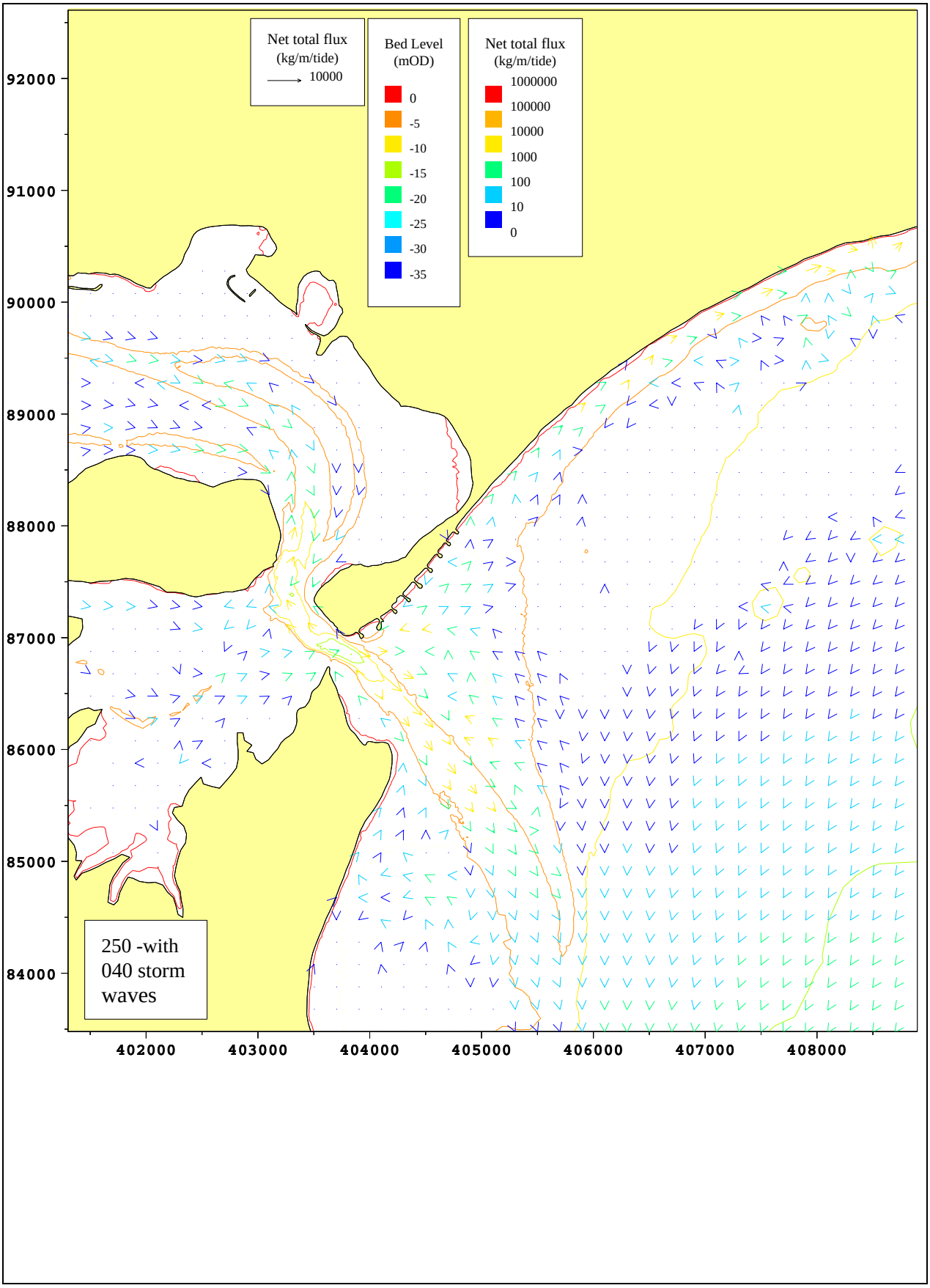

Figure 43 Net sediment flux over spring tide with storm waves from 220N, Poole Harbour Entrance

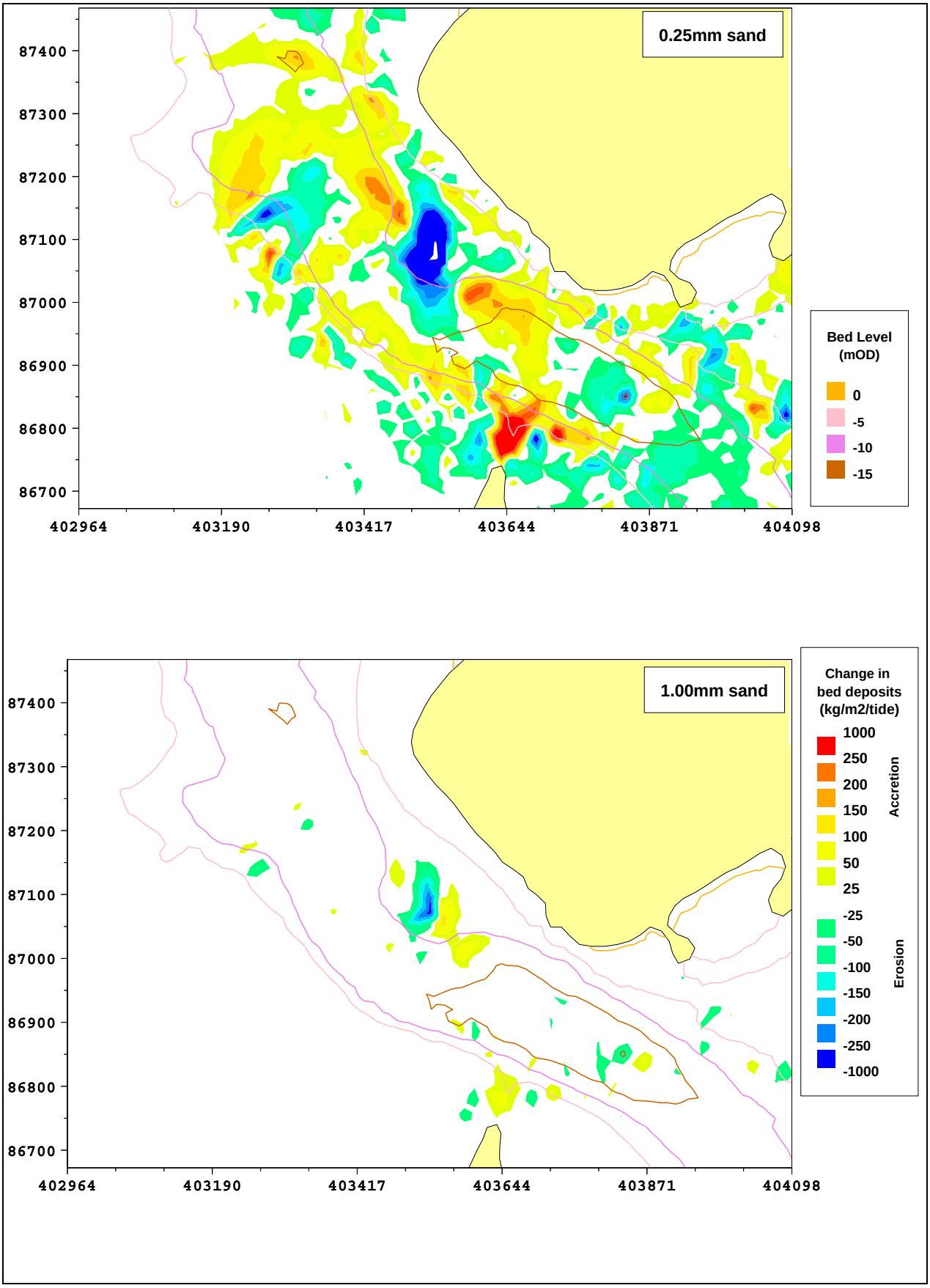

Figure 44 Net deposits over a spring tide in the area of Chapmans Peak

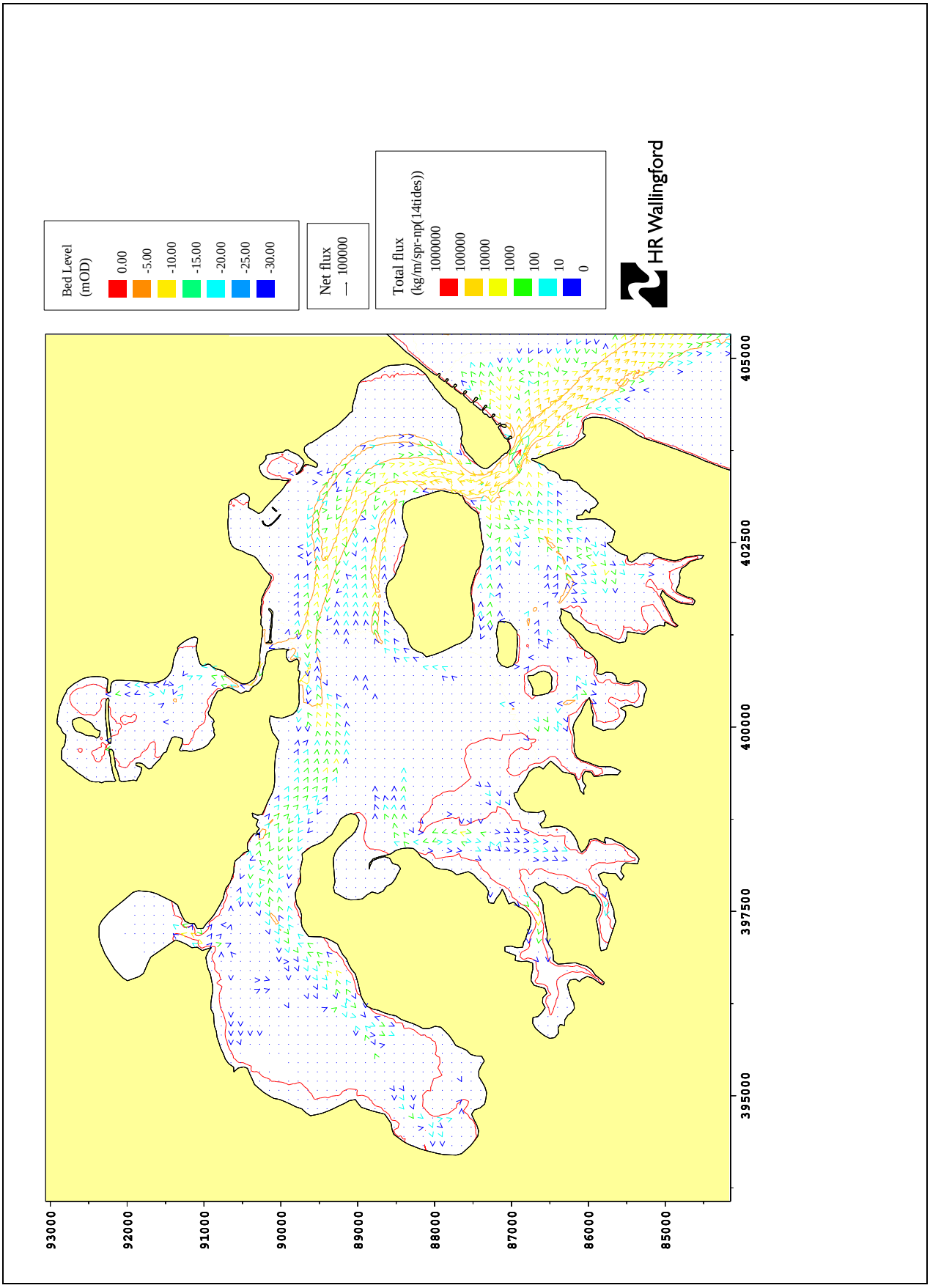

Figure 45 Net sediment flux over a spring/neap period, Poole Harbour

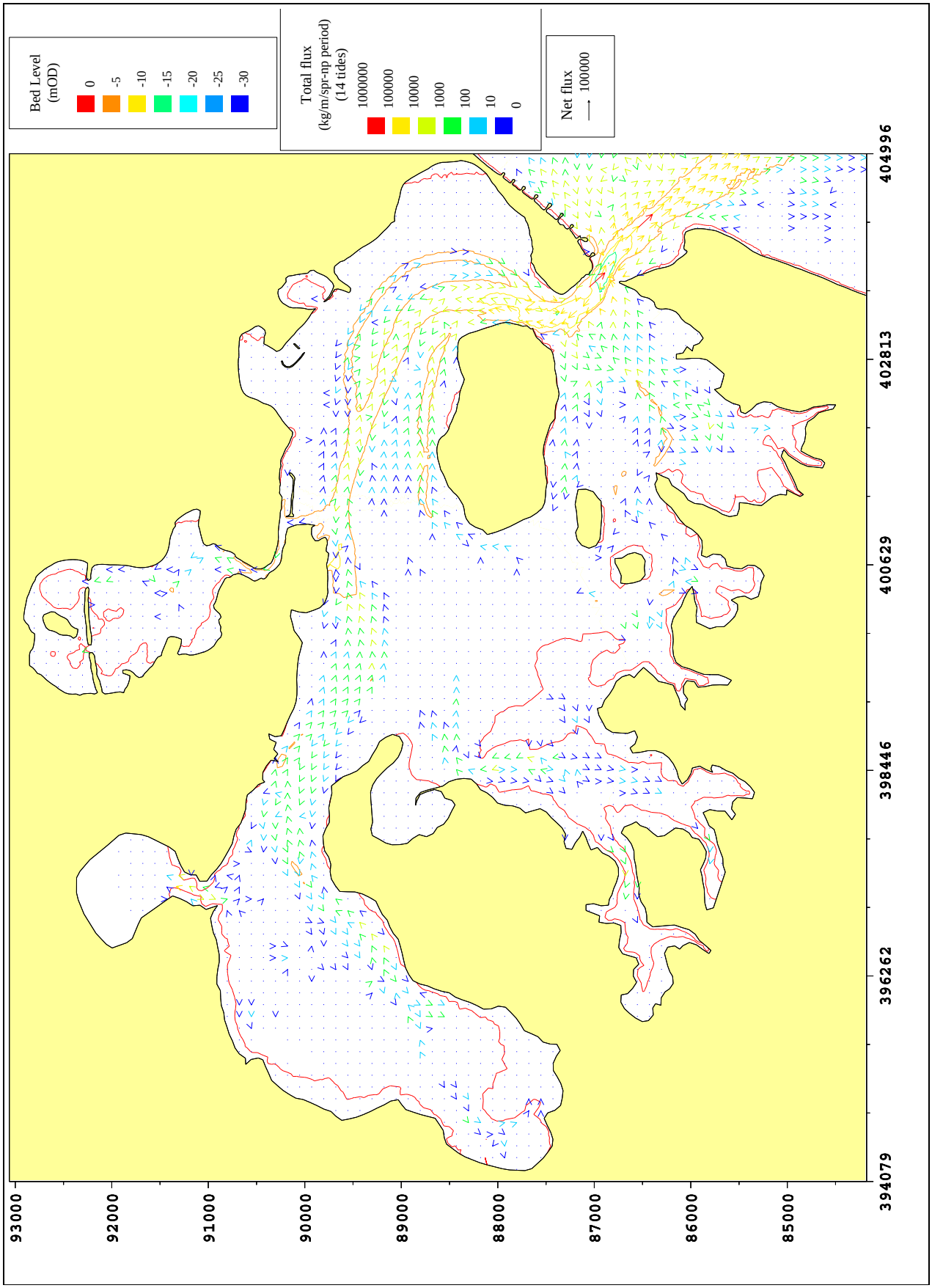

Figure 46 Net sediment flux over a spring/neap period with wave stirring due to wave propagation from offshore, Poole Harbour

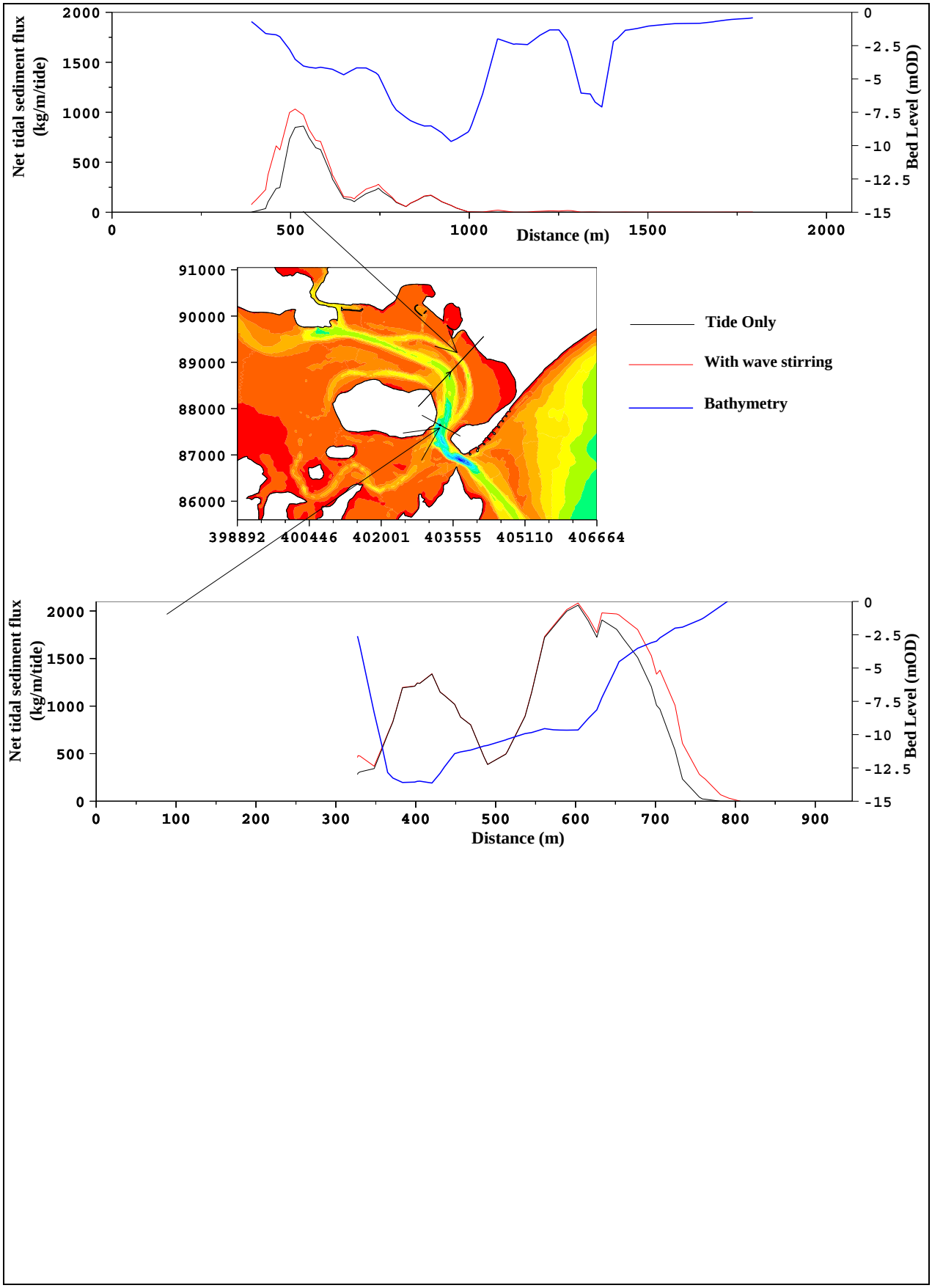

Figure 47 Net sediment flux over a spring tide with local wave stirring

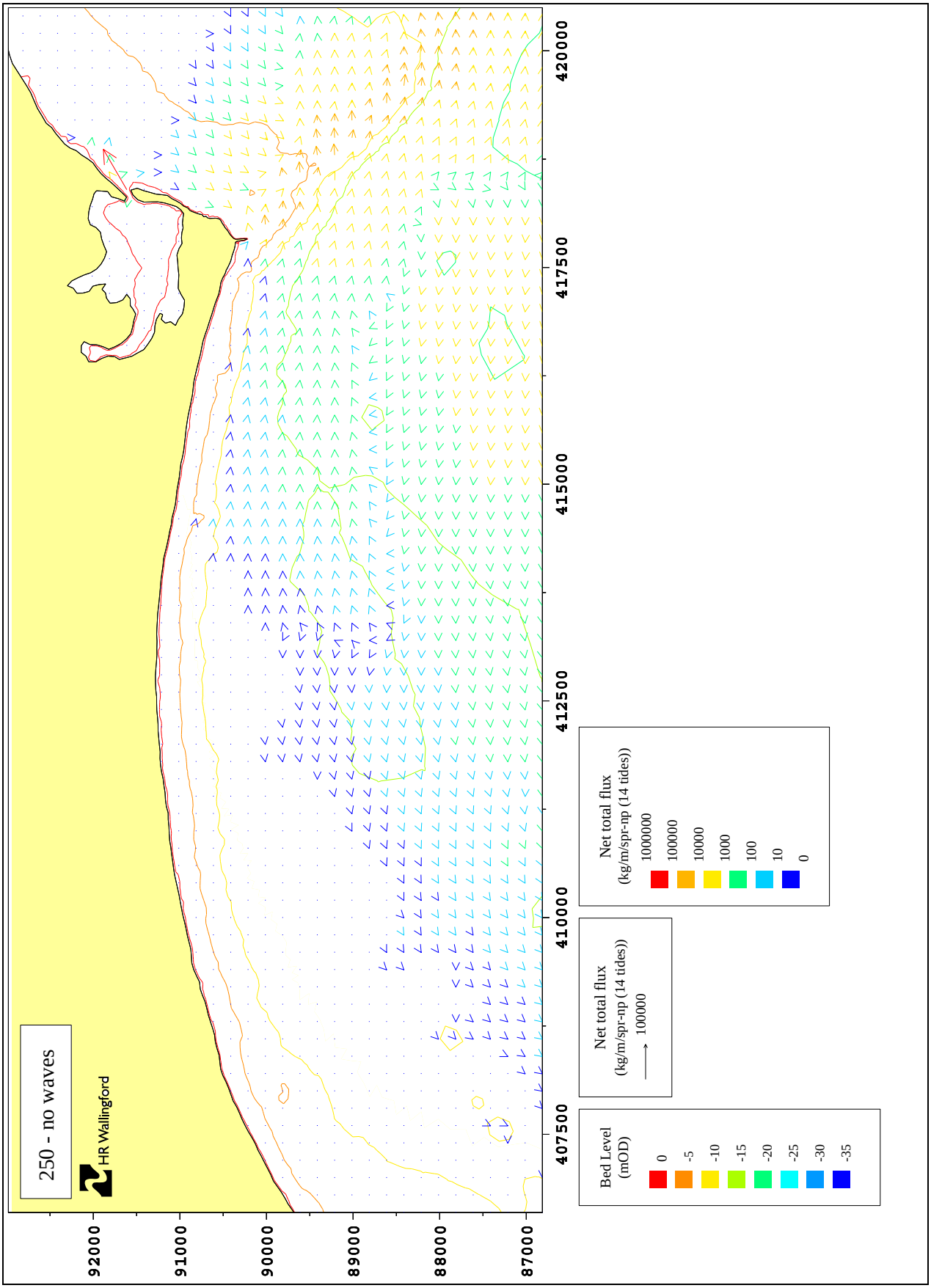

Figure 48 Net sediment flux over spring/neap period, Bournemouth to Christchurch

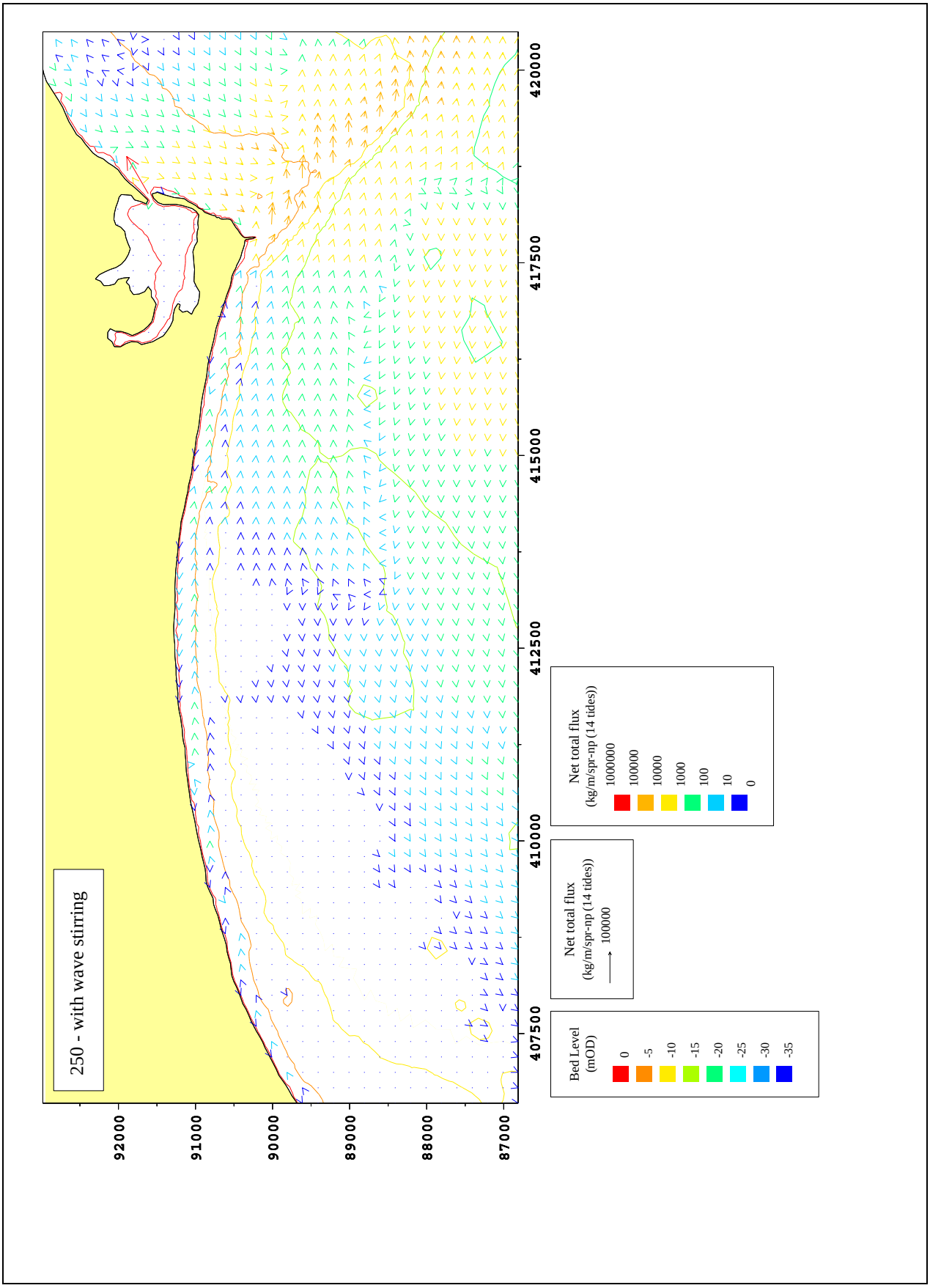

Figure 49 Net sediment flux over spring/neap period with wave stirring, Bournemouth to Christchurch

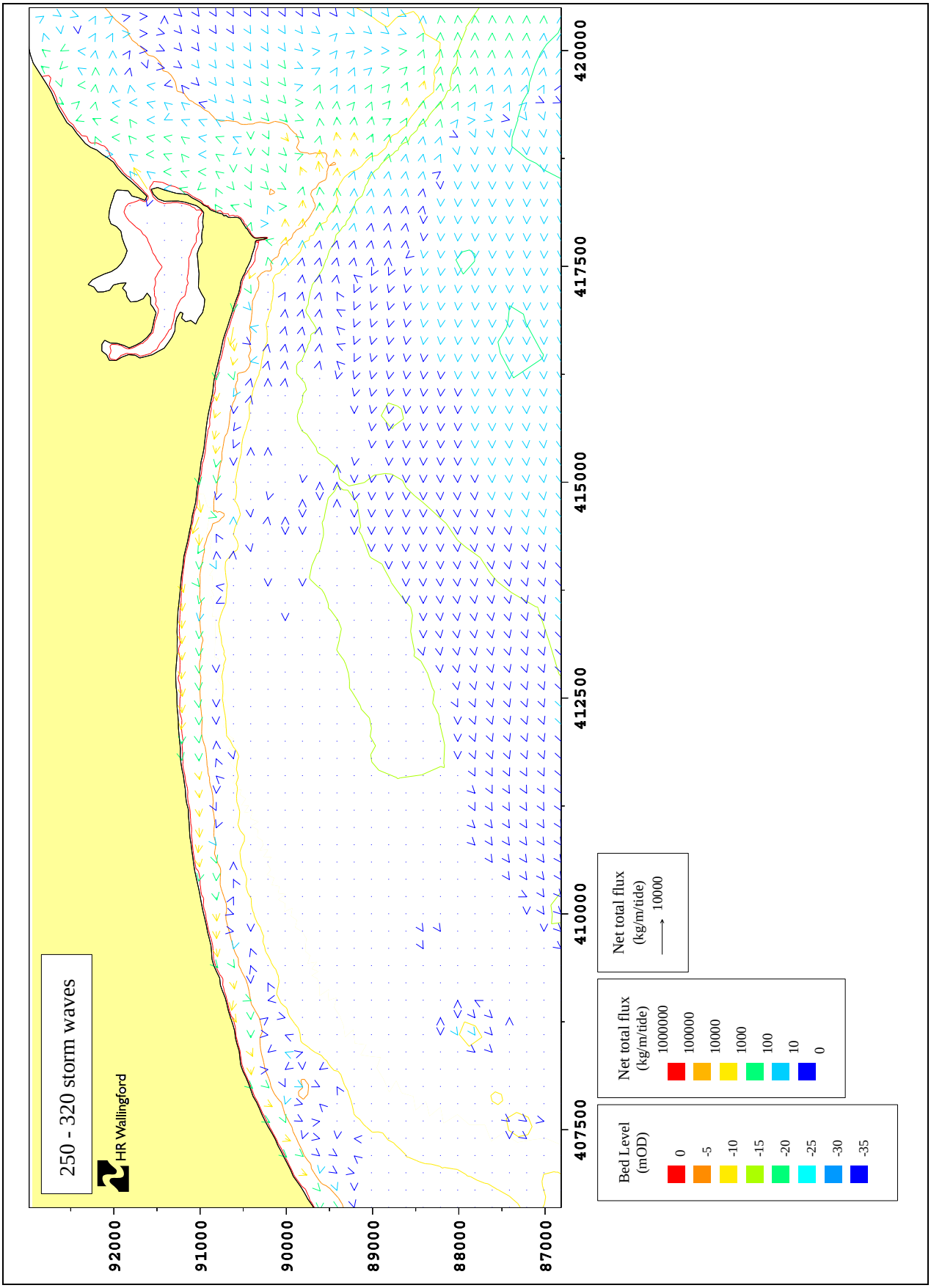

Figure 50 Net sediment flux over spring tide with storm waves from 140N, Bournemouth to Christchurch

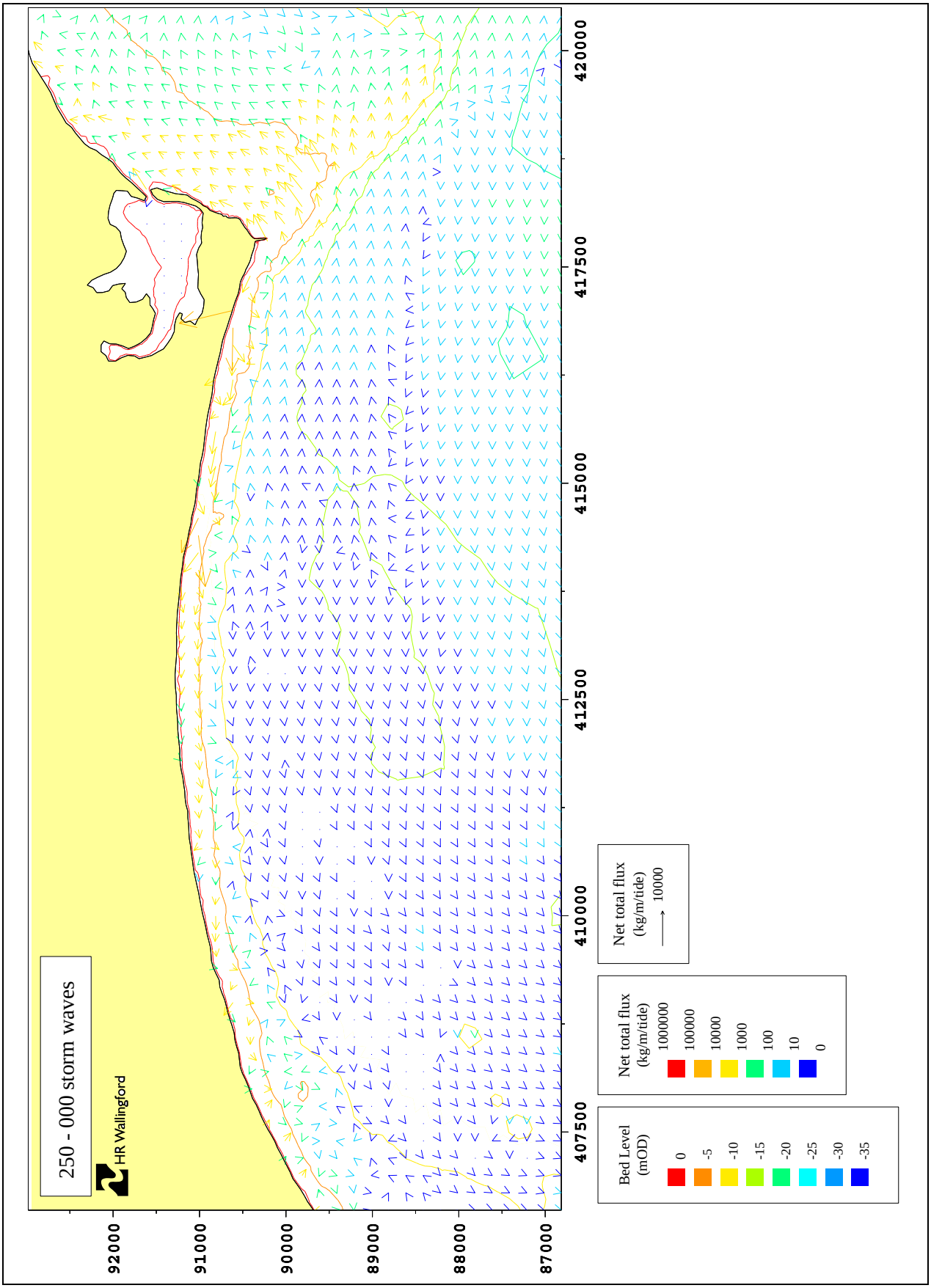

Figure 51 Net sediment flux over spring tide with storm waves from the South, Bournemouth to Christchurch

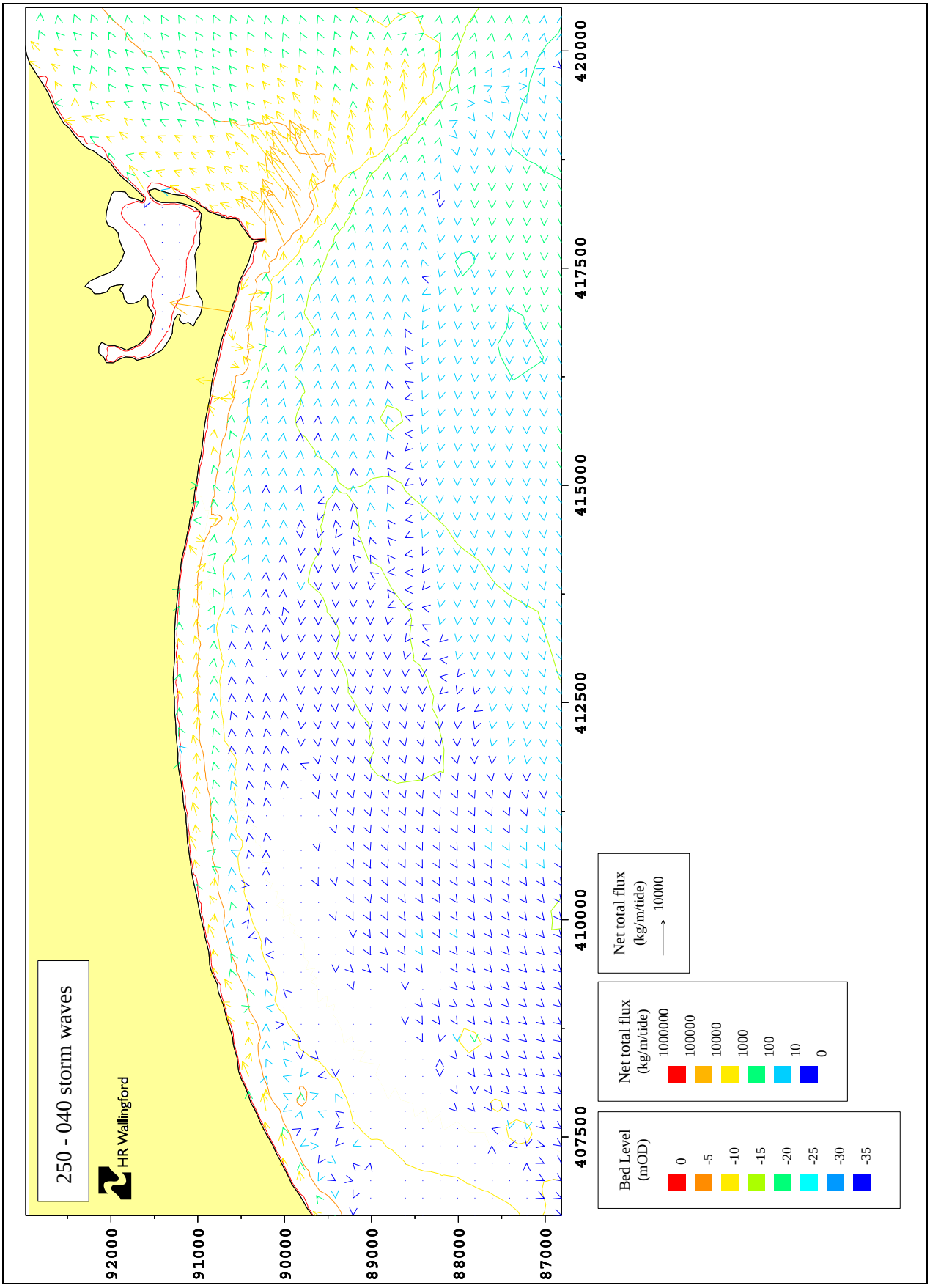

Figure 52 Net sediment flux over spring tide with storm waves from 220N, Bournemouth to Christchurch

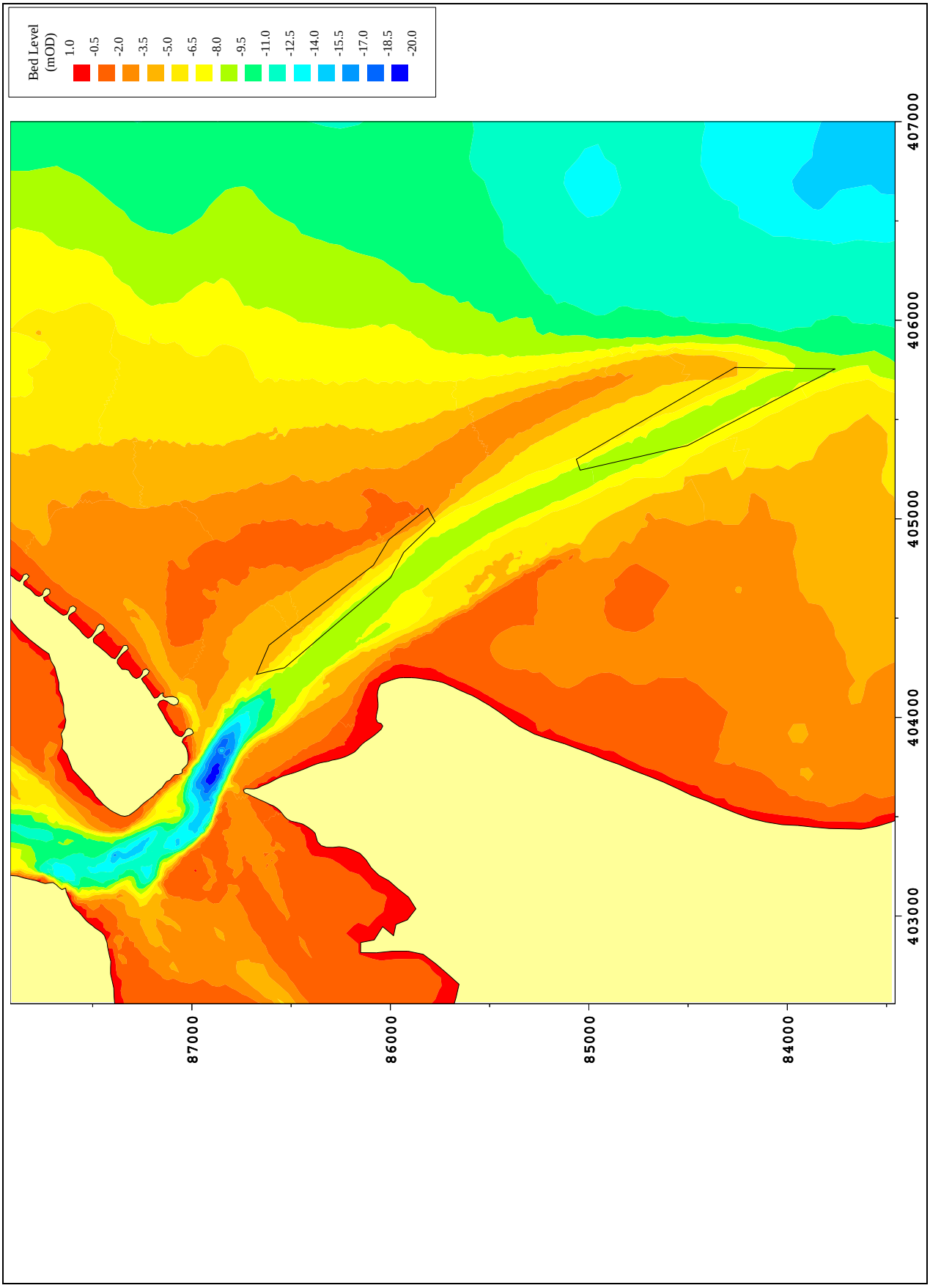

Figure 53 Existing bathymetry in the vicinity of the proposed dredging

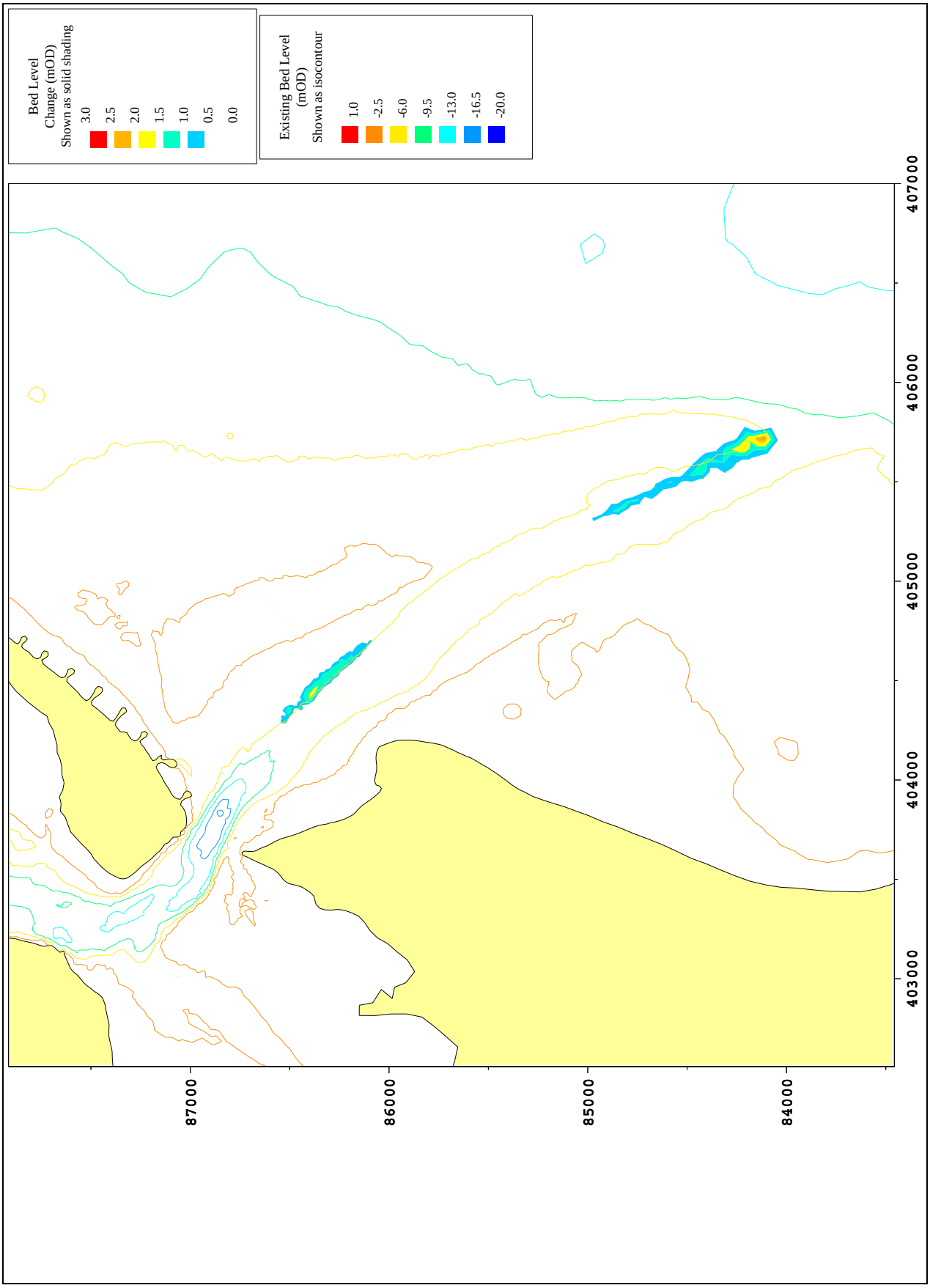

Figure 54 Change in bathymetry following dredging

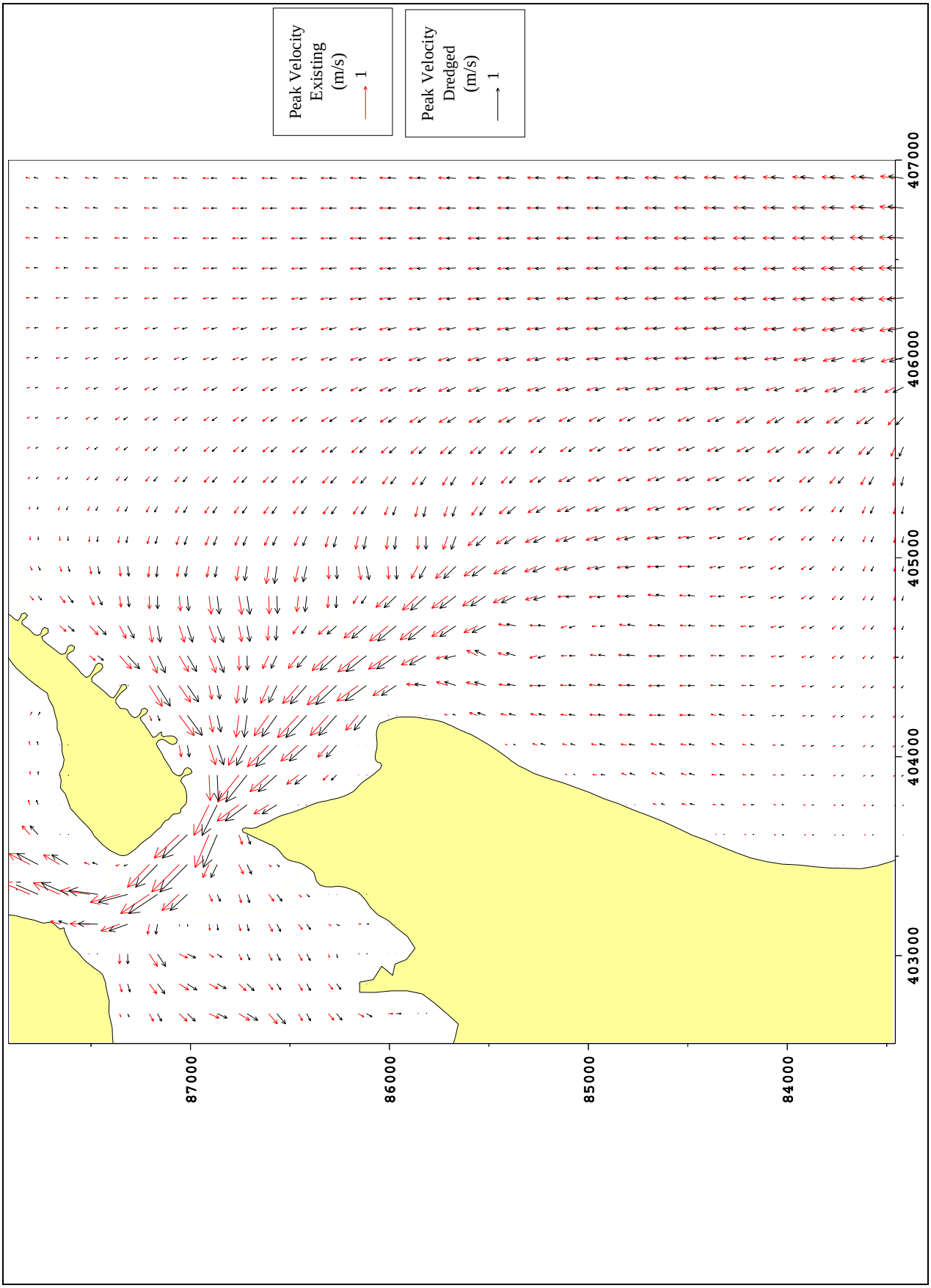

Figure 55 Spring peak flood currents: existing and dredged scenario

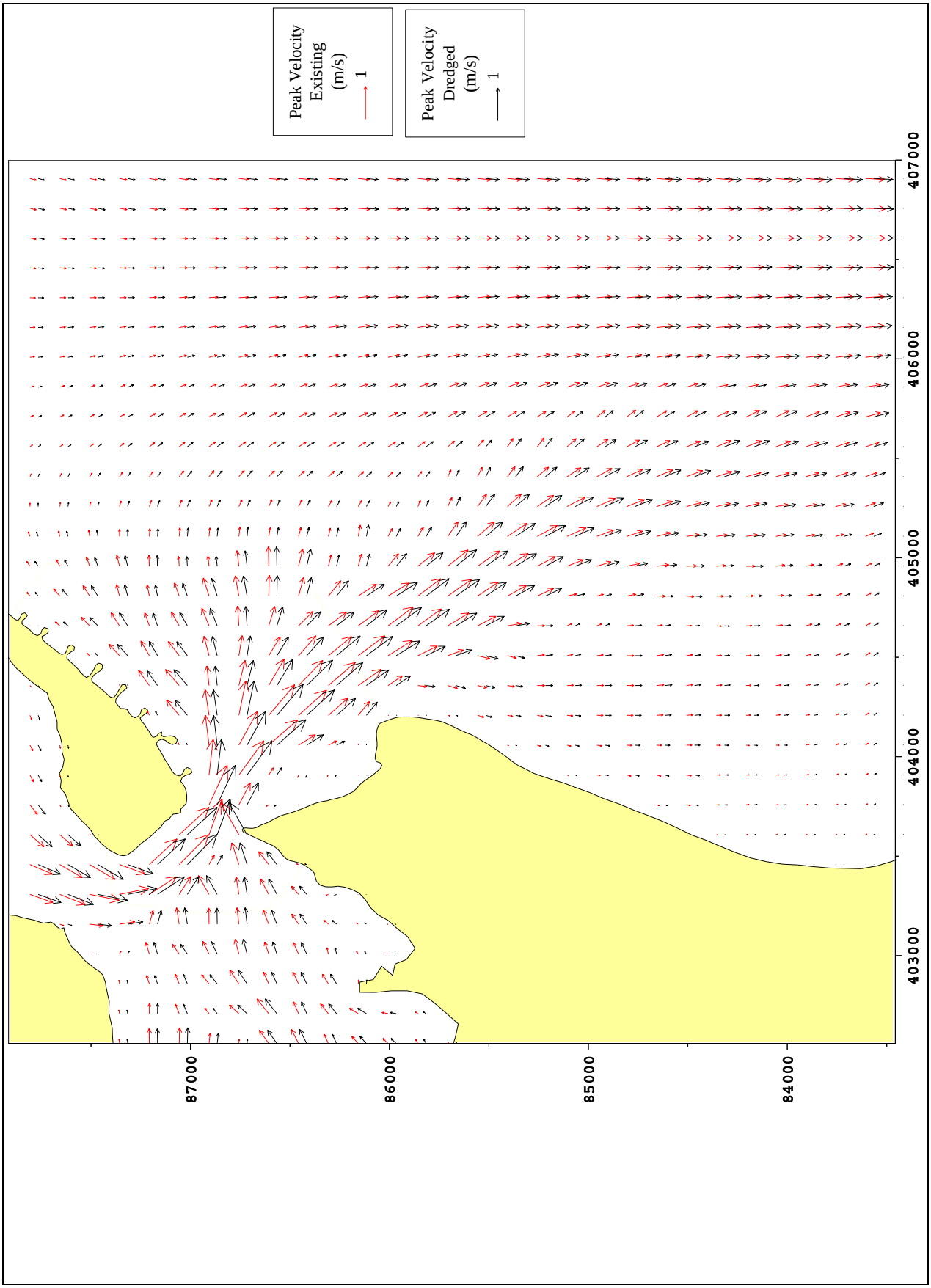

Figure 56 Spring tide peak ebb currents: existing and dredged scenario

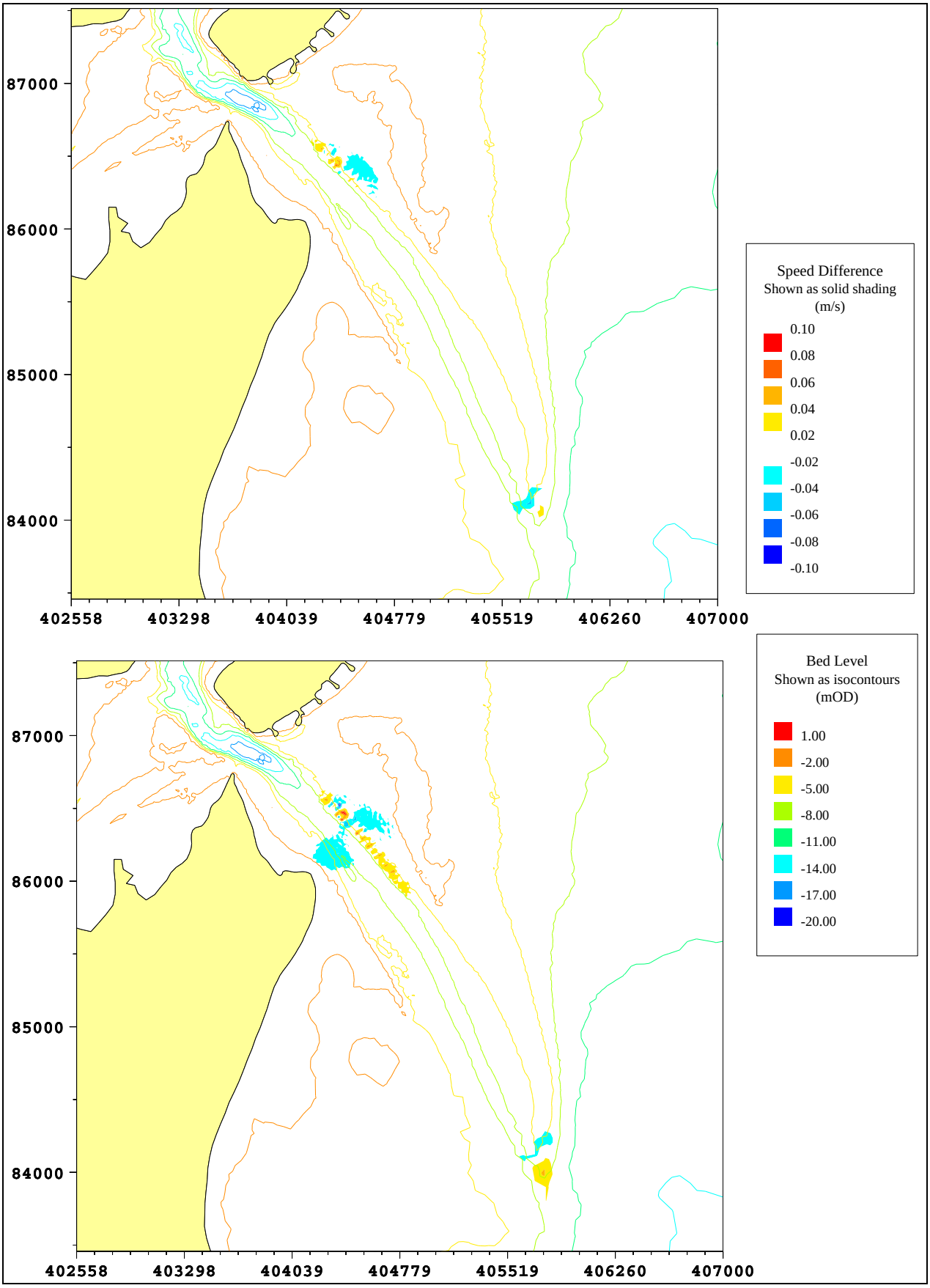

Figure 57 Change in peak tidal currents following dredging (top: flood, bottom: ebb)

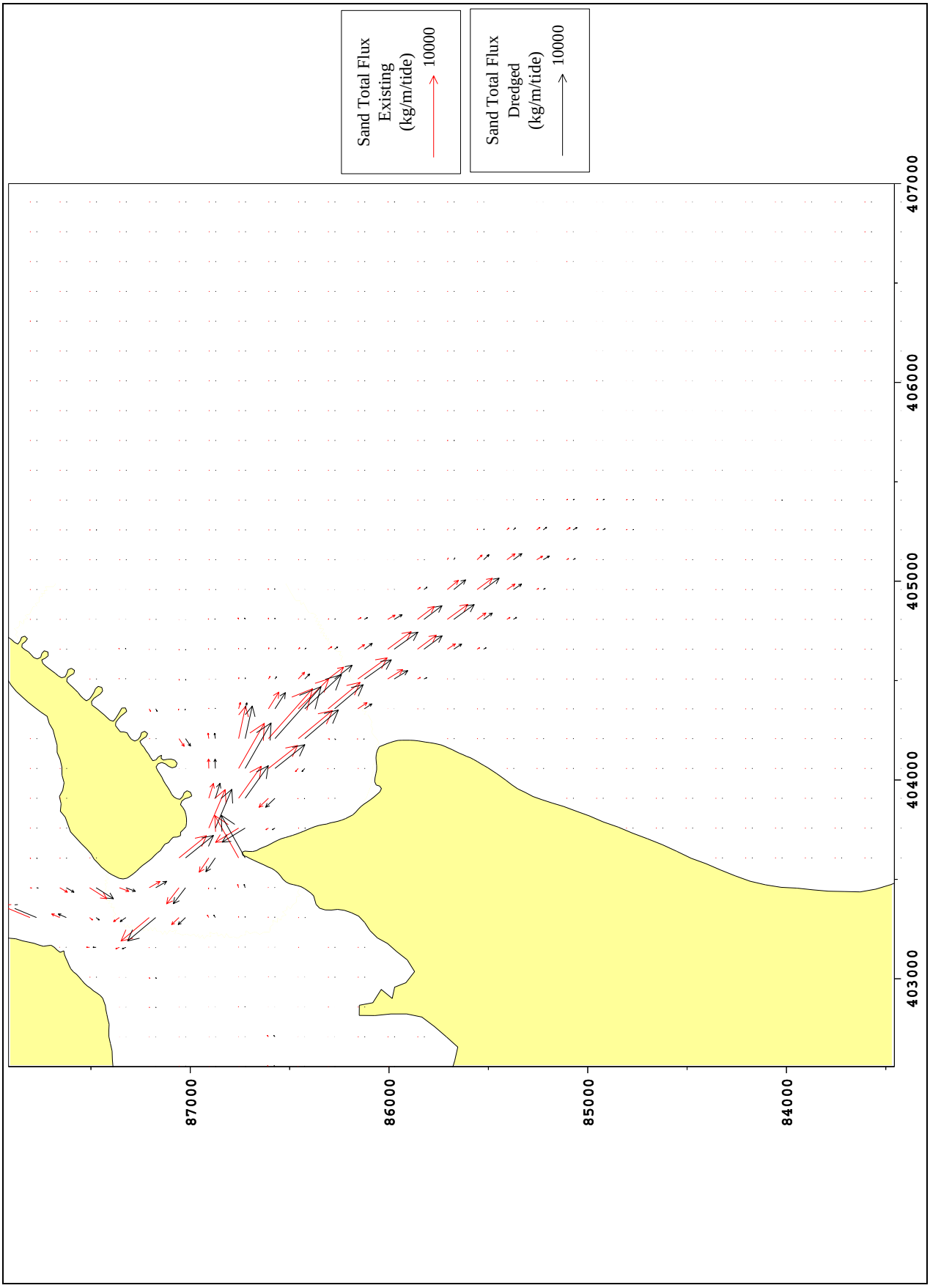

Figure 58 Spring tide net tidal sediment transport vectors: Existing and dredged scenario

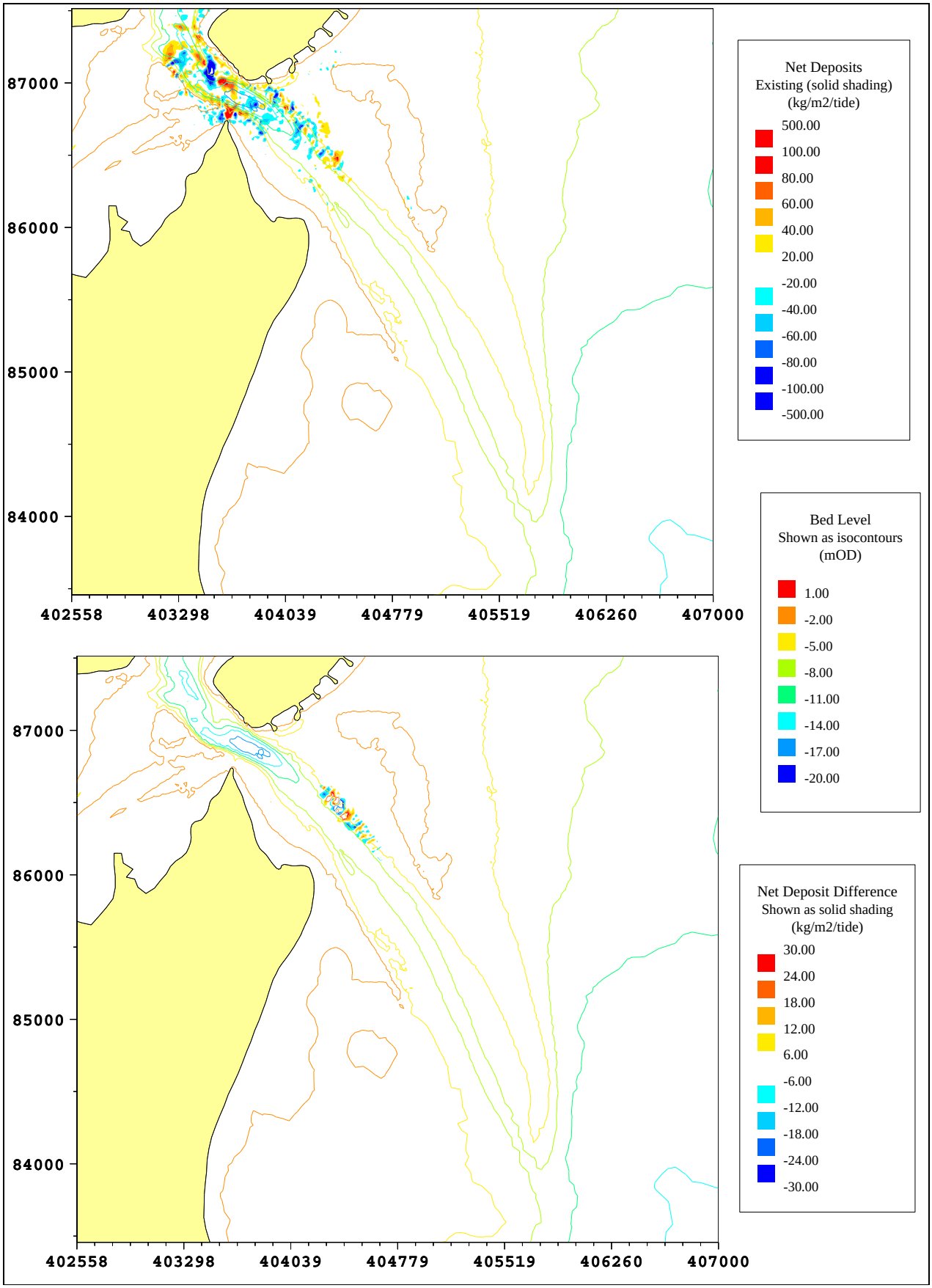

Figure 59 Existing net spring tide patterns of erosion and deposition (top), and changes due to dredging (bottom)

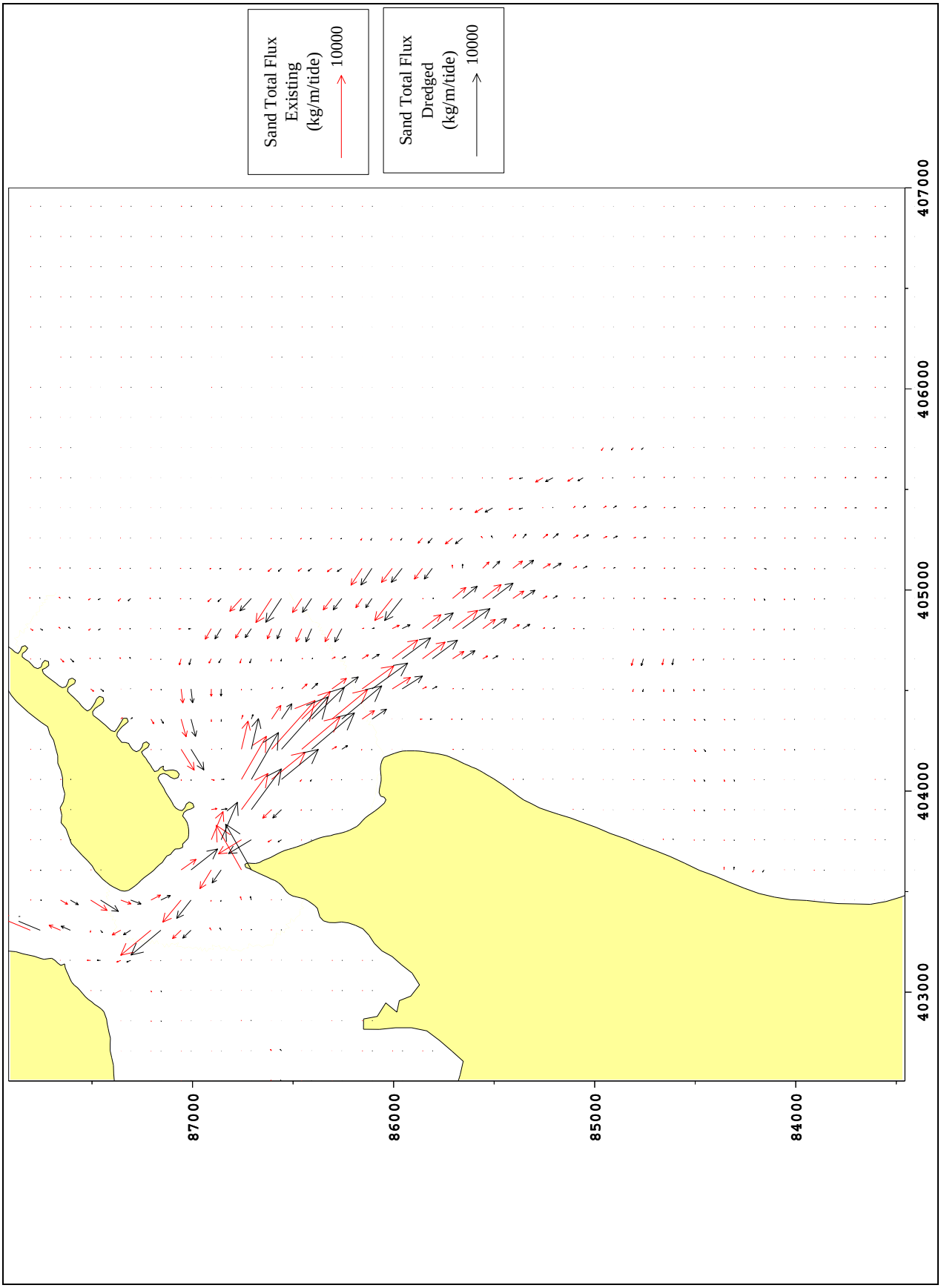

Figure 60 Net tidal sediment transport vectors under spring tides with storm waves from 140°N: existing and dredged scenario

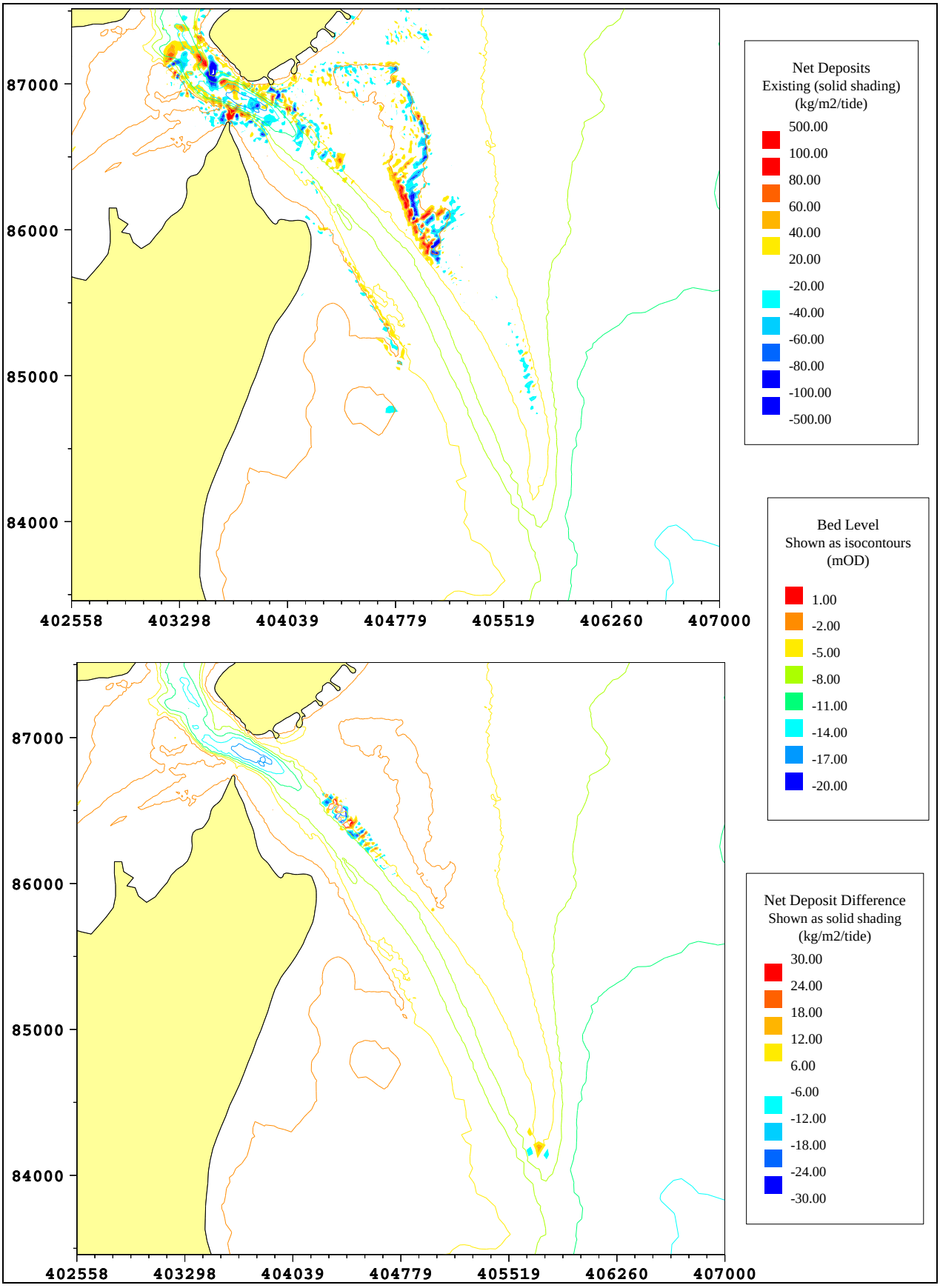

Figure 61 Existing net tidal patterns of erosion and deposition under spring tides with storm waves from 140°N (top), and changes due to dredging (bottom)

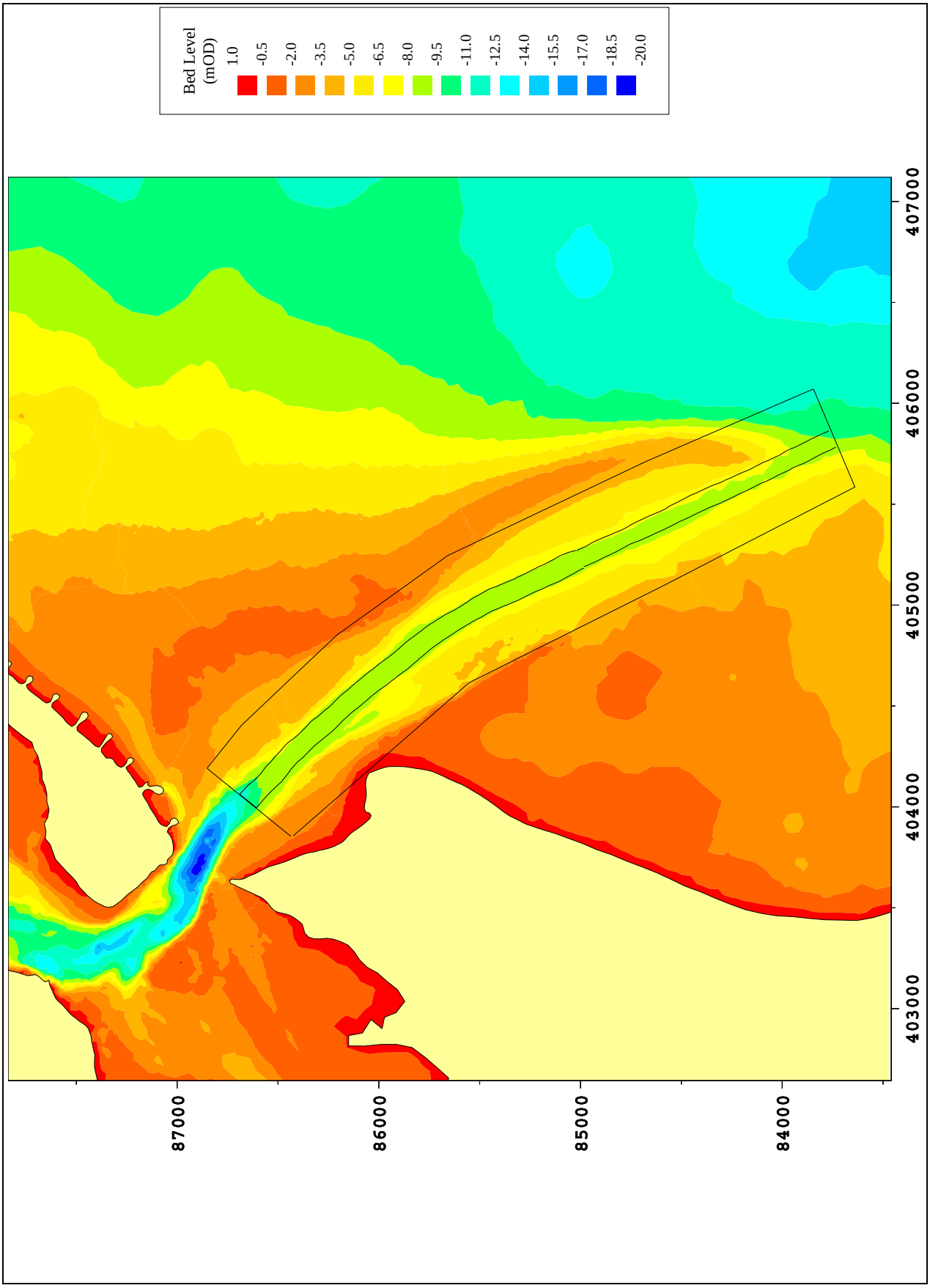

Figure 62 Existing bathymetry in the vicinity of the proposed dredging

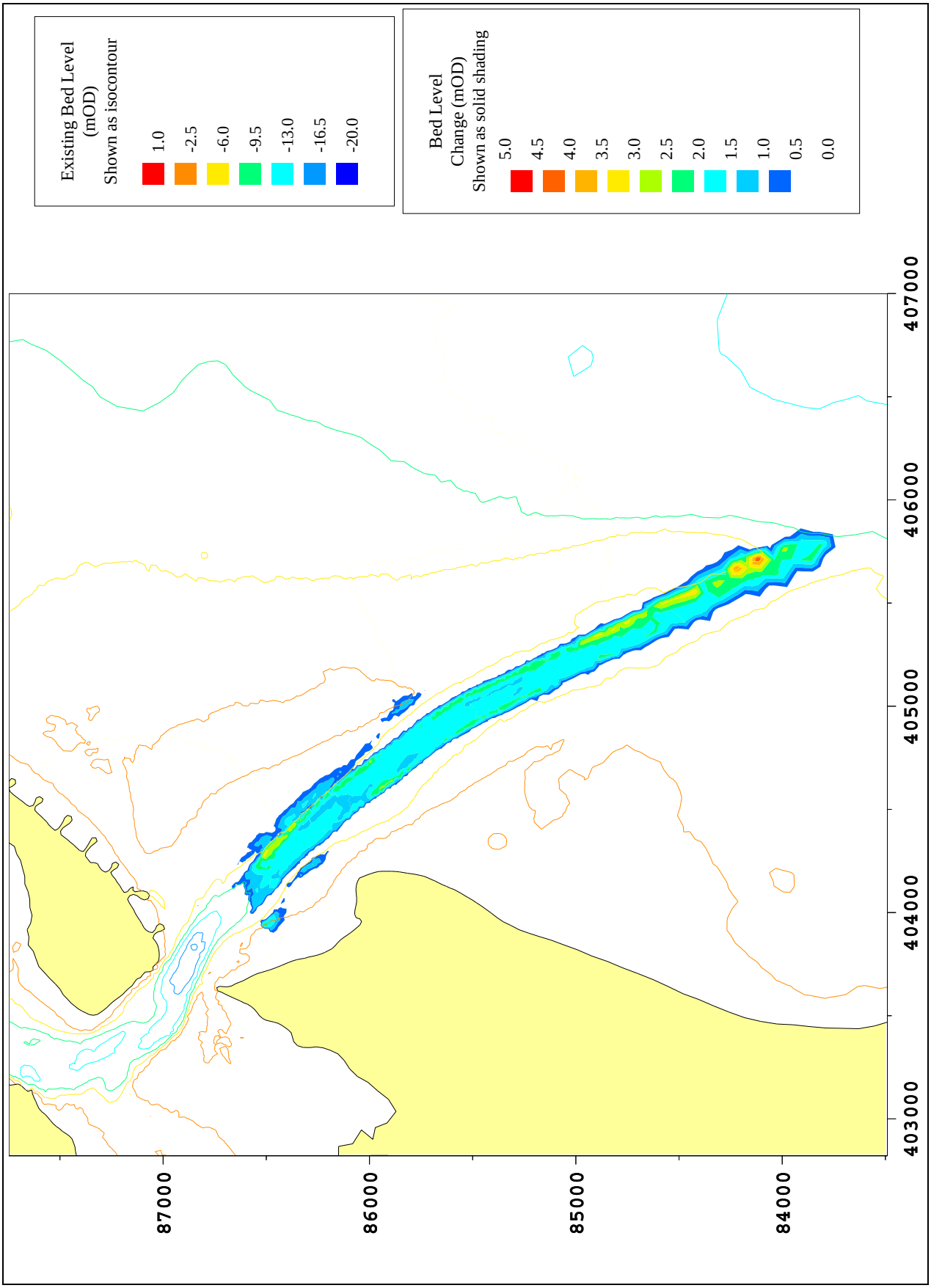

Figure 63 Change in bathymetry following dredging

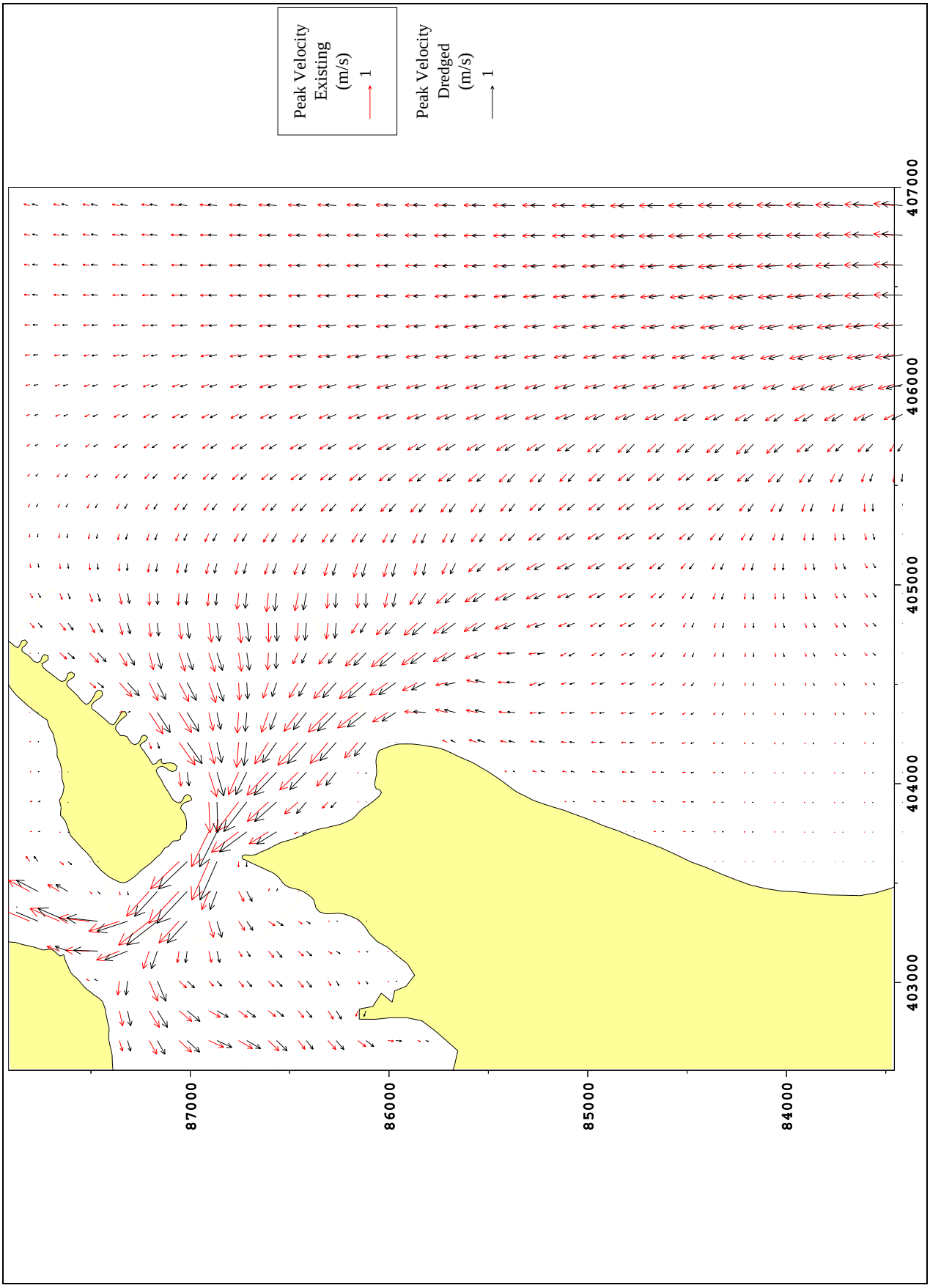

Figure 64 Spring tide peak flood currents: existing and dredged scenario

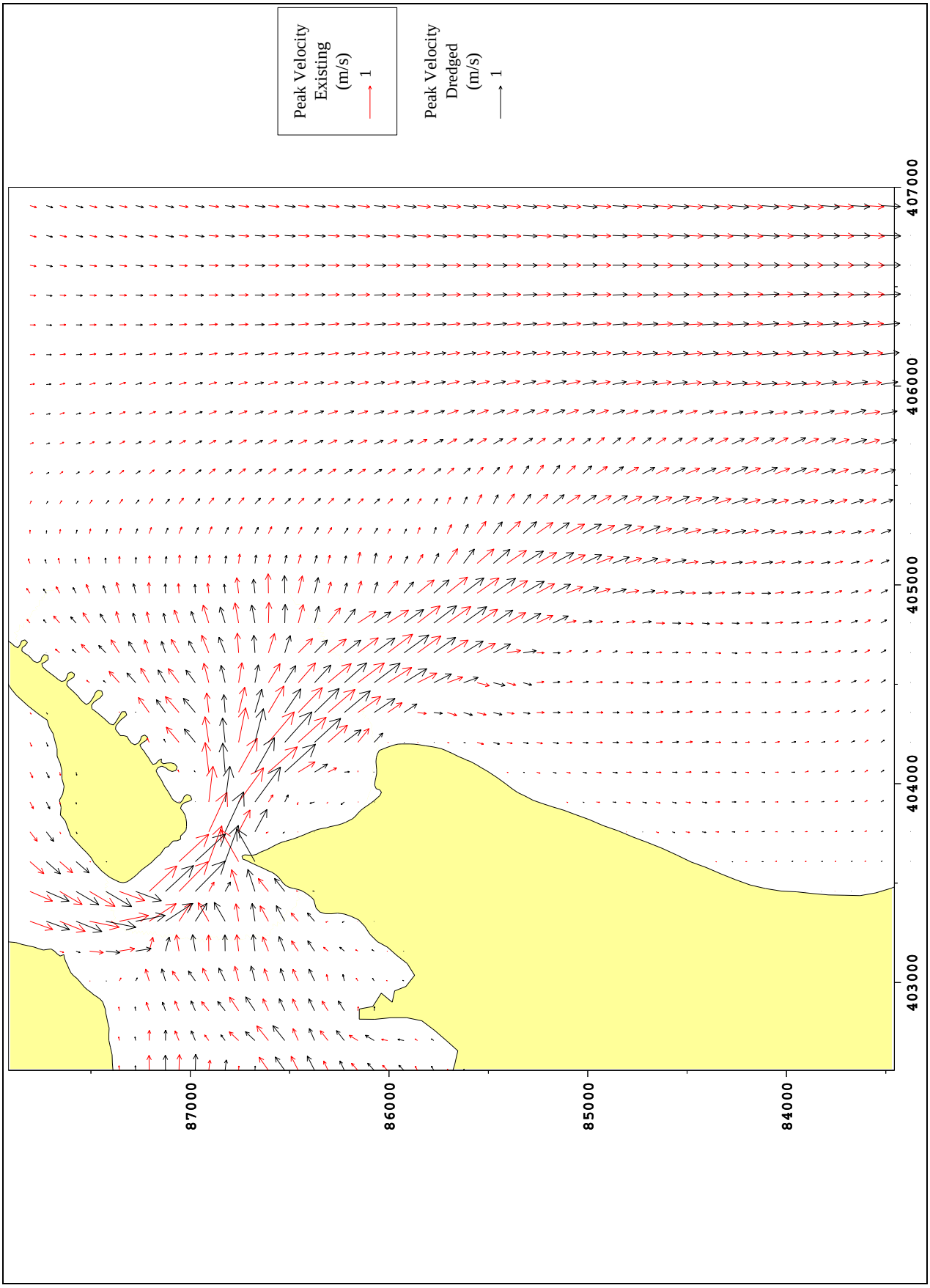

Figure 65 Spring tide peak ebb currents: existing and dredged scenario

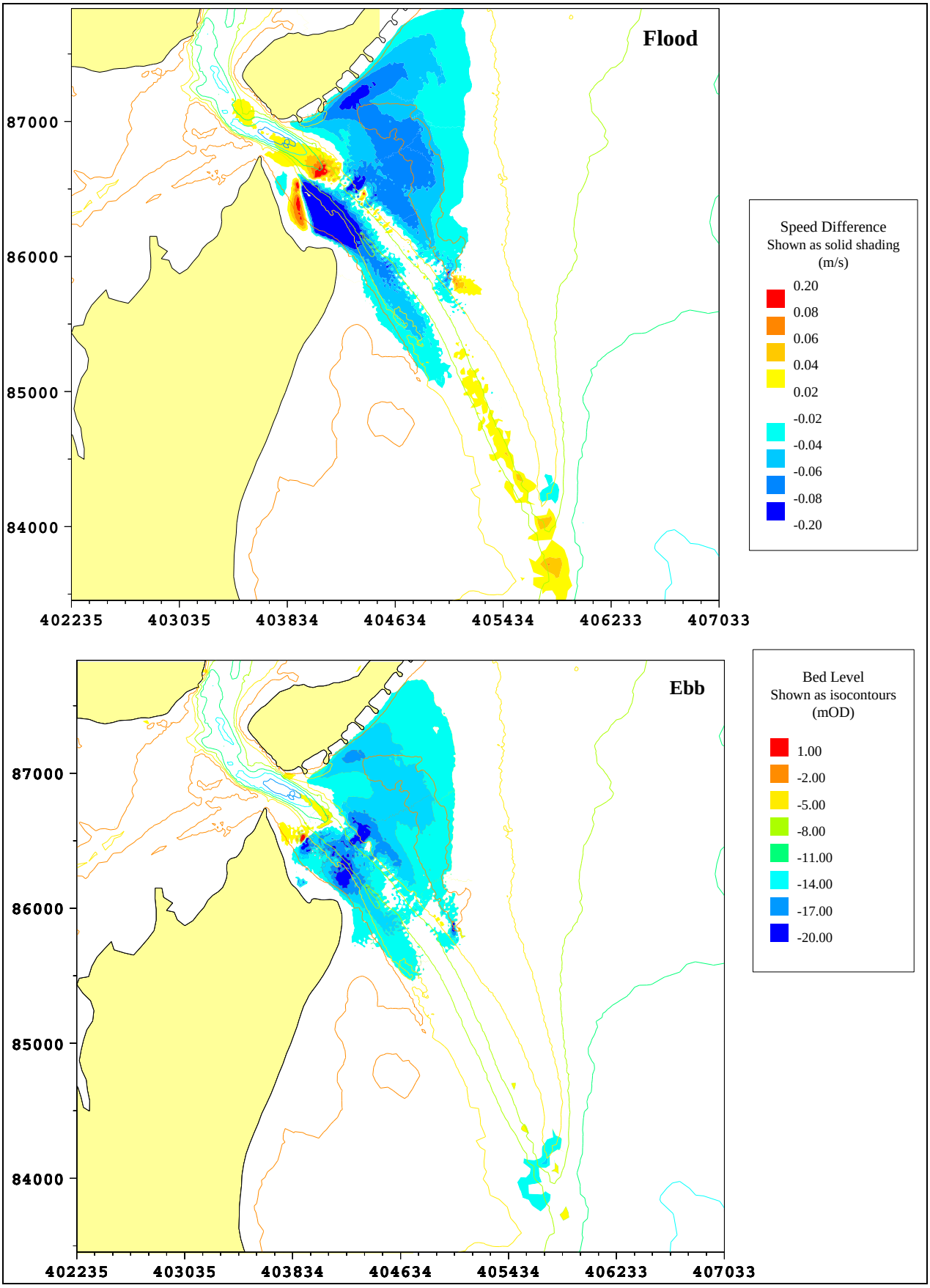

Figure 66 Change in peak tidal currents following dredging (top: flood, bottom: ebb)

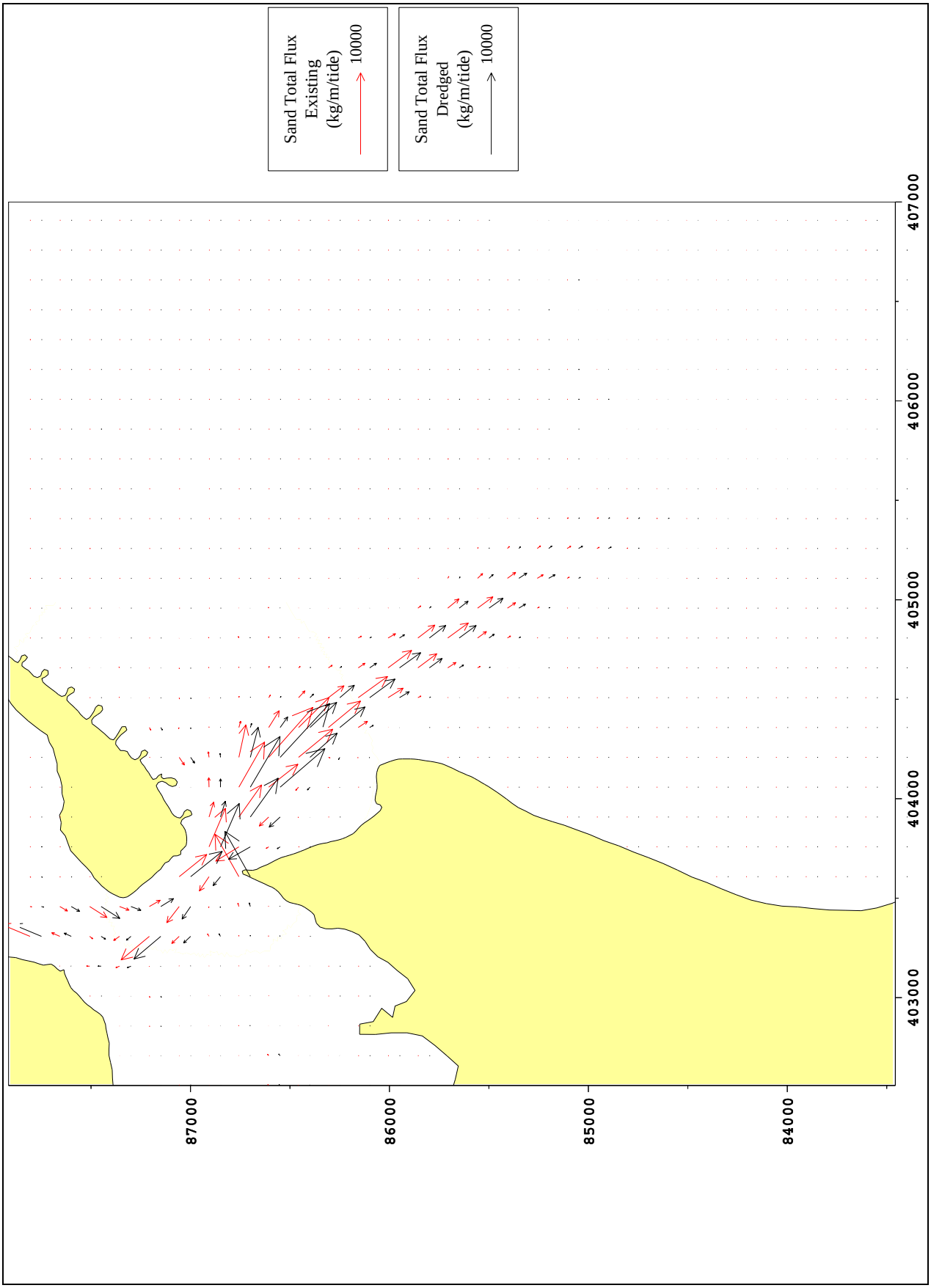

Figure 67 Net tidal sediment transport vectors under spring tides: existing and dredged scenario

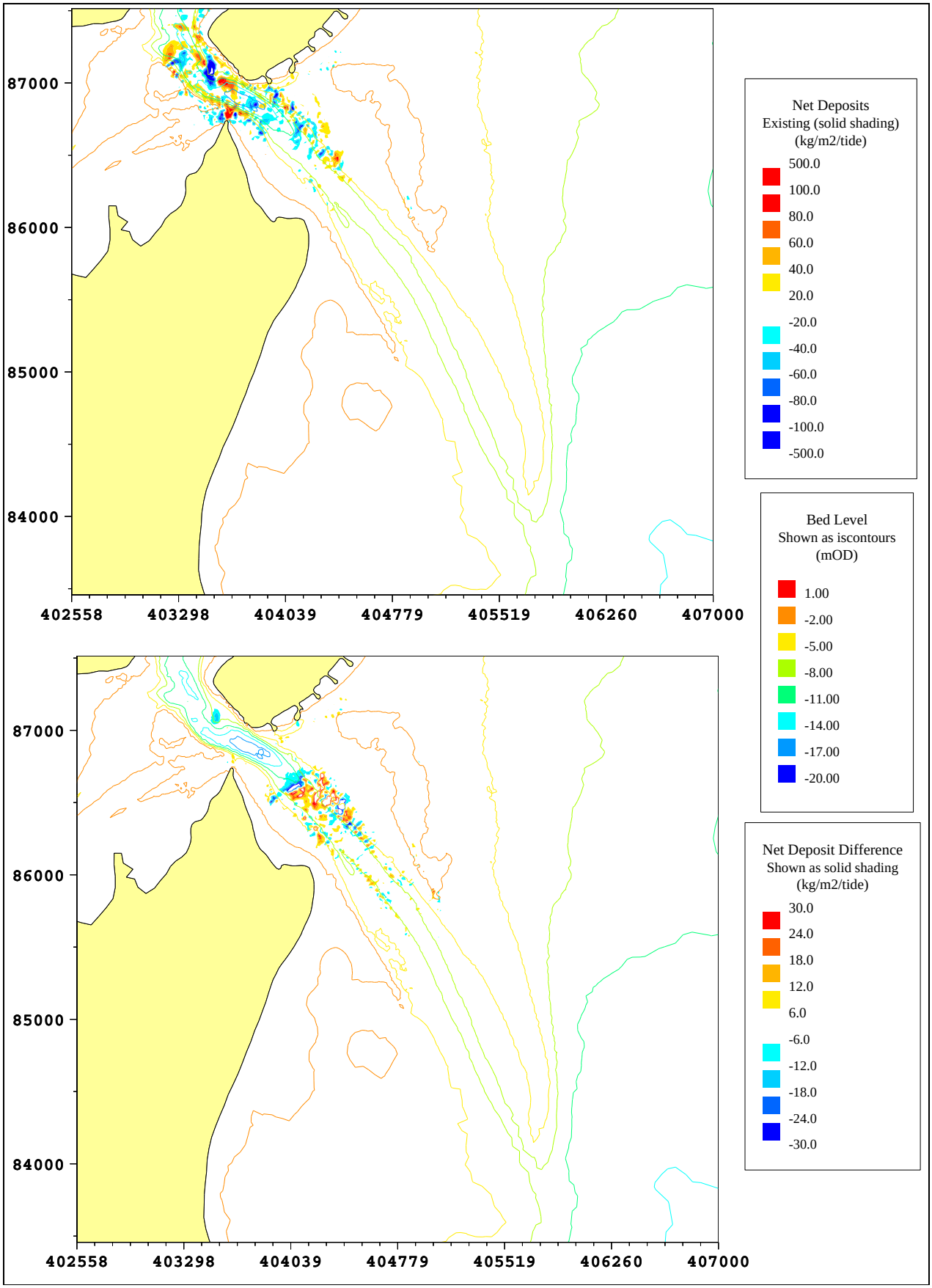

Figure 68 Existing net tidal patterns of erosion and deposition under spring tides (top) and changes due to dredging (bottom)

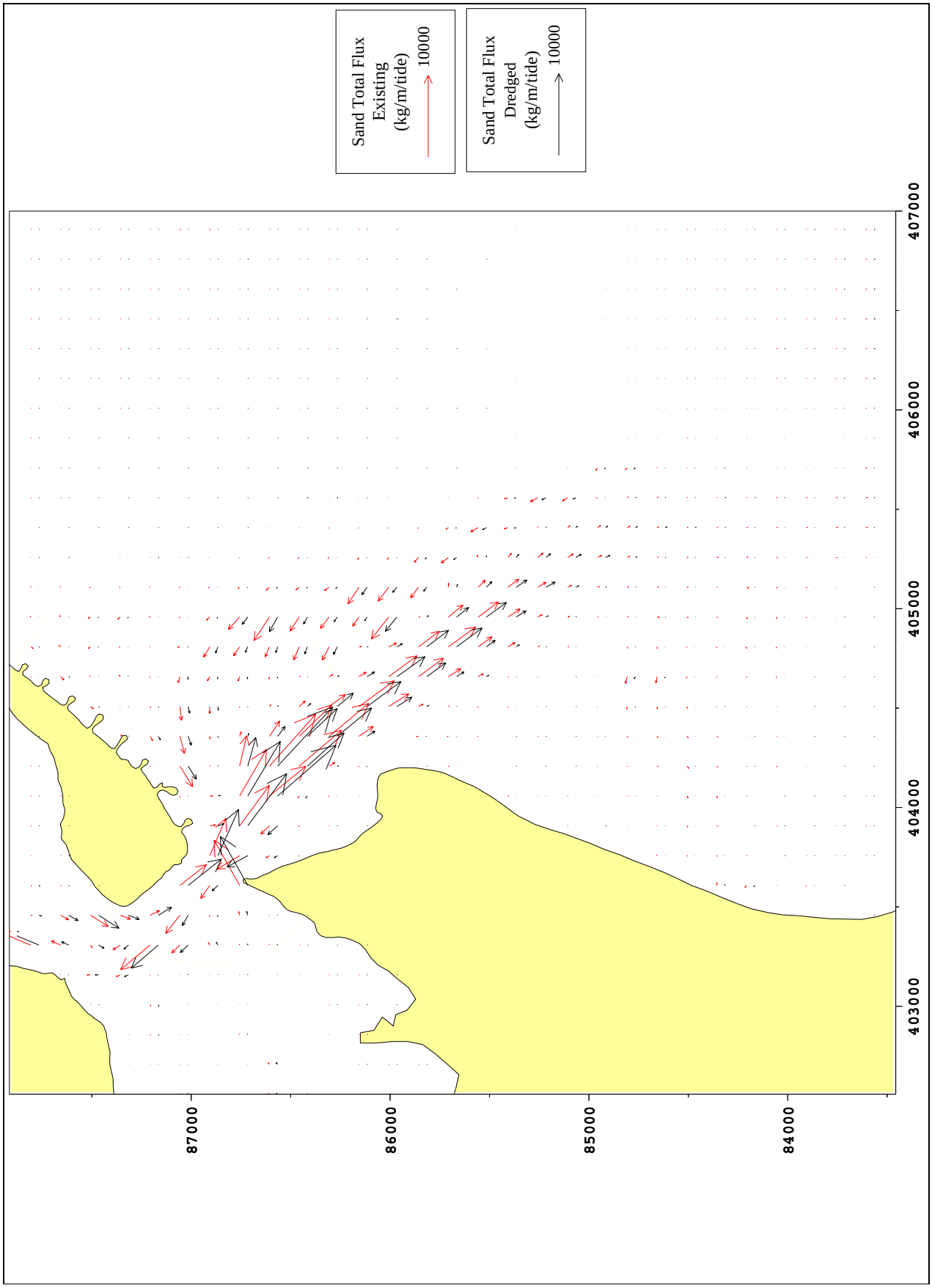

Figure 69 Net tidal sediment transport vectors under spring tides with storm waves from 140°N: existing and dredged scenario

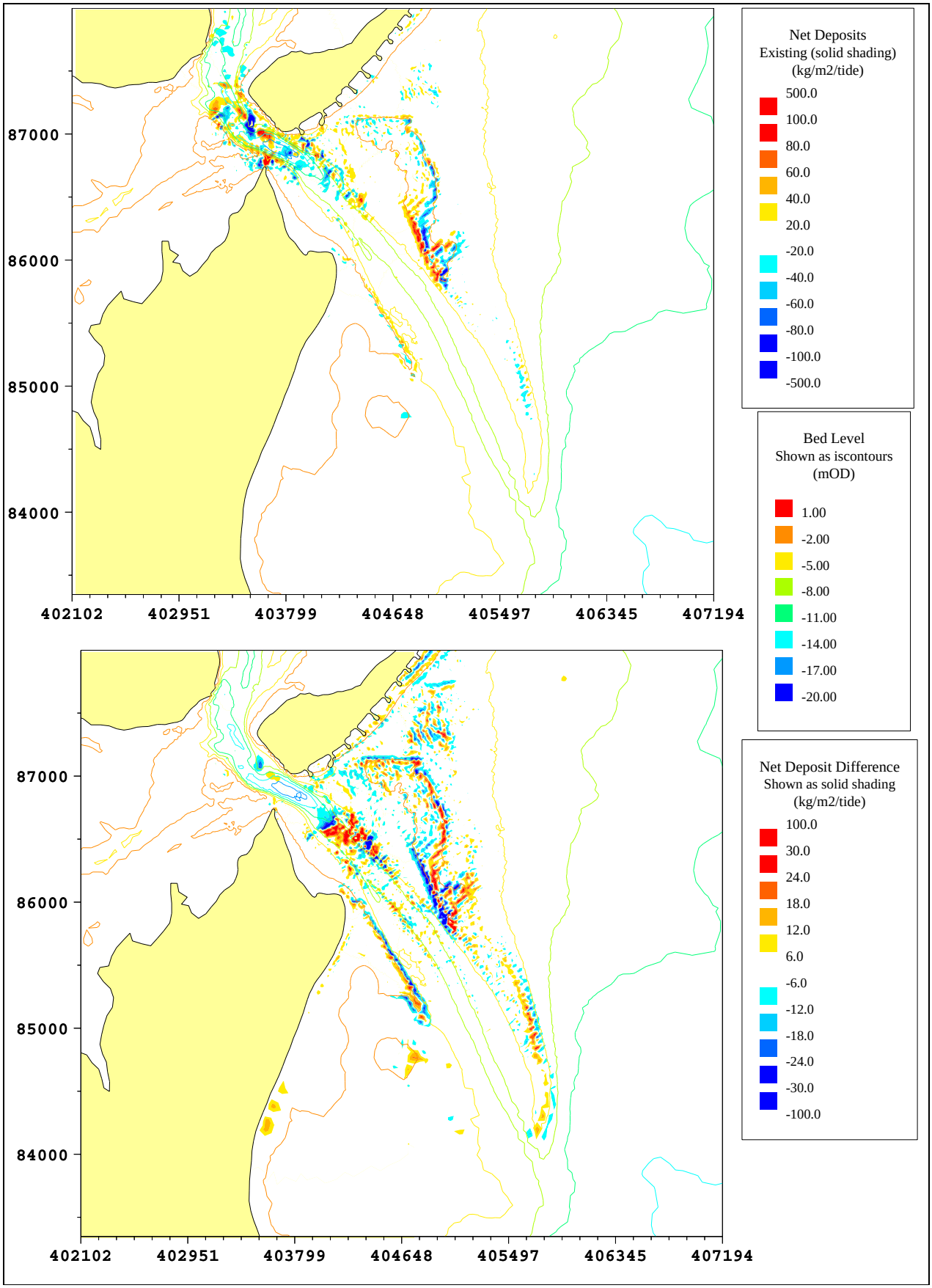

Figure 70 Existing net tidal patterns of erosion and deposition under spring tides with storm waves from 140°N (top), and changes due to dredging (bottom)

Appendices

Appendix 1

TELEMAC, COWADIS and SANDFLOW model details

Appendix 1 TELEMAC, COWADIS and SANDFLOW model details

TELEMAC-2D Model Description

Description of model and main areas of application

TELEMAC-2D is a sophisticated flow model, which was originated by LNH in Paris, for free surface flows. It solves the 2D depth-integrated shallow water equations that are used to model flows in rivers, estuaries and seas. It uses finite element techniques so that very flexible, unstructured triangular grids can be used. It has been developed under a quality assurance system including the application of a standard set of validation tests.

The model can simulate depth integrated tidal flows in estuaries and seas including the presence of drying banks. It can also simulate flows in rivers including turbulence structures resulting from flow obstructions and transcritical flows.

The advantage of using finite elements lies primarily in the possibility of using a very flexible grid. This is superior to using an orthogonal curvilinear grid as the user has far more complete control over grid refinement with a finite element system.

The applications of TELEMAC have included studies of tidal flows, storm surges, floods in rivers, dam break simulations, cooling water dispersion and infill of navigation channels.

Theoretical background and solution methods

TELEMAC solves the shallow water equations on an unstructured finite element grid (usually with triangular elements). The various variables (bed elevation, water depth, free surface level, and the **u** and **v** velocity components) are defined at the nodes (vertices of triangles) and linear variation of the water and bed elevation and of the velocity within the triangles is assumed.

When the model is used a time-step is chosen and the computation is advanced for the required number of time-steps. There is no particular limit on the time-step for a stable computation but it is best to ensure that the Courant number based on propagation speed is less than about 10. It is found that if the solution is nearly steady then few computational iterations are required at each step to achieve the required level of accuracy, which in TELEMAC is computed according to the actual divergence from the accurate solution. The computation at each time-step is split into two stages, an advective step and a propagation-diffusion step.

The advective step

The advective step is computed using characteristics or stream-wise upwind Petrov-Galerkin. The characteristic step makes it possible for the code to handle such problems as flow over a bump giving rise to locally supercritical flow and eddies shedding behind flow obstructions.

The propagation/diffusion step

The finite element method used is based on a Galerkin variational formulation. The resulting equations for the nodal values at each time-step are solved using an iterative method based on pre-conditioned conjugate gradient (PCG) methods so that large problems are solved efficiently. Several PCG solvers are coded and a selection is available to the user. The complete matrix is not assembled. Instead an element by element method is used so that most of the operations are carried out on the element matrices; this is computationally more efficient, both in speed of execution and in memory requirements. Rather than using Gauss quadrature exact analytical formulae are used for the computation of matrices. Symbolic software was used to draw up the formulae used. The software makes it possible to carry out a second iteration of the solution at each time-step in order to represent the non-linear terms in a time centred way, otherwise these terms are treated explicitly.

Boundary conditions

Boundary conditions are applied at solid boundaries where a "zero normal flow" and either a slip or non-slip boundary condition are applied. At open boundaries a selection of possibilities can be invoked depending on whether the flow is subcritical or supercritical or whether a wave absorbing boundary using a Riemann invariant is needed. A water discharge along a boundary segment can also be applied and the software distributes the flow along the segment chosen. This facility is valuable when running models of river reaches and the discharge in a cross section may be known rather than the velocity at each point in the cross-section.

Grid selection

The model can be run with a Cartesian grid for modelling rivers, estuaries and small areas of sea, with the possibility to apply a uniform Coriolis parameter, or on a spherical grid for larger areas of sea in which case the Coriolis parameter is computed from the latitude at each node. The effect of a wind blowing on the water surface and causing a set-up or wind induced current or of an atmospheric pressure variation causing an inverted barometer effect can be included, as can a k-epsilon model of turbulence if required.

Friction

The bed friction can be specified via a Chezy, Strickler or linear coefficient, or a Nikuradse roughness length. A variable friction coefficient over the model area is a possibility. Sidewall friction can also be included if wanted. Viscosity can be imposed as a given eddy viscosity value or a k-epsilon model can be used if needed.

Tracer calculation

TELEMAC-2D includes also the capability to simulate the transport of a tracer substance. The tracer is again computed using an advective step followed by a propagation/diffusion step. Tracer boundary conditions can be applied at model inflow boundaries. The tracer calculation has been used in order to simulate cooling water dispersion and mud transport. Sources of water and/or of tracer can be specified in terms of the discharge required and the x and y co-ordinates of the location.

INPUTS

TELEMAC requires as input a finite element grid of triangles covering the area to be modelled. Bathymetric data from which the bed elevation at each node can be computed is also required covering the area. A file of keyword values is used to steer the computation (supplies bed roughness, time-step, duration of run etc).

Methods of inputting the data

The finite element grid may be provided by a standard FE grid generator such as I-DEAS or SIMAIL. The software STBTEL (part of the TELEMAC suite) is used to read the output file from the grid generation software. The bathymetry is input using a digitising tablet and the SINUSX software is used to capture the bathymetry data. The data is stored in a form to be read into the TELEMAC system and depths interpolated to the model nodes.

Methods of checking and amending input data

SINUSX is a powerful interactive graphical software that can be used to check and amend the input data. Bathymetric curves can be duplicated, deleted, smoothed, moved etc.

Time to set up/calibrate/run/amend model

This depends on the form in which the data is supplied. Typically 1-2 days to digitise the chart data and 1-2 days to create the finite element grid. Boundary conditions may take a day to prepare. A run may take 1

to 5 hours to run a tide (for a 2000 cell model). The duration of the calibration process is hard to generalise as it depends entirely on particular circumstances.

OUTPUTS

Output parameters

The user can select from a range of output parameters including u and v velocity, u and v discharge, water level, bed level, water depth, tracer concentration and Froude number.

Output files

The TELEMAC output is contained in a single binary file which can be input to the graphics post-processor RUBENS. A listing file contains reflection of the input keywords and information on time-step reached, number of iterations to convergence etc. This file can be used to monitor the progress of a run.

Output plots

Results from the TELEMAC system are processed using the interactive graphics system RUBENS. This is a powerful and friendly environment in which figures can be produced interactively. By pointing and clicking time history plots, cross sections, vector plots and contour plots of any parameter at any position can be produced. Parameters other than those input can be calculated in RUBENS and plotted.

GENERAL

Interaction and compatibility of the model with other models

The main modules apart from TELEMAC-2D itself (the 2D flow model code) are SINUSX and RUBENS (described above).

The TELEMAC suite includes a bed load transport model (TSEF) and a suspended load model (SUBIEF). Also a wave model ARTEMIS that solves the mild slope equation.

The TELEMAC modelling suite also includes a quasi-3D random walk model for pollution transport modelling and a detailed water quality model with many water quality parameters including dissolved oxygen balance and particulates.

Quality Assurance

The software has been developed under the quality assurance procedures required by the French Electricity Industry. This has included the production of an extensive dossier of validation tests.

Validation

Validation tests on TELEMAC include:

- Simulation of eddies produced behind bridge piers. This test case includes the ability of the model to produce an unsteady solution from steady boundary conditions (von Karman vortex street).
- Drying on a beach.
- Simulation of the tides on the continental shelf including the Bay of Biscay. This model has been closely compared with the observed tides at coastal sites.
- Flow over a step in the bed with critical flow and a hydraulic jump. This solution is compared with the analytically known solution to this problem.

The COWADIS spectral wave model

Introduction

COWADIS (Computation Of WAve Density Integrated Spectrum) computes the generation and propagation of waves in coastal waters for given wind, seabed and current conditions. It is particularly suited to the generation and transformation of waves over relatively large coastal areas. COWADIS is part of the TELEMAC suite and is based on the finite element method used throughout TELEMAC.

COWADIS is a second generation wave model, in that it restricts the two dimensional energy density to a pre-defined spectral shape in the frequency range (e.g. a JONSWAP spectrum). The model is based on the numerical solution of the wave action density balance equation, given in terms of unknown quantities m_0 and m_1, where m_0 and m_1 respectively are the zeroth and first moments of spectral density. COWADIS is based on the assumption of steady state conditions, i.e. no variation in time. These features result in a model that is computationally efficient in terms of both memory and floating point operations.

The model has been validated for a variety of test cases and has already been used in numerous studies. It is designed to represent the following wave propagation processes:

- shoaling due to spatial variations in seabed and current
- refraction due to spatial variations in seabed and current
- blocking by opposing currents
- generation by wind
- dissipation by whitecapping
- dissipation by depth-induced wave breaking
- dissipation by seabed friction or percolation
- wave-wave interactions (quadruplets).

Diffraction by coastal structures or features of the seabed is not modelled in COWADIS, nor are reflections due to structures or significant seabed irregularities. Because of this, the wave field computed by the model will generally not be as accurate in the vicinity of obstacles.

The COWADIS wave model

The COWADIS model represents waves in terms of the two-dimensional wave action density spectrum $N(f_a,\vartheta)$. The independent variables are the absolute frequency f_a and the wave direction ϑ. The action density is equal to the energy density divided by the relative frequency, σ: i.e.

$$N(f_a,\vartheta) = F(f_a,\vartheta)/\sigma \qquad (1)$$

A more detailed explanation of the terms given in this equation and those proceeding are given in Reference 5.

In COWADIS the two-dimensional wave action density spectrum may vary only in space (unsteady effects due to variations in seabed, currents or winds in time are not taken into account). A simplified action balance equation describes its evolution, of which only the equations corresponding to the first two frequency moments m_0 and m_1 of the spectrum are solved:

$$\dot{x}_0 \frac{\partial}{\partial x}(B_0 m_0) + \dot{y}_0 \frac{\partial}{\partial y}(B_0 m_0) + \dot{\vartheta}_0 \frac{\partial}{\partial \vartheta}(B_0 m_0) = B_0 S_F \qquad (2)$$

$$\dot{x}_0 \frac{\partial}{\partial x}(B_0 m_1) + \dot{y}_0 \frac{\partial}{\partial y}(B_0 m_1) + \dot{\vartheta}_0 \frac{\partial}{\partial \vartheta}(B_0 m_1) = B_0\left(\frac{m_1}{m_0} S_F + m_0 S_\omega\right) \qquad (3)$$

where B_0 is a factor dependent on $\omega_0 = m_1 / m_0$.

The first and second terms on the left-hand side represent the propagation of waves in geographical x - and y - space. The third term represents propagation in ϑ - space (depth-induced and current-induced refraction). Shifting of the absolute frequency due to variations in depths and currents in time is not modelled since only steady state regimes are considered in COWADIS. The terms on the right hand side of the action balance equation are the source and sink terms representing the effects of generation, dissipation and non-linear wave-wave interactions. These are expressed as a function of the variance S_F and the mean angular frequency of the energy spectrum S_ω .

The wave action density spectrum integrated in frequency is hereafter referred to as $F_0(\vartheta)$ (= m_0), while the wave action density spectrum integrated in both frequency and direction is referred to as F_1 . A directional spreading function $D_{ideal}(\vartheta)$ is defined as $F_0(\vartheta) = F_1 \times D_{ideal}(\vartheta)$.

Wind generation

The wind generation source term is intended to combine all the processes in addition to wave generation by the wind that occurs in deep water. This includes whitecapping and non-linear interactions between quadruplets of frequencies.

Whitecapping is a form of energy dissipation primarily controlled by the steepness of the waves.

Non-linear (quadruplet) wave-wave interactions between waves of different frequencies result in the transfer of energy from the peak frequency to lower frequencies (thus shifting the peak frequency to lower values) and to higher frequencies (where the energy is dissipated by whitecapping). In shallow water, non-linear triad wave-wave interactions result in transfer energy from lower frequencies to higher frequencies. However, triad interactions are not modelled in COWADIS.

The formulation used in COWADIS to represent these processes is derived from Holthuijsen et al. (1989) and assumes the idealised case of a wind field uniform in space and time and is given by:

$$S_F(\vartheta) = \frac{U^3}{g} abD_{ideal}(\vartheta)\left[\frac{g^2 F_0(\vartheta)}{aU^4 D_{ideal}(\vartheta)}\right]^{\frac{b-1}{b}} \quad if \quad \tilde{t} < \tilde{t}_m \qquad (4)$$

$$S_F(\vartheta) = 0 \quad if \quad \tilde{t} \geq \tilde{t}_m$$

and

$$S_\omega(\vartheta) = S_{\omega ideal}(\vartheta)\left[\frac{U\omega_0(\vartheta)}{gc}\left(\frac{g^2 F_0(\vartheta)}{aU^4 D_{ideal}(\vartheta)}\right)^{\frac{-d}{b}}\right]^m \qquad (5)$$

where

$$S_{\omega ideal}(\vartheta) = \frac{U^2}{g^2} cd\left[\frac{U\omega_0(\vartheta)}{gc}\right]^{\frac{b-1}{b}} \quad if \quad \tilde{t} < \tilde{t}_m$$

$$S_{\omega ideal}(\vartheta) = 0 \quad if \quad \tilde{t} \geq \tilde{t}_m$$

with $\tilde{t} = \left(\frac{U\omega_0(\vartheta)}{gc}\right)^{\frac{1}{b}}$

where a , b , c and d are wind generation constants that can be tuned by the user.

Seabed Friction

The model used for seabed friction-induced energy loss in COWADIS accounts for the various contributions related to wave-seabed interactions including seabed motion, percolation or back-scattering due to seabed irregularities. These processes are represented in COWADIS by:

$$S_F(\vartheta) = -(\Gamma + CU_k)\frac{\sigma_0^2(\vartheta)}{g^2 \sinh^2(k_0 d)} F_0(\vartheta) \qquad (6)$$

$$S_\omega = A\frac{C_{g0}(\vartheta)k_0(\vartheta)}{m_0(\vartheta)} S_F(\vartheta) \qquad (7)$$

in which Γ is a seabed friction coefficient for waves, C is a seabed friction coefficient for currents and A is a seabed friction coefficient for mean frequency. A large number of models have been proposed for Γ. Hasselmann et al. (JONSWAP, 1973) suggested an empirically obtained constant. This performs well in many different conditions provided a suitable value is chosen (typically different for swell and wind sea; Bouws and Komen, 1983).

Wave breaking

In addition to seabed friction effects, wave energy can be dissipated in shallow water due to wave breaking. The process of depth-induced wave breaking is still poorly understood and little is known of the effects on each component of a wave spectrum. Despite this, the total dissipation (i.e. integrated over the spectrum) can be accurately modelled using the assumption of the dissipation of a bore applied to the breaking waves in a random field. Battjes and Janssen's expression (1978) has been expanded in the COWADIS model to include wave direction and based on the assumption that wave breaking does not alter the directional distribution of energy, this source/sink term is applied to all the propagation directions:

$$S_F(\vartheta) = -\frac{\alpha Q_b \omega_0(\vartheta) H_m^2}{8\pi}\frac{F_0(\vartheta)}{F_1} \qquad (8)$$

$$S_\omega(\vartheta) = 0 \qquad (9)$$

in which α is a numerical constant of the order of 1, Q_b is the rate of breaking and H_m is the maximum possible individual wave height in the local water depth d, according to Battjes and Janssen (1978). The value of Q_b depends critically on the breaking parameter $\gamma = H_{\max}/d$. In COWADIS γ has a constant value (default is 0.8).

Wave blocking

The wave blocking term in COWADIS accounts for energy dissipation due to opposing currents.
The source/sink term is based on the formulation proposed by Holthuijsen et al. (1989) and is given by:

$$SF(\vartheta) = \frac{k_c^{-n}(1-n)}{k_c^{-n} - k_p^{-n}}\frac{dk_c(\vartheta)}{dt} F_0(\vartheta)$$

and

$$S\omega(\vartheta) = \frac{C_g(\vartheta)\left(k_c(\vartheta) - k_0(\vartheta)\right)}{F_0(\vartheta)} S_F(\vartheta)$$

where:

k_0 is the mean wave number

k_p is the peak wave number

k_c is the critical wave number

C_g is the mean group velocity

Computational Methods

In COWADIS the steady state problem is solved by considering the solution as the limit of an unsteady problem. Within each virtual time increment, the model performs two steps: a convection step to determine the wave propagation and an iteration step to solve for the source/sink terms. Depth induced wave breaking is carried out as a sub-iteration process. The propagation step is solved using the method of characteristics, which is carried out only once per time increment. Furthermore, since the speed of this approach is not dependent on the computational grid spacing, local refinement to accurately represent seabed irregularities or coastal features does not significantly affect the overall run times of the model. With the exception of depth induced wave breaking the source/sink term integration is based on a semi-implicit scheme. For the wave breaking sink term an explicit scheme is used and the model allows sub-increments in time to be defined to ensure wave breaking is not overestimated due to the length of the main time increment.

Typical results

(i) Tables of H_s, T_z, and mean direction at a selection of inshore locations. For example the model can be used to investigate which offshore wave conditions lead to the worst inshore wave heights at a particular site.

(ii) COWADIS also calculates wave-induced currents, orbital velocities and radiation stresses suitable for sediment transport calculations.

(iii) The model can also be used to provide boundary conditions for the ARTEMIS wave disturbance model from the TELEMAC suite to investigate different options of harbour layout.

References

1. Battjes, J.A. and J.P.F.M. Janssen, 1978: Energy loss and set-up due to breaking of random waves, *Proc. 16 th Int. Conf. Coastal Engineerin*g, ASCE, 569-587.

2. Bouws, E. and G.J. Komen, 1983: On the balance between growth and dissipation in an extreme, depth-limited wind-sea in the southern North Sea, *J. Phys. Oceanog*r., **1**3, 1653-1658.

3. Hasselmann, K., T.P. Barnett, E. Bouws, H. Carlson, D.E. Cartwright, K. Enke, J.A. Ewing, H. Gienapp, D.E. Hasselmann, P. Kruseman, A. Meerburg, P. Müller, D.J. Olbers, K. Richter, W. Sell and H. Walden, 1973: Measurements of wind-wave growth and swell decay during the Joint North Sea Wave Project (JONSWAP), *Dtsch. Hydrogr.* Z. Suppl., **1**2, A8.

4. Holthuijsen, L.H., Booij, N. and Herbers, T.H.C., 1989, A prediction model for stationary, short crested waves in shallow water with ambient currents, *Coastal Engineerin*g, 13, 23-54

5. Marcos, F., 1998: COWADIS software for finite element wave propagation in coastal areas – Principle Note – Release 1.0, *HE-42/98/056/A*, *EDF-DER*

The SANDFLOW-2D Model Description

Description of model and main areas of application

SANDFLOW-2D is the sand transport modelling module of the TIDEWAY-2D system. SANDFLOW-2D uses the flows calculated by TIDEFLOW-2D to study the transport, deposition and erosion of non-cohesive (sandy) sediment and thereby identify areas of potential siltation and erosion. SANDFLOW-2D has also been adapted to use the flows produced by the TELEMAC flow model for sand transport calculation.

Theoretical background and solution methods

The sediments under consideration here are very fine and fine sands (d_{50}~ 0.06 to 0.25 mm) which mainly move in suspension. The model can also be used to identify trends in the case of medium sand (d_{50}~ 0.25 to 0.5 mm). If the sediment contains a high proportion of clay or silt particle sizes less than 0.06 mm, it would be more appropriate to use the MUDFLOW-2D (TIDEWAY) or SUBIEF (TELEMAC-2D) models.

The main factors controlling sand transport are:

- advection by currents
- settlement under gravity
- turbulent diffusion in all directions (but only the vertical component is of significance under most circumstances)
- exchange of sediment between the flow and the bed

The study of sand transport generally is very difficult but more so in the case of estuaries or coastal areas. This is because the water movements are continually changing, with the rise and fall of the tide, and there is usually a wide range of sediments on the bed and areas without mobile sediment, leading to unsaturated loads in the water.

Method

Although sand transport in estuaries is really an unsteady, 3D problem, it has been shown by HR Wallingford that it can be dealt with using a 2D, depth-averaged model provided special provision is made to account for the vertical profile effects of the sediment concentration. Under these circumstances the depth-averaged, suspended solids concentration c(x, y, t) satisfies the conservation of mass equation.

$$\frac{\partial}{\partial t}(dc) + \alpha\left[\frac{\partial}{\partial x}(duc) + \frac{\partial}{\partial y}(dvc)\right] = \frac{\partial}{\partial s}\left(dD_s \frac{\partial c}{\partial s}\right) + \frac{\partial}{\partial n}\left(dD_n \frac{\partial c}{\partial n}\right) + S \qquad (1)$$

where

(u,v)	=	depth-averaged components of velocity (m/s)
D_s	=	longitudinal (shear flow) dispersion coefficient (m^2/s)
D_n	=	lateral (turbulent) diffusivity ($m^{½}/s$)
(x,y)	=	Cartesian co-ordinates in horizontal plane (m)
(s,n)	=	natural co-ordinates (parallel with and normal to mean flow) (m)
t	=	time (sec)
d	=	water depth (m)
S	=	erosion from or deposition on the bed ($kg/m^{½}/s$)
α	=	advection factor to recover the true sediment flux from the product of depth-averaged quantities

Advection factor (α)

This is introduced to compensate for the omission of the vertical profile in the sediment flux terms.

$$\alpha = T/qcd \qquad (2)$$

where

T = $\int_o^d q'c'dz$ is the sand transport (kg/m width/s)
q = the depth-averaged water speed $(u^2 + v^2)^{1/2}$

and q',c' are the full three-dimensional velocity and concentration variables.

Since the highest concentrations occur near the bed it follows that $\alpha \leq 1$. Typical values of α can be obtained by evaluating equation (2) for sand transport profile observations or from the integration of theoretical solutions for suspended solids profiles. However, in practice, it is usually acceptable to take $\alpha = 1$ on the grounds that the external and internal sources of mobile sediment are not well enough known to justify a more precise formulation.

Bed exchange relations

The simplest formulation of the bed exchange relation is

$$S = ß_s \omega_s (c_s - c) \qquad (3)$$

where

c_s is the depth-averaged concentration when the flow is saturated with sediment (kg/m^3)
ω_s is the representative settling velocity (m/s)
$ß_s$ is a profile factor to compensate for integrating out the vertical profile of suspended sediment ie to correct for higher sediment concentrations near the bed.

Deposition or erosion takes place depending on whether the instantaneous sediment load (c) exceeds or is less than the saturated value (c_s). Pick up of sediment from the bed is prevented if there is no sediment available on the bed. A shortage of material on the bed is reflected in a low concentration of suspended solids being advected away by the flow.

Typical values of $ß_s$ could be obtained from actual observations of sediment profiles or from theoretical considerations. However, HR Wallingford has derived an analytical expression for this so that bed exchanges are performed automatically. This involves simplifying the vertical diffusivity relation and a profile mixing factor is introduced to enable the user to increase or decrease the effective mixing during calibration of the model.

Sediment transport relation

The evaluation of bed exchanges requires a depth-averaged sediment concentration (c_s). Sandflow-2D obtains this from a sediment transport relation specified by the user. Three sand transport relations are supplied in the package (Ackers-White, van Rijn and a simple power law) and since the source code is provided other relationships can be added by the user if preferred.

The choice of sand transport relation needs care. It should be borne in mind that most relationships found in the literature are based on river or channel data where sediments are more narrowly graded than in estuaries. Also there is normally a small proportion of cohesive material in estuary sediments and this can alter the transport properties. If possible, sand fluxes should be measured at the study site, and if such data is available it may be best to use it to obtain the best-fit power law relation for the site.

Diffusion

The dispersion (D_s) and diffusion (D_n) coefficients are not well defined. When viewed in close enough detail the whole motion appears advective; but when viewed on a coarser grid the smallest motions appear diffusive. Thus selection of the appropriate diffusion or dispersion coefficients depends on the grid size of the model - one model will treat as advection what a coarser grid model will treat as diffusion or dispersion.

Fortunately, the solutions to the equation are not normally sensitive to D_s and D_n. As a first approximation, $D_n = Bdu$, where d and u are representative depths and velocities. It has been found that B is usually in the range 0.01 (for fairly uniform depths and smooth beds) to 0.1 (for irregular geometry and/or rougher beds).

D_s is automatically calculated by the program for each model cell depending on the local depth and velocity to give more diffusion in the direction of flow. The overall scale of D_s can be changed using the relative dispersion parameter (in keyword DIFFUSION). This normally has the value unity but it can be adjusted upwards or downwards during calibration to get agreement between the model results and any dispersion observations that may be available.

Numerical model

A simple, explicit, upstream finite difference technique is used to solve the advection - diffusion equation. Flux corrections are not considered to be necessary because the background concentrations of suspended sand are normally fairly uniform throughout the model in contrast to POLLFLOW-2D applications that have one or two point sources and correspondingly steeper concentration gradients.

The use of an explicit method introduces a stability constraint on the computing time step (Δt).

$\Delta t < \Delta s/(\text{maximum flow velocity})$

where Δs is the grid size (TIDEWAY) or separation between nodes (TELEMAC-2D) in metres.

Generally, this does not pose any problems in practice because the allowable Δt is usually much larger than the TIDEFLOW-2D time step and there is only a single equation to solve in the process model compared to three in TIDEFLOW-2D. Under these circumstances an explicit method is preferred because it enables the user to understand the code more easily and to modify the treatment of the physics of the processes being simulated. Note that where TELEMAC-2D is being used the values of Δs will vary and so the minimum value of Δs is the most important in terms of stability.

The treatment of the dispersion (D_s) and diffusion (D_n) terms introduces another stability constraint.

$\Delta t < \Delta s^{½}/4\ D_{max}$

where D_{max} is the maximum of D_s and D_n.

This constraint is normally weaker than the advective stability limit but the user should be aware that a high value of diffusivity can lead to an instability. In the event of problems the possible violation of both limits should be checked.

Application of the model

The application of the model and interpretation of the results requires a good understanding of sand physics. Firstly it is important to choose representative values for the main parameters. Ideally these should be based on laboratory tests of actual sediment samples from the site. It is also important for the modeller to be aware of the limitations of this type of model when applied to real sites.

In addition it should be appreciated that sand transport is not an exact science. Accordingly, whatever model is used, and whatever parameter values are chosen it is essential that results are interpreted correctly. Provided this is done the model will be a valuable engineering tool.

Calibration/validation

Calibration of sediment models is difficult because bed changes are usually too slow or too variable to measure anything significant for comparison. Sometimes historical charts or dredging records may be available but even then it is unlikely that the sources of suspended sediment can be quantified for the relevant period. Sometimes it is possible to get scaling factors for model results in cases where information is available and use these to estimate siltation in the new situation, but in many cases one is forced to use the best available values for the parameters and to demonstrate that the siltation and erosion patterns produced by the model agree with the observed state of the estuary or coastal region being studied.

Some evidence to support the physical realism of the model is given by the following results of simulation of sand transport in a flume and of observations from the Thames estuary.

The computer model results were compared with the results of a laboratory experiment performed in a flume with a length of 30m, a width of 0.5m and a depth of 0.7m. The discharge was measured by a circular weir. The mean flow depth was 0.25m and the mean flow velocity was 0.67 m/s. The bed material had a d_{50} = 230μm and a d_{90} = 320 μm. The median diameter of the particles in suspension was estimated to be about 200 μm, resulting in a representative fall velocity of 0.22 m/s (water temperatures 9°C). The stream bed was covered with bed forms having a length of about 0.1m and a height of about 0.015m. Small Pitot tubes were used to determine the vertical distribution of flow velocity. Water samples were collected simultaneously by means of a siphon method at four locations to determine the spatial distribution of the sand concentrations. At each location (profile) five samples were collected at a height of about 0.015, 0.025, 0.05 and 0.22m above the average bed level and these were integrated to give the suspended load transport. The HR SANDFLOW-2D model was run for the same conditions assuming the overall shear velocity was 0.0477 m/s and the results in Figure 1 shows that the model could be calibrated if suitable data is available.

The model was compared with some flume data to test its response to a change in the sediment load. It was shown that the model simulation could be calibrated by adjusting the settling velocity and vertical diffusivity parameters. This procedure is justified for practical applications because in nature these parameters are not well defined. For example, there is no unique settling velocity because the suspended load would contain a range of sediment sizes and the true nature of the vertical diffusivity is not yet fully understood.

The basic physics of the model was then checked against real field data from Foulness in the Thames Estuary. There was a wide range of sediment sizes in the data but the model was only used to simulate individual fractions. The saturation concentrations in the model were calculated using a cubic velocity relation derived from the observed sand fluxes.

Results from the model simulation of the 75 to 100 μm sand fraction are shown in Figures 2 and 3 plotted at half hourly intervals with a sequence number showing the progression through the tide. The model has a similar hysteresis effect to the observations on both stages of the tide. The systematic underestimation of concentrations during the ebb is probably due to a different availability of sediment sizes not allowed for in the simplified model. Nevertheless the demonstration confirms the general validity of the model in a natural situation.

An example of the agreement achieved during validation, between the SANDFLOW-2D model results and observed sediment distribution is shown in Figure 4. Note in particular the agreement between the areas of potential erosion predicted by the model and areas of rock bed, and also the areas of potential deposition and areas of sand bed observed.

INPUTS

Input data required

SANDFLOW-2D requires as input the elevation and flow results from a TIDEFLOW-2D run or a TELEMAC-2D run, together with information describing the initial distribution of sand on the bed. A boundary data file is also required to specify sediment concentrations at the model edges with respect to time. Other parameters required include the typical size of sand and its basic properties such as settling velocity and threshold stress for initiation of motion.

Methods of inputting the data

Data is input to SANDFLOW-2D using ASCII data and steering files and unformatted direct access results files from TIDEFLOW-2D or the TELEMAC-2D equivalent. The steering files are set up using the context sensitive editor included in the user interface.

User interface

A keyword driven interface controls all aspects of using SANDFLOW-2D from setting-up a model through to analysis of the results. The interface includes file management functions, graphical presentation of results and utilities for results analysis and file format conversion.

OUTPUTS

Output parameters

SANDFLOW-2D calculates concentrations of suspended sediment and distributions of erosion and deposition are stored at user selected intervals during the run. SANDFLOW-2D calculates suspended sediment concentration, erosion and deposition throughout the model area for each time step through the tide.

Output files

Each run of the SANDFLOW-2D model generates three output files. Two of these files contain the suspended concentrations and bed deposits. The third output file; the List File contains run information.

Output plots

The results from the SANDFLOW-2D may be represented using report quality-graphics utilities included in the TIDEWAY-2D system or, where TELEMAC-2D has been deployed, the RUBENS visualisation system. Contour plots of suspended concentrations and/or bed deposits at user selected times and concentration-time and deposit-time plots at selected locations can be produced.

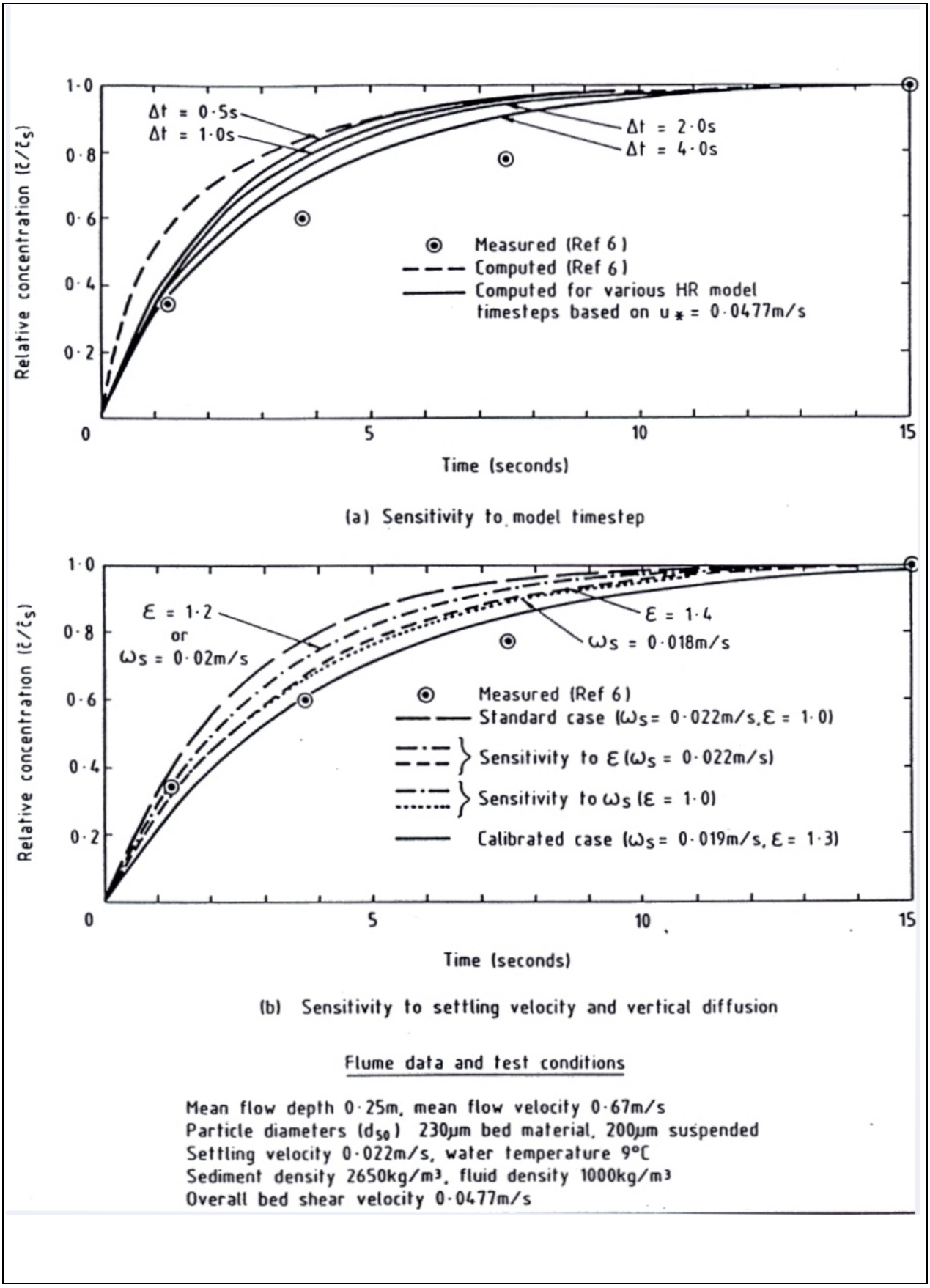

Figure 1 Computed and measured evolutions of sediment load

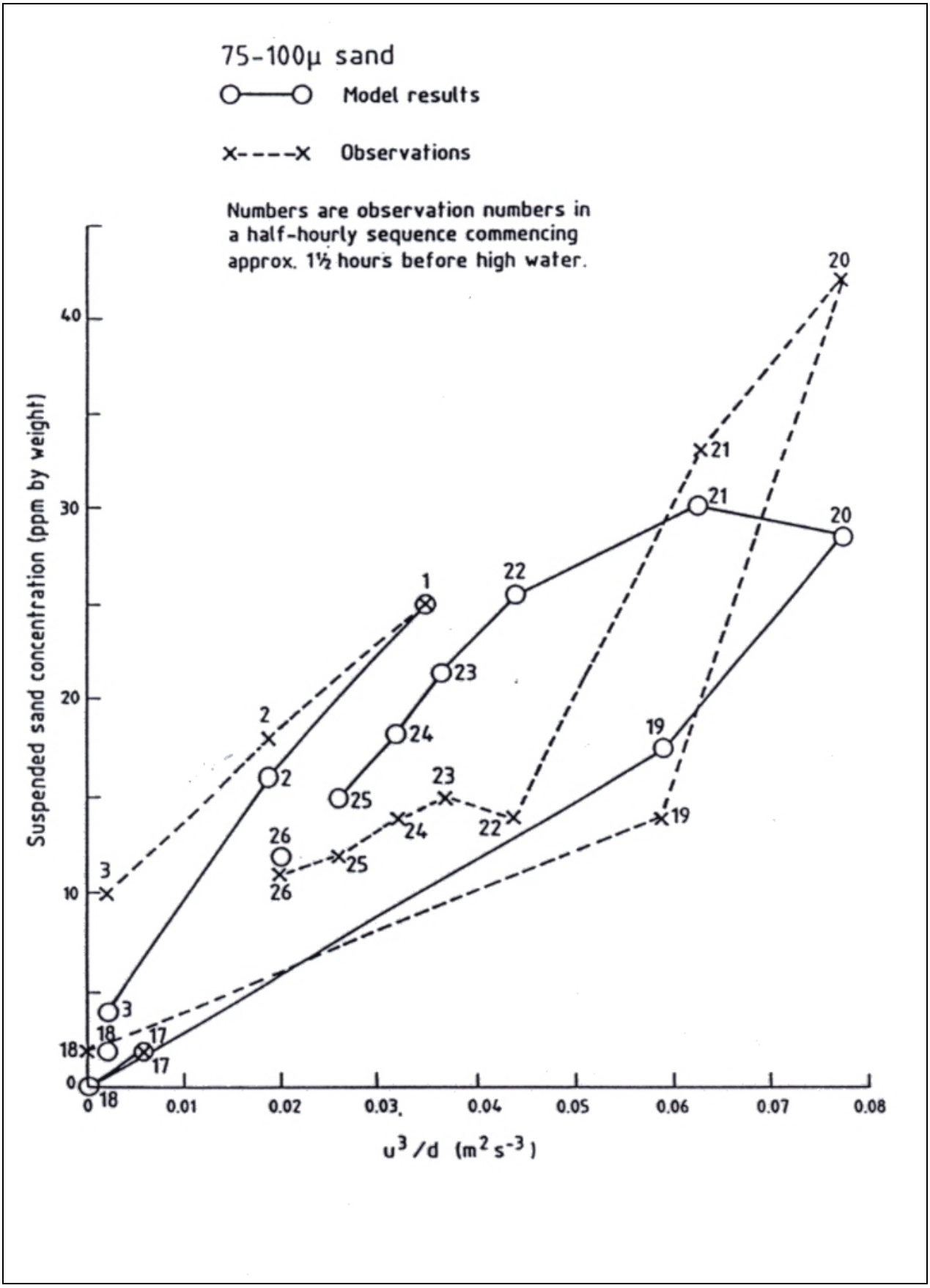

Figure 2 Simulation of Foulness position 1 flood tide

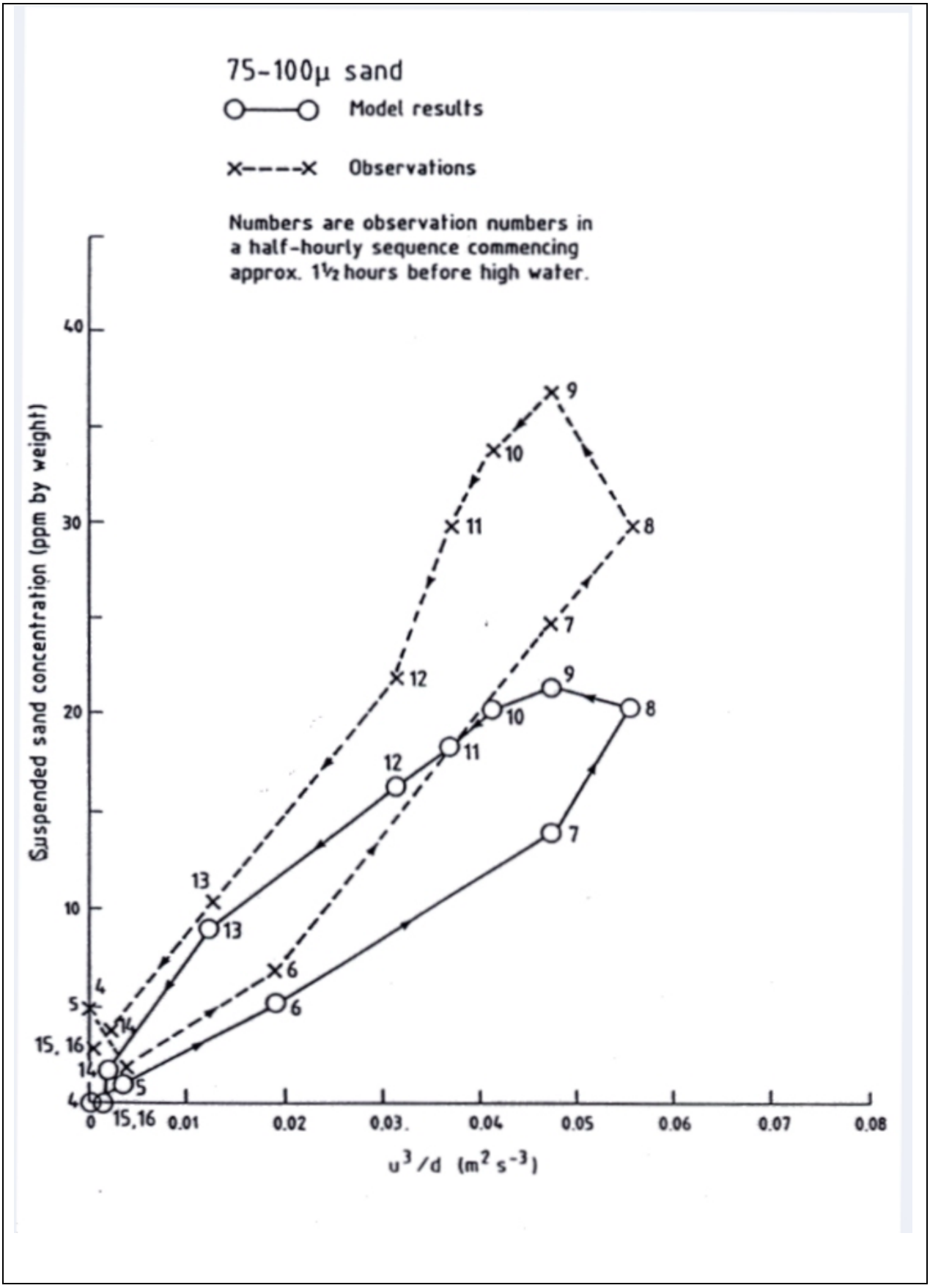

Figure 3 Simulation of Foulness position 1 ebb tide

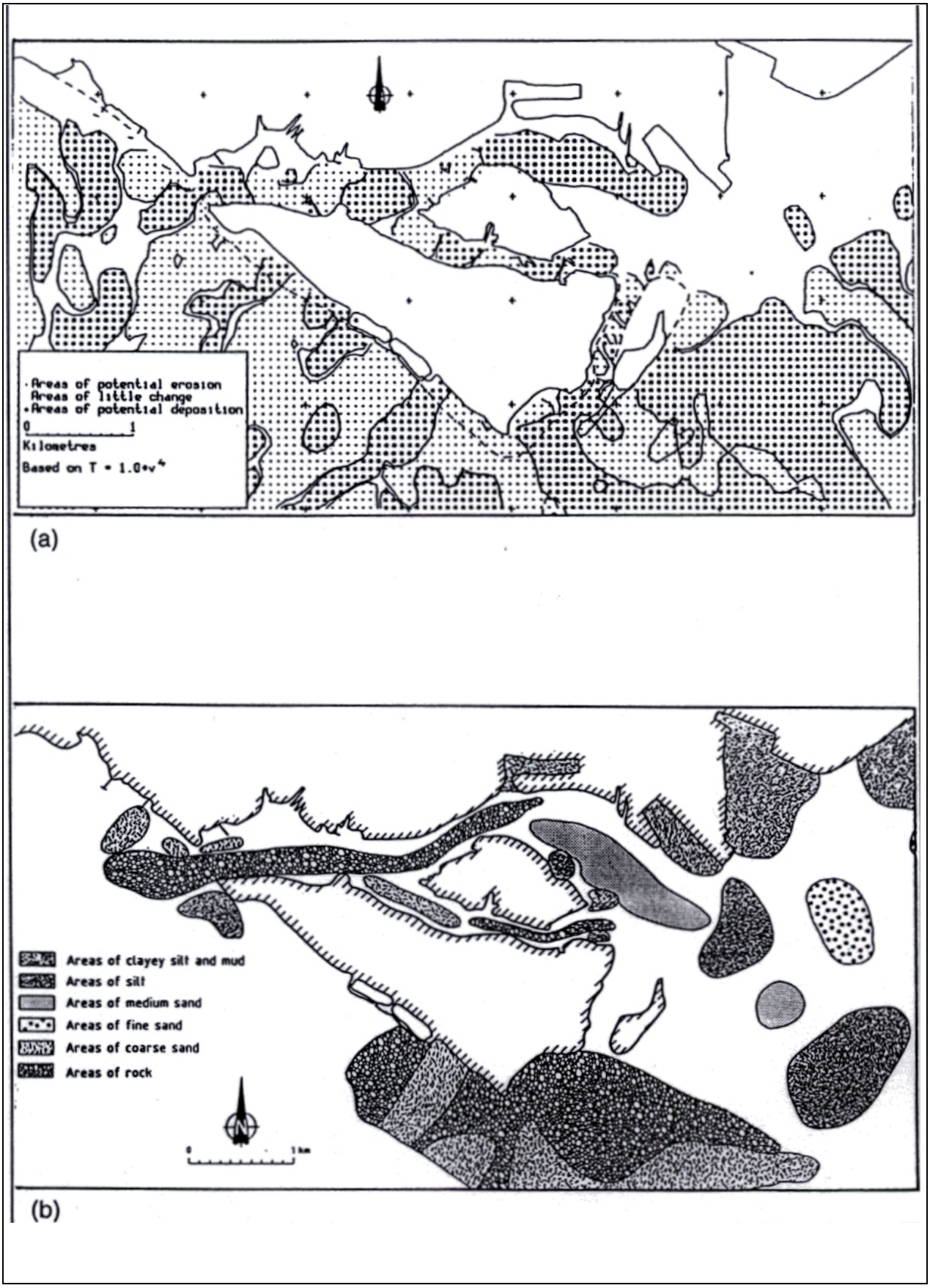

Figure 4 Comparison of sand erosion/deposition areas in model (a) with observed sediment distribution (b)

Appendix 2

Derivation of representative wave conditions for sediment transport

Hydraulic and Environmental Modelling: Coastal Waters

Proceedings of the Second International Conference on Hydraulic and Environmental Modelling of Coastal, Estuarine and River Waters
Volume 1

Edited by
R. A. Falconer
S. N. Chandler-Wilde
S. Q. Liu

ASHGATE

Published by
Ashgate
Ashgate Publishing Limited
Gower House
Croft Road
Aldershot
Hants GU11 3HR
UK

Ashgate Publishing Company
Old Post Road
Brookfield
Vermont 05036
USA

A CIP catalogue record for this book is available from the British Library and the US Library of Congress.

All royalties from the sale of this book will be donated to the Save the Children Fund

ISBN 1 85742 055 1
Printed in Great Britain at the University Press, Cambridge

31 The concept of a single representative wave for use in numerical models of long term sediment transport predictions

T. J. Chesher and G. V. Miles

Abstract

A method is proposed for the schematisation of wave fields into one single, representative field for use in long-term sand transport predictions. The concept comprises determining the optimum wave (in terms of sediment transport) from each direction and combining them, taking into account their relative frequency.

Combination of the waves into one wave field requires the determination of weighting factors. Sensitivity tests based on a coastal study area indicated that weighting factors based on the longer, "classical" approach gave qualitatively the same result, although quantitatively the total sedimentation prediction was underestimated.

Errors as a result of the schematisation are considered in relation to the overall accuracy of the sediment transport system, which includes both process filtering (e.g. the use of a 2DH model) and other input filtering (e.g. single grain size).

Introduction

In order to make long term sand transport predictions in the coastal zone it is often important to consider the effects of both currents and waves. By the very nature of a typical wave climate it is clear that some degree of schematisation is required so that the various combinations of tides and currents is reduced to an acceptable level.

Typically the schematisation of waves takes the form of a choice of a particular wave height (e.g. significant wave height) or a particular exceedence (eg. 1 in 1 year event). Having determined the input wave conditions the wave, tidal current, and sediment transport models are run for each wave direction and long term predictions are made by considering the relative frequency of the particular waves from each direction.

A method is proposed whereby this schematisation process is carried one stage further and, having chosen a particular wave type, waves from all directions are combined into one single

representative wave field (SRW), again taking into account the relative occurrence of each wave direction.

The concept represents a means of substantially reducing the computational expense incurred in making long term predictions by averaging over the directional space of a particular wave type.

Philosophy of the method

The SRW method is presented as a schematisation based on an order-of-operators concept; rather than predicting sand transport patterns for a particular wave type by combining the individual results for each wave direction, the individual wave fields are first combined into one wave field by averaging over the directions. This is then used to represent the whole wave field in the flow and sand transport models.

Figure 1 shows in schematic form how these two predictive approaches compare. With the "classical" approach the final sediment transport patterns are combined, with weighting factors (WC) determined by their occurrence in order to generate an overall prediction. With the SRW approach new weighting factors (WS) must be applied to generate a single wave field, which is then employed in the flow and sand transport models.

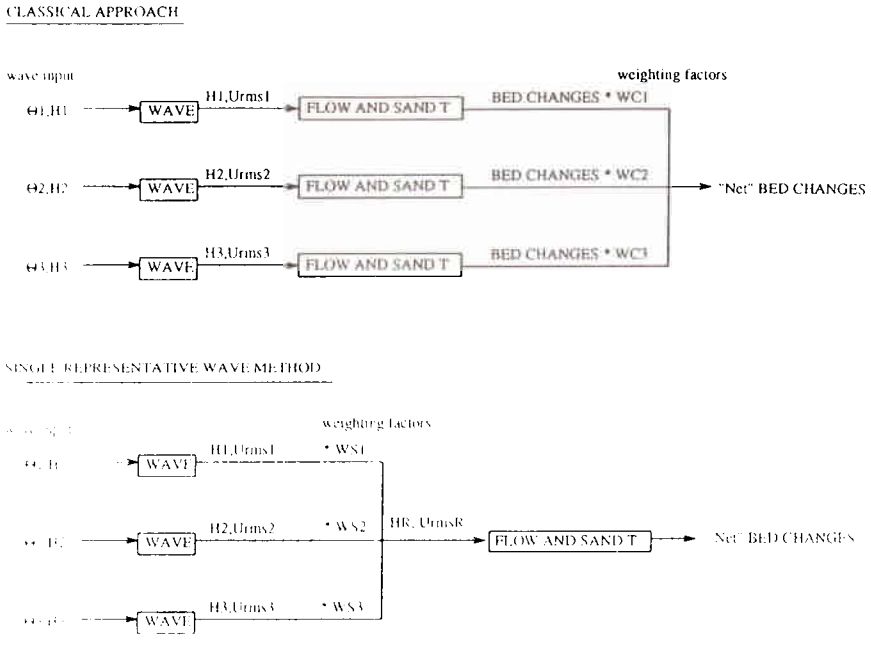

Figure 1 The concept of the single representative wave

Clearly, the method would lead to considerable saving in time and computational expense since the flow and sand transport models would need to be run once only. The efficacy of

this method in providing a valid means of schematising the complete wave climate into this more acceptable and manageable field depends on how the waves affect the sediment transport patterns.

Waves affect sediment transport in two main ways ; firstly by affecting the tidal currents via wave radiation stresses, mass transport and enhanced friction at the bed, and secondly by stirring up the bed and increasing the mass of suspended sediment which is subsequently advected away by the flow.

The stirring effect of even relatively small waves can give rise to vast increases in sediment transport [5] and it is this mechanism which is exploited in the SRW concept since the stirring is independent of direction.

Model details

The numerical modelling of sediment transport under combined waves and currents can take a variety of levels of complexity, eg fully coupled flows considering the effects of both the waves on the currents and the currents on the waves followed by a sediment transport relation including wave stirring, wave asymmetry and gravity (slope) effects. Conversely a simplified approach including waves as a stirring parameter in the sand transport relation may be adopted.

The choice of method will be determined by the relative importance of the waves and the currents, as well as by other external factors such as financial and time management considerations.

This schematisation study is based on a semi-coupled approach whereby 2DH models are coupled to include the effects of waves on currents as above, followed by sediment transport based on these combined flows with the inclusion of wave stirring. A short description of each module follows.

Wave module

The wave fields are determined by solution of the parabolic approximation to the mild slope equation

$$\nabla(C\ C_g\ \nabla\phi) + \frac{C_g}{C}\omega^2\phi = 0 \qquad (1)$$

where ∇ is the horizontal gradient operator
C is the wave celerity ($= \omega/k$)
C_g is the group velocity $d\omega/dk$
$\phi = \phi(x)$ a complex velocity potential at the mean free surface,
ω is the angular frequency

After further approximation the mild slope equation is solved on a finite difference grid to yield wave heights and periods over the model area.

Using these fields wave radiation stresses and orbital velocities are derived based on the method of Longuet-Higgins and Stewart [4] and Soulsby and Smallman [6] respectively.

Tidal current module

The appropriate equations for studying water movements in tidal areas are the shallow water equations. These are obtained by vertically integrating the equation of motion governing mass and momentum and making the following simplifying assumptions:

(i) the flow is incompressible;
(ii) it is well mixed (no variations in density);
(iii) vertical accelerations are negligible (the hydrostatic pressure assumption);

(iv) the effective lateral stresses associated mainly with shearing in the horizontal, and to a small extent with the averaging of sub-grid scale turbulence, may be approximated by a constant eddy viscosity;
(v) bed stress can be modelled using a quadratic friction law.

The equations then take the following form:

Conservation of mass:

$$\frac{\partial z}{\partial t} + \frac{\partial}{\partial x}(ud) + \frac{\partial}{\partial y}(vd) = 0 \tag{2}$$

Conservation of momentum:

$$\frac{\partial u}{\partial t} + u\frac{\partial u}{\partial x} + v\frac{\partial u}{\partial y} = -g\frac{\partial z}{\partial x} - f\frac{u}{d}(u^2 + v^2)^{1/2} + D\left[\frac{\partial^2 u}{\partial x^2} + \frac{\partial^2 u}{\partial y^2}\right] + \Omega v + \frac{\tau_{sx}}{\rho d} + \frac{\tau_{wx}}{\rho d} \tag{3}$$

$$\frac{\partial v}{\partial t} + u\frac{\partial v}{\partial x} + v\frac{\partial v}{\partial y} = -g\frac{\partial z}{\partial y} - f\frac{v}{d}(u^2 + v^2)^{1/2} + D\left[\frac{\partial^2 v}{\partial x^2} + \frac{\partial^2 v}{\partial y^2}\right] - \Omega u + \frac{\tau_{sy}}{\rho d} + \frac{\tau_{wy}}{\rho d} \tag{4}$$

where t = time (s)
z = elevation above datum (m)
u,v = depth averaged component of velocity in x,y direction (m/s)
d = total depth
f = friction coefficient
D = horizontal eddy viscosity coefficient (m^2/s)
Ω = Coriolis parameter (s^{-1})
τ_{sx}, τ_{sy} = x and y components of surface windstress. (N/m^2)
τ_{wx}, τ_{wy} = x and y components of the wave radiation stress. (N/m^2)

For conditions with wave activity the calm conditions friction factor is modified to

$$f_w = f(1+\alpha(\frac{W}{U})^n) \tag{5}$$

based on the method of Yoo and O'Connor [8] where

$$(8f)^{-1/2} = 2\log_{10}(14.8d/k_s) \tag{6}$$

and W = wave orbital velocity (m/s)
k_s = roughness length (m)
U = current speed (m/s) $=(u^2 + v^2)^{0.5}$
α and n are set to 0.72 and 1 respectively.

Sediment transport module

Although sand transport in estuaries is really an unsteady, 3D problem it can be dealt with using a 2D, depth-averaged model provided special provision is made to account for the

vertical profile effects of the sediment concentration. Under these circumstances the depth-averaged, suspended solids concentration c(x, y, t) satisfies the conservation of mass equation

$$\frac{\partial}{\partial t}(dc) + \alpha[\frac{\partial}{\partial x}(duc) + \frac{\partial}{\partial y}(dvc)] = \frac{\partial}{\partial s}(dD_s\frac{\partial c}{\partial s}) + \frac{\partial}{\partial n}(dD_n\frac{\partial c}{\partial n}) + \beta w_s(c_s - c) \quad (7)$$

where D_s = longitudinal (shear flow) dispersion coefficient (m^2/s)
D_n = lateral (turbulent) diffusivity (m^2/s)
(s,n) = natural coordinates (parallel and normal to mean flow (m))
w_s = settling velocity (m/s).

The parameters α and β are introduced to account for vertical profile effects lost during the depth-averaging.

$$\alpha = \int_o^d u(z)c(z)dz/(ucd) \quad (8)$$

represents the factor required to recover the true transport from the product of depth-averaged quantities.

β represents the factor to recover the correct rate of exchange of sediment at the bed. In its simplest form $\beta = c_{bed}/c$ but a better relation can be derived from the underlying 3D equation

$$\frac{\partial c}{\partial t} + u\frac{\partial c}{\partial x} + v\frac{\partial c}{\partial y} + (w - w_s)\frac{\partial c}{\partial z} = \frac{\partial}{\partial x}(D_x\frac{\partial c}{\partial x}) + \frac{\partial}{\partial y}(D_y\frac{\partial c}{\partial y}) + \frac{\partial}{\partial z}(D_z\frac{\partial c}{\partial z}) \quad (9)$$

with the usual meaning for the variables. By considering uniform horizontal flow conditions this reduces to

$$\frac{\partial c}{\partial t} = \frac{\partial}{\partial z}(D_z\frac{\partial c}{\partial z}) + w_s\frac{\partial c}{\partial z} \quad (10)$$

An analytical solution by Laplace Transform is possible for a depth independent eddy viscosity (D_z) which can be integrated to yield an expression for β in terms of error functions for each velocity, depth and sand size [2].

c_s is the depth-averaged concentration when the flow is saturated with sediment. Deposition or erosion takes place if the instantaneous model concentration exceeds or falls short of the saturated load at each point.

The saturation concentration, c_s is calculated by appealing to an empirically based sand transport law after van Rijn [7] with enhancement due to wave stirring after Grass [1].

The van Rijn formula for currents only is

$$\textbf{Bedload: } q_b = 0.005\rho_s Ud[\frac{U - U_{cr}}{[(s-1)gd_{50}]^{0.5}}]^{2.4}(\frac{d_{50}}{d})^{1.2} \quad (11)$$

$$\textbf{Suspended load: } q_s = 0.012\rho_s Ud[\frac{U - Ucr}{[(s-1)gd_{50}]^{0.5}}]^{2.4} D_*^{-0.6} \quad (12)$$

where q_b, q_s represent mass of sediment/unit width/unit time
d_{50} = median grain diameter (m)
ρ_s = sediment density (kg/m^3)
s = sediment specific gravity
g = gravitational acceleration (m/s^2)
U_{cr} = threshold speed (m/s)

$$D_* = d_{50}\left[\frac{(s-1)g}{\upsilon^2}\right]^{1/3} \quad (13)$$

υ = kinematic viscosity of water (m^2/s)

These formulae for currents only are written in total load flux form as

$$q_t = Au\,(U-U_{cr})^{n-1}\ (kg/m/s) \quad (14)$$

where A is a constant for a given grain size
n = 3.4

By appealing to the method of Grass, the wave enhanced sediment transport formula, including a threshold velocity is defined as

$$q_{t*} = Au[(U^2 + BW^2)^{0.5} - U_{cr}]^{n-1}\ (kg/m/s) \quad (15)$$

where B = $0.08/C_D$
W = wave orbital velocity (m/s)
C_D = drag coefficient

Methodology

Having defined the SRW concept it remains to determine the method of choosing the particular wave type and estimating the new weighting factors, WS. As expected, the manner in which the choice of wave is made would have a direct consequence on the determination of the weighting factors. The method described in this study is clarified by referring to the arbitrary annual wave height exceedence data in Table 1.

Table 1 Annual wave height exceedence diagram for wave model point X

H1	to H2	Wave angle (degrees N)											
		-30 0	0 30	30 60	60 90	90 120	120 150	150 180	180 210	210 240	240 270	270 300	300 330
0.00	0.20	3044	2888	1088	1344	1149	705	654	1566	2347	530	1444	3345
0.20	0.40	2144	1599	2200	1666	2072	983	1018	2221	2734	678	2200	3065
0.40	0.60	1611	1010	1665	2389	1557	756	779	1999	4000	0	1546	1965
0.60	0.80	268	250	575	1524	1949	860	1208	2446	2934	0	547	560
0.80	1.00	47	49	103	544	887	444	437	929	1577	0	213	139
1.00	1.20	9	10	81	612	410	514	686	851	1367	0	444	35
1.20	1.40	2	2	4	266	411	240	588	585	999	0	134	15
1.40	1.60	0	0	5	198	357	303	468	287	567	0	15	6
1.60	1.80	0	0	9	85	221	289	416	178	202	0	6	2
1.80	2.00	0	0	0	16	59	440	402	199	117	0	0	0
2.00	2.20	0	0	0	55	109	227	328	21	156	0	0	0
2.20	2.40	0	0	0	11	115	167	317	30	11	0	0	0
2.40	2.60	0	0	0	23	40	148	361	5	20	0	0	0
2.60	2.80	0	0	0	10	109	205	234	5	1	0	0	0
2.80	3.00	0	0	0	0	121	157	232	2	6	0	0	0
3.00	3.20	0	0	0	0	43	132	124	1	2	0	0	0
3.20	3.40	0	0	0	0	47	87	193	2	1	0	0	0
3.40	3.60	0	0	0	0	35	57	88	0	0	0	0	0
3.60	3.80	0	0	0	0	23	35	134	0	0	0	0	0
3.80	4.00	0	0	0	0	14	29	53	0	0	0	0	0
4.00	4.20	0	0	0	0	26	22	33	0	0	0	0	0
4.20	4.40	0	0	0	0	14	18	19	0	0	0	0	0
4.40	4.60	0	0	0	0	8	29	8	0	0	0	0	0
4.60	4.80	0	0	0	0	0	7	10	0	0	0	0	0
4.80	5.00	0	0	0	0	0	3	6	0	0	0	0	0
5.00	5.20	0	0	0	0	0	3	5	0	0	0	0	0
parts per thousand for each direction		73	59	58	89	100	70	90	115	174	12	67	93

Table 1 Annual wave height exceedence diagram for wave point X

The first stage of the schematisation comprises selection of a particular wave height from each direction. The wave model is then run for each chosen wave height from each direction.

Since the schematisation comprises averaging over the wave direction field each individual wave direction must be weighted according to its relative frequency. The most simple schematisation comprises combining all waves from a particular direction into one representative wave height, H_R for that direction. This is calculated by appealing to the sediment transport law and weighting according to the wave height, H and occurrence, f in the following way :

$$H_\theta = [\Sigma(f.H^{2.4})/\Sigma f]^{1/2.4} \qquad (16)$$

Further filtering of the wave input data could be carried out by neglecting those waves that are below a certain threshold and as such are considered to play only a minor role in the overall system.

Having generated the input wave fields for the tidal current and sand transport models in the classical approach each wave directional case H_θ would be run and the sediment transport patterns combined using as weighting factors the relative frequencies shown at the base of the table.

In the SRW approach the waves are firstly combined into one wave field H_R by averaging over the directional space with suitable weighting factors. The method of choice of weighting factors is not altogether clear since the whole sediment transport system is highly non-linear with respect to the wave input.

Results are presented in this paper for a sensitivity test on the sediment transport patterns for a particular study area between the classical approach and the SRW approach using the same weighting factors (i.e. assuming a linear response) based on the occurrence and the wave height for each direction.

Model Application

The schematisation concept was applied to an open coastal study area at Poole Bay in S. England where the sedimentation regime is strongly influenced by the effects of both currents and waves. This was confirmed by initial sedimentation sensitivity tests with and without waves where the sediment transport was minimal under currents alone but increased by an order of magnitude after inclusion of average-sized waves [3]. That there is considerable sedimentation at the site is confirmed by the need for capital dredging in order to keep the approach channel clear.

The wave data in Table 1 is based on data from a waverider buoy at this site. It can be seen that the waves are largest from the south and the east. Using this information it was assumed that waves below a wave height of 1m would play only a minor part in the overall sedimentation prediction and hence only three direction bands were considered, viz. 090-120, 120-150 and 150-180 degrees (N).

The weighting factors WC1, WC2, WC3 were calculated from the relative frequencies (f) from table 1 (ie assuming only these waves were present).

As indicated above the first guess at the schematised method weighting factors WS1, WS2, WS3 was made by setting them equal to WC1, WC2, WC3 respectively.

Net sedimentation patterns based on a spring tide using the classical approach and the SRW approach (Fig 1) were calculated and the results for each test are presented in Figures 2 and 3 respectively. Differences between the two approaches are presented in Figure 4.

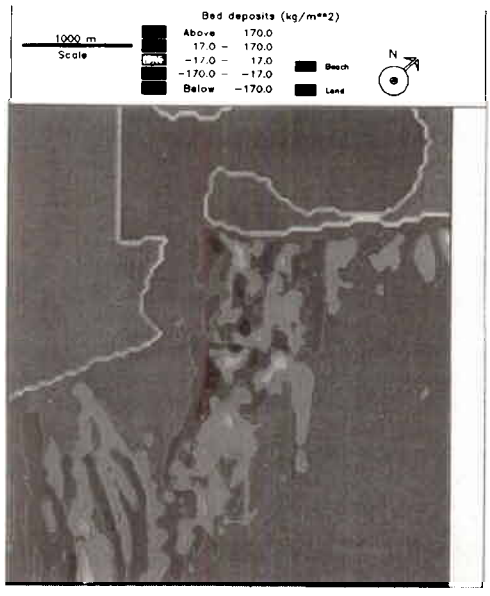

Figure 2 Net sedimentation based on the classical approach

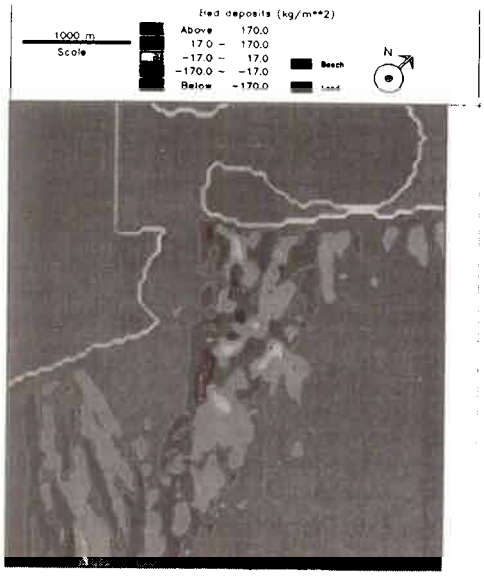

Figure 3 Net sedimentation based on the single representative wave approach

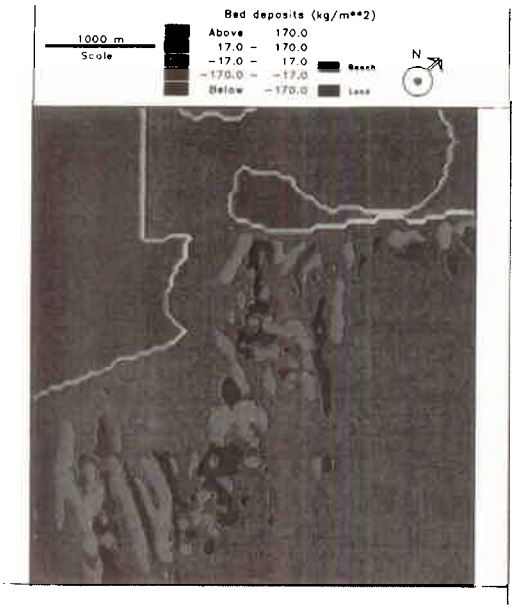

Figure 4 Net sedimentation differences (SRW - classical)

Discussion

Clearly there are differences (errors) as a result of the schematisation. However these errors must be considered in relation to the many other deficiencies involved even in this relatively elaborate system. Also, these errors should be considered against the expense of the classical method, the flow model being by far the most expensive module to run (in terms of time and expenditure).

The first check of the SRW method against the classical method is purely qualitative whereby one approach predicts erosion while the other predicts deposition (or vice versa). In this test 524 model cells out of a total of 14490 cells conflicted, which is less than 4%.

A closer quantitative assessment identified the cell with the worst error of 145 kg/m^2 deposition versus 44 kg/m^2 erosion. This is equivalent to an error of about 10cm.

Globally, a comparison of $\Sigma|\text{deposits(kg/m}^2)|$ indicated rather more (20%) total bed changes with the classical method than with the SRW method, which suggests that the weighting factors should be adjusted.

Conclusions

A schematisation method has been devised which appears to give rise to comparable predictions of sedimentation with the more detailed, full analysis, based on semi-coupled waves+currents at a particular test site.

The method comprises the generation of a single representative wave field by schematising results from repeated applications of the wave module (for a particular wave from a particular direction), prior to inclusion of the wave field into flow and sediment transport modules. It should be stressed that more than one wave propagation exercise is considered so that, for

example, a long breakwater would not be mis-represented unduly since the effect of the breakwater on the waves from all relevant directions would be included in the definition of the SRW.

The validation of the method is by no means rigorous, with a sensitivity test based on identical weighting factors for the classical method and the SRW method (i.e. assuming a linear response). Further tests, or a more detailed analysis of the method should be carried out to yield a more satisfactory set of weighting factors.

The test considered only waves from three dominant directions. A more open site would require consideration of waves from more directions. However, in these cases the successful derivation of a satisfactory SRW field would result in a considerable time and cost saving.

It is appreciated that the method will break down in the case of large waves with small currents, since the wave-driven currents from two or more directions could not be represented by one single wave from one single direction.

In the sensitivity test a representative wave from each direction was derived based on the stirring term in the sediment transport algorithm. Storm waves present an additional problem. In many coastal areas the sediment regime is dominated by the effects of storm conditions. For the reasons given above it is not expected that the method would give a satisfactory prediction under these conditions. However, in the cases where storm waves occur from a dominant direction the SRW schematisation for typical waves (using the method described in this paper) could be supplemented with individual "storm" cases. More importantly, in these storm cases the prediction of sediment transport remains a more elusive problem.

Acknowledgements

The author gratefully acknowledges financial support for research underpinning this work from the UK Department of the Environment under Research Contract PECD 7/6/161, and from the Commission of the European Communities Directorate General for Science, Research and Development under Contract No. MAST-0035-C as part of the G6M Coastal Morphodynamics research programme.

References

[1] Grass AJ (1981). *Sediment Transport by Waves and Currents.* SERC London Centre for Marine Technology Report FL29, University College, London.

[2] HR Wallingford (1988). *A numerical sand transport model with time dependent bed exchange.* Report No. SR 148.

[3] HR Wallingford (1991). *Poole Bay Phase II - Hydraulic Study.* Report No. EX 2228

[4] Longuet-Higgins MS and Stewart RW (1964). "Radiation stress in water waves; a physical discussion with applications". *Deep-Sea Research,* **XI.**

[5] Owen MW and Thorn MFC (1978). "Effects of Waves on Sand Transport by Currents." *Proc 16th Coast Eng Conf Hamburg.*

[6] Soulsby RL and Smallman JV (1986). *A Direct Method of Calculating Bottom Orbital Velocity under Waves.* HR Wallingford Report No. SR 76.

[7] van Rijn LC (1984). "Sediment Transport, Part III. Bed Forms and Alluvial Roughness." *J. Hydr Eng,* **110**, 12.

[8] Yoo D and O'Connor BA (1987). "Bed Friction Model of Wave-current Interacted Flow." *ASCE Spec Conf on Coastal Hydrod, Delaware, USA.*

Appendix 3

Example of sediment transport vectors using traditional plotting

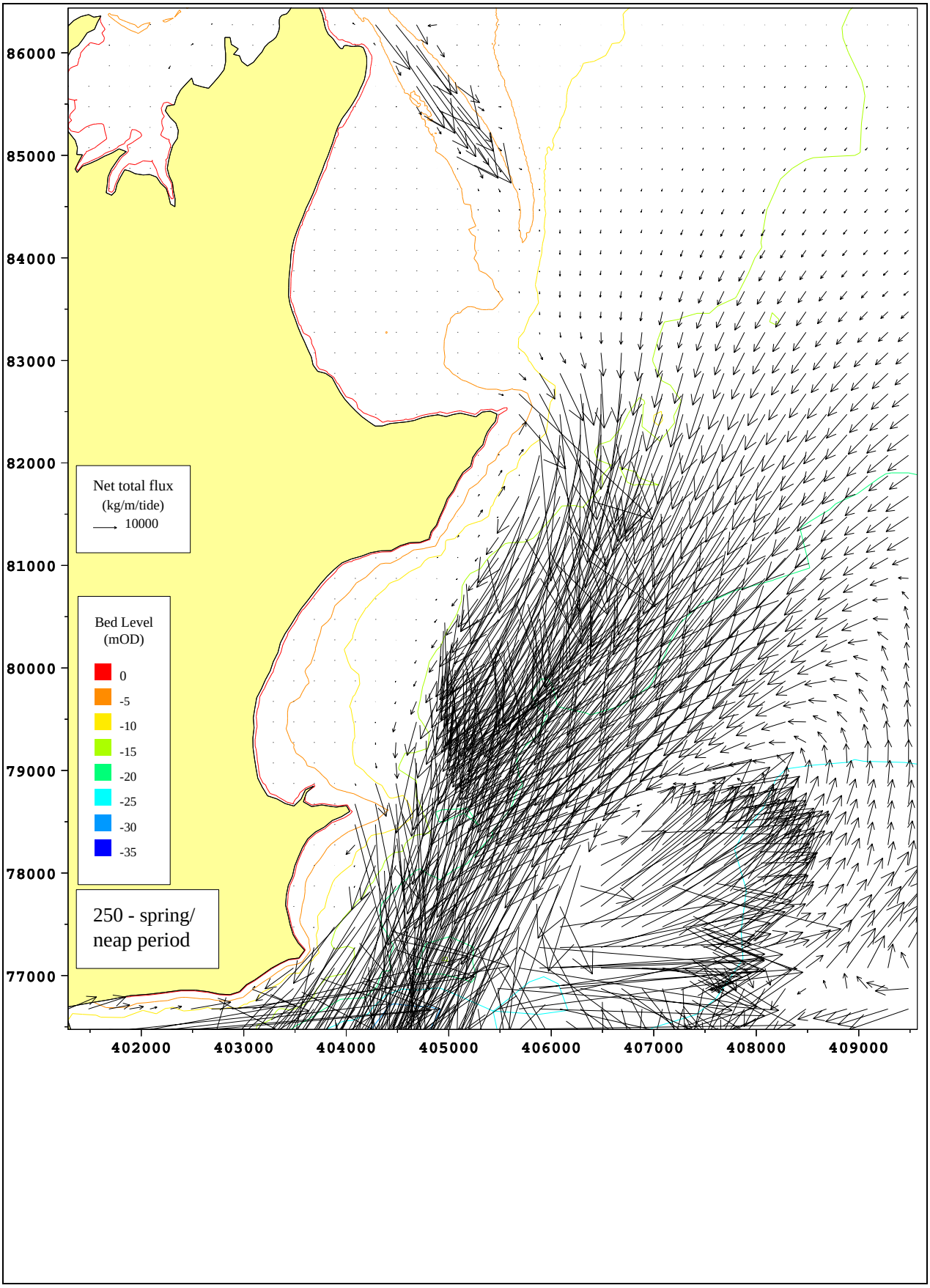

Figure A3.1 Reproduction of Figure 34